Université de Liège
Faculté des Sciences
Unité de recherche CESAM
GRASP

Université Libre de Bruxelles
École Polytechnique
TIPs

Leidenfrost effect at its limits

Laurent Maquet

In partial fulfillment of the requirements
For the degree of
Doctor of Philosophy
In the subject of physics
Academic year 2016-2017

Thanks

Tout a commencé il y a un peu plus de cinq ans, lors du mémoire de master... Cinq ans que je traîne dans les couloirs du 3$^{\text{ème}}$ étage, et pas que. La liste des personnes à remercier pour ces années est longue.

Merci aux différents membres du jury. Ça me fait particulièrement plaisir d'avoir pu constituer un jury avec tant de diversité tant sur les compétences que sur les points d'intérêts. Merci à Alejandro Silhanek d'avoir accepté d'être président du jury, dans un domaine qui n'est pas le sien; à Geoffroy Lumay, la petite secrétaire, et bien plus encore; to Neil Shirtcliffe, who accepted to come from Germany and who will be the guarantor of English in a french jury; à Philippe Brunet que j'avais eu plaisir à rencontrer à Paris, et qui, par son intérêt, avait réussi à me faire parler de Leidenfrost dans des circonstances festives. Et enfin merci à Denis Terwagne, pour sa présence dans le jury autant que pour ses années au labos et la trace qu'il y a laissée, et que pour son enseignement qui a fait partie des personnes qui font que je suis à l'ULg depuis dix ans.

Ensuite, bien sûr, il y a Pierre Colinet. Durant ces années de collaborations, nous avons régulièrement eu des points de vue différents sur certains sujets et notamment sur l'écriture, mais cette thèse n'aurait définitivement pas été la même sans ton apport de rigueur et de théorie.

Enfin, last (of the jury) but not least, Stéphane Dorobolo... Doroblo... Dorbolo ! Je pense que tu sais déjà assez bien à quel point tu as été incroyable pendant ces années, bien que tu sois trop modeste pour l'avouer. Scientifiquement, ça a été un plaisir de devenir un peu ton troisième fils spirituel après Denis et Martin, en travaillant sur un sujet aussi passionnant que l'effet Leidenfrost, et en laissant libre court à toutes les idées et en les nourissant de ton imagination et de tes questions. Ensuite, personnellement, ça a été par-

ticulièrement enrichissant. Pour les débats du matin, pour les pcr, pour la culture cinématographique, pour le punk...

Il y a encore plusieurs ribambelles de gens qui ont encore joué un rôle tout particulier dans cette thèse. Ceux qui ont eu un apport direct... D'abord bien sûr, mon frère de thèse, Martin Brandenbourger. Ton intérêt pour tout ce qui t'entoure a peut-être carrément été plus inspirant que nos discussions de geek et que les innombrables cocktails que tu as pu inventer. Ensuite, Baptiste Darbois-Texier. Peut-être le scientifique le plus impressionnant de son âge que j'aie rencontré, pour sa culture, sa capacité à s'intéresser à absolument tout... En science comme ailleurs dans le monde. Ma thèse ne serait certainement pas aussi chouette sans les manipes qu'on a pu faire ensemble et toutes les discussions qu'on a pu avoir. Et puis, Alexis Duchesne, le petit dernier. Et pourtant, à l'origine d'une idée de manipe qui a finallement été à l'origine d'une petite moitié de ma thèse. Au final, on a assez peu manipé ensemble, mais sans toi et Martin, je ne me serai jamais demandé si mes setup expérimentaux étaient un peu foireux. Enfin, ceux qui ont eu les mains dans le cambouis pour moi, qui ont fait que certaines mes manipes étaient propres : Samuel Rondia et Médéric Mélard, les mécaniciens et électroniciens que tout le monde regrette en quittant Liège.

Puis il y a tous les autres du labo, avec qui j'ai eu plus ou moins de rapports scientifiques et humains... Le très ancien, Christophe, qui m'a donné la confirmation que mettre de la musique et des blagues dans mes talks était une bonne chose, avant mê que je ne rentre à l'université. Les anciens, Florian, mon premier copromoteur à l'époque du mémoire; François, le numéricien-mathématicien qui m'aura fait exploser le plus souvent; Nicolas, dit Bob, avec ses bouibouibouiiis; Charles, dix ans de course pour savoir qui serait diplômé en premier, et j'accepte ma défaite. Ceux qui sont encore là: Eric, l'un de ceux qui m'ont aidé dans ma thèse-bis, même si je ne suis pas sûr d'avoir déjà mon titre de docteur ès Magic; Marti le puissant, pour avoir renforcé mon corps en le défonçant au foot; Sofienne, le quatrième fils, celui que j'ai enfermé; Pierre-Brice, le dernier Français qu'on a ramené de Paris dans nos valises, aussi fort que les autres même s'il ne le sait pas; Hervé, dont je me demande toujours si c'est son ouverture sur le monde qui lui donne son côté aigre-doux; Nicolas, le chef; Maxime, l'elfe avec la hallebarde, dit aussi, le magicien qui rate ses sorts; Sébastien, le plus nouveau des nouveaux, ma relève au labo; Boris, la preuve que les métalleux sont très urbains (mais un peu sâles quand même); Floriane et Antonella, la touche féminine du labo, expertes en presque-germanisme et

pisco (resp.); Martin, deuxième du nom, la force tranquille, toujours prêt à aider; Galien, un mec qui s'appelle trop-cool-Grosjean et qui est la preuve que même sans cheveux longs, les métalleux sont très urbains (mais un peu sâles quand même). Et puis, Alice, qui n'est pas vraiment du labo, mais qui a facilement trouv le moyen de s'intgrer dans la bande. Et enfin, mes co-bureau, Sébastien, il me semble qu'il est un peu nerveux. Et puis Julien, dix ans de non-course pour savoir qui ne sortirait pas en premier, j'admets ma défaite, mais c'est bien parce que bon, hein, voilà, OK ?! Tu te calmes !

Ensuite, ce n'est pas fini... Il y a les Bruxellois avec qui j'ai eu des discussions et avec qui j'ai pu collaborer aussi. Benjamin et Alex, deux moitiés fort différentes d'un même duo. Vous aussi, votre contribution directe à cette thèse est non-négligeable, même si je ne suis toujours pas complètement certain d'avoir saisi la différence entre patching et matching.

Quand je suis passé à Paris, j'ai eu la chance de travailler avec des gens qui n'ont eu finalement que peu d'apport direct, dans cette thèse, mais qui en vrai, ont eu un très gros apport indirect. Christophe Clanet, pour sa rigueur, son exigence, et le fourmillement d'idées qui passent par sa tête, reste un modèle pour moi. Et bien entendu, Éline. Les trois mois que j'ai passé à Paris, et le mois et demi que tu as passé à Liège ont été fantastiques, et ton entrain, ton sourire et tes gentils mots ont, alors et depuis, été très agréables et motivants. Il y a aussi Pascal, Adrien, Caro, Guillaume, Dan, Loïc, Thomas, et je pourrais même citer Mourad... Mais en vrai, la liste ne s'arrête pas là.

For a few month, I also had the opportunity to work with Tadd Truscott. The coolest guy I met from the United States, and one of the coolest guy ever.

Une mention spéciale pour l'homme qui m'a donné l'envie de faire de la physique mon métier. Michel Kapenyak, toi et tes folles expériences dans les couloirs et en classe (au hasard, monter sur un chariot pour illustrer le MRUA, le slinky pour illustrer les propriétés des ondes, et la séance de Star Wars en électro-magnétisme) avez été capitaux pour me pousser jusqu'ici.

Enfin, il y a tous les autres qui m'ont entouré ces dernières années. Impossible de tous les citer, sinon je vais oublier des gens, mais les gars de Black Sun Act, et en particulier François, les gens de l'univ, les touristes et assimilés, ceux du badminton, de l'université Magic, et de la team JangaDa...

Et puis bien entendu, ma famille qui a été la première à me donner la passion des sciences il y a bien longtemps, en me faisant jouer avec des légos, des dinosaures et en me faisant lire des bouquins sur l'astro. Heureusement que je n'ai pas viré ingénieur ou gratteur de caillou, quand même...

Liège, November 2016
Laurent Maquet

Table of Contents

Summary

For more than ten years, the Leidenfrost effect has focused the attention of many physicists with an interest in drops. It appeared that the drops in the Leidenfrost state are convenient to manipulate fluids and particles, and are a good example of the ability of drops to be used as micro-reactors. However, many things are still to be understood, especially when the drops are pushed towards their limits. For instance, the Leidenfrost Point, *i.e.* the temperature above which the drops can experience this effect on a given substrate, still lacks of understanding. In this thesis, through five different experiments, we point out some of the ingredients that are crucial to understand why the theory and experiments usually do not match regarding this problem, and how interesting properties emerge when the drops are settled in specific conditions.

In the first experiment, the drops are studied under hypergravity conditions. This experiment shows well how the hypergravity can be used to suppress the regimes dominated by capillary effects in the physics of drops. Moreover, we show that the Leidenfrost Point increases with the gravity. This increase is explained via the observation that the minimal thickness of the vapor film is decreasing with the gravity.

In the second experiment, we demonstrate that it possible to make drops levitate on a heated liquid pool as soon as its temperature is larger than the boiling point of the liquid of the drop. This fact that had never been observed on any other substrate is expected to originate from the absence of roughness of liquid substrates. However, it appears that making Leidenfrost drops on highly viscous substrates at the temperatures considered is impossible. The velocity fields of the liquid of the pool are analyzed, and we conclude that the mechanism for this suppression of the Leidenfrost effect does not find its origin in the large toroidal vortex that appears under the drop.

In the third experiment, we show that Leidenfrost drops on an oscillating substrate can exhibit classical features of the bouncing objects, such as phase locking, bifurcations and transition to chaos. Drops are observed to have a contact time that does not depend on the parameters of the oscillation of the substrate and that is the same as the one on a static substrate. This induces that when the substrate oscillates too fast, the drop can undergo a transition towards a bouncing mode where it bounces once every two oscillations of the substrate.

In the fourth experiment, we show that the way drops are deposited on a hot liquid pool, *i.e.* the velocity at the moment of the impact, is of tremendous importance to determine how the drop will behave. We observed four different regimes by increasing this impact velocity. At very low impact velocity, the drop deforms the substrate, and then bounces without any contact with the surface. At the end of this process, the drop ends in the Leidenfrost state described in the second experiment. For slightly larger impact velocities, the drop may cross the interface and form a thermal antibubble, *i.e.* a drop inside a shell of its own vapor, inside the liquid pool. At even larger velocities, the release of the antibubble disrupts the vapor film around the drop, leading to a sudden evaporation. At the larger impact velocities investigated, the drop does not create any vapor film and directly touches the substrate.

Finally, in the last experiment, we show that microbeads can be organized in Leidenfrost drops and lead to the formation of monolayers at their surface. We also show that these beads tend to reduce the evaporation when they are located at the surface of the drop, by reducing the surface available for evaporation. This decrease of the surface of evaporation is linked to the contact angle between the liquid of the drop and the surface of the microbeads, and to the surface packing fraction of the beads.

Résumé

Depuis plus de dix ans, leffet Leidenfrost a focalisé lattention dun grand nombre de physiciens intéressés par la physique des gouttes. Ces gouttes sont apparues comme un moyen pratique pour manipuler fluides et particules. Elles ont prouvé leur capacité à servir de micro-réacteurs. Cependant, de nombreux aspects de ce phénomène sont toujours mal compris, en particulier lorsque ces gouttes sont poussées à leurs limites. Par exemple, lorigine de la température de Leidenfrost, cest-à-dire la température à partir de laquelle une goutte est en état de Leidenfrost sur un substrat donné, est toujours sujette à débat. Dans cette thèse, à travers cinq expériences, nous étudions différents ingrédients cruciaux pour une meilleure compréhension de cette limite, et de quelle manière dintéressantes propriétés des gouttes en Leidenfrost apparaissent lorsquelles sont placées dans des conditions spécifiques.

Dans la première expérience, nos gouttes sont étudiées en hypergravité. Nous montrons à quel point les conditions dhypergravité peuvent être intéressantes pour supprimer les régimes capillaires en physique des gouttes. De plus, nous montrons que la température de Leidenfrost augmente lorsque la gravité augmente. Cette augmentation est imputée au fait que lépaisseur minimale du film de vapeur sous la goutte diminue lorsque la gravité augmente.

Dans la seconde expérience, nous démontrons quil est possible de faire léviter des gouttes sur un bain liquide chauffé dès que sa température est supérieure à la température débullition du liquide de la goutte. Ce fait na jamais été observé sur des substrats solides et semble provenir de labsence de rugosité des substrats liquides. Cependant, déposer des gouttes en Leidenfrost sur des substrats liquides très visqueux semble impossibles aux températures de substrat considérées. Les champs de vitesse dans les bains sous la goutte sont étudiés, et nous concluons que le mécanisme de cette suppression de leffet Leidenfrost ne provient pas du vortex toroïdal apparaissant sous la goutte.

Dans la troisième expérience, nous montrons que le comportement de gouttes en Leidenfrost sur un substrat oscillé verticalement possède des caractéristiques classiques des objets solides sur de tels substrats, comme le verrouillage de phase, les bifurcations, et les transitions vers le chaos. Les gouttes en Leidenfrost ont un temps de contact qui ne dépend pas des paramètres de loscillation du substrat, et qui est le même que celui sur des substrats statiques. Cela implique que lors doscillations trop rapides, la goutte transite vers un mode de rebond où elle rebondit une fois toutes les deux oscillations du substrat.

Dans la quatrième expérience, nous montrons que la façon de déposer des gouttes sur des bains liquides chauffés, cest-à-dire la vitesse dimpact, a une importance capitale pour déterminer le comportement de la goutte. Nous avons observé quatre régimes différents en augmentant la vitesse dimpact. A basse vitesse dimpact, la goutte déforme le substrat, rebondit, puis se stabilise en état de Leidenfrost. Pour des vitesses légèrement supérieures, la goutte peut déformer suffisamment linterface et être libérée dans le bain pour former une antibulle thermique, cest-à-dire une goutte dans une couche de sa propre vapeur, à lintérieur du bain liquide. A des vitesses encore un peu supérieures, la libération de lantibulle provoque la rupture du film de vapeur, menant à la perte de létat de Leidenfrost. Aux plus grandes vitesses dimpact explorées, la goutte ne crée pas de film de vapeur suffisamment vite, et touche directement le substrat.

Enfin, dans la dernière expérience, nous montrons que des micro-billes peuvent être organisées par les gouttes en Leidenfrost et mener à la création de mono-couches de ces micro-billes à leur surface. Nous avons aussi montré que la présence de ces billes à la surface de la goutte tend à diminuer son évaporation en réduisant la surface dévaporation de la goutte. Cette diminution est liée à la manière de sorganiser des micro-billes à la surface, et à langle de contact du liquide de la goutte avec la surface des billes.

Il est permis d'espérer que l'état sphéroïdal, qui comprend la nature entière, depuis les plus grands corps célestes jusqu'aux infiniment petits des corps organisés, sera tôt ou tard l'objet de l'attention universelle.

Boutigny P. H.

I

Introduction

I.1 A story of drops

As any work in the field of the physics of fluids, this thesis may begin in a sea. Its characteristic size would be 10^6 m. But that is quite large for the lab. Let us take it smaller...

As any work in the field of the physics of fluids, it may begin with a molecule of fluid. Its characteristic size would be 10^{-9} m. But that is quite small for my eyes... Let us then take it bigger...

A drop is quantity of liquid that may be described as an amount of liquid that is not too big, and not too small. Usually, the size of water drops as we imagine them is of the order of 10^{-3} m. The reason why this scale is so special is that this scale is precisely the one where objects made of fluids are on the edge of the transition between large size objects like seas, that are dominated by gravitationnal forces, and small size objects, where molecular forces (grouped under the name of capillary forces) dominate. A dimensionless number is particularly adapted to determine what are the dominant forces applying on a liquid object in a surrounding fluid : the Bond number, Bo.

$$\mathrm{Bo} \;=\; \frac{\Delta\rho \; g \; L^2}{\gamma} \tag{I.1}$$

In this number, $\Delta\rho$ is the difference of densities between the densest and the less dense of both fluids, g is the acceleration of the gravity, L is the characteristic length of our object, and γ is the surface tension associated to both fluids. From this number, we can build a significant length, the capillary length

$$\ell_c = \sqrt{\frac{\gamma}{\Delta\rho\, g}}\,. \tag{I.2}$$

When the size of our system is larger than the capillary length, the gravitationnal forces dominate and the liquid volume tends to adapt to the shape of the container. When the surface tension forces dominate, the liquid tends to stay in a spherical shape. For water in air at 20°C, this length is equal to 3 mm.

From this property to be at the limit between two regimes, many interesting features arise. In this thesis, we will work with drops slightly smaller, as well as slightly larger than the capillary length.

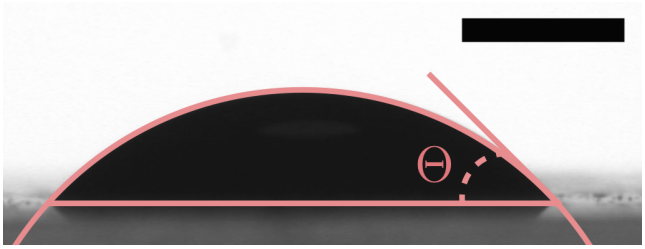

Figure I.1: Photography of a drop on a glass slide. The scale bar represent 1 *mm.*

When they are deposited on a flat solid isotropic substrate, in most case, we can observe that small drops enter in contact with the substrate, spread quite a bit on it, then stabilize (at least when the drop does not evaporate). At that moment, its shape is a sherical cap, and the line at the frontier between the two fluids and the solid is circular, and is called the contact line. By looking at the drop from the side, we can easily define the contact angle Θ, the angle between the plane of the substrate and the tangent to the surface of the drop at the contact line (see Fig. I.1). For example, in that case, the contact angle of the water drop in this picture is 53°. In some particular cases, playing with the chemistry of the surfaces, contact angles can be above 90°. These surfaces are called hydrophobic substrates. But it is even possible to go quite close to 180°...

I.1.1 A way to overcome contacts

Indeed, considering a small drop on lotus leaf, one can see that this drop seems extremely mobile and has a spherical shape. Measuring the contact angle gives a value around 160°. This kind of contact angles cannot be achieved by simply playing with the chemistry of surfaces. The trick to get this exceptionnal behavior is to play on the roughness of the substrate in addition to the chemistry of the interface. The characteristic of these surfaces is to have microstructures on them, and in some case, multiscale structures. The advantage of this roughness is that the liquid does not penetrate in the roughnesses like in the so-called Wenzel state [1] (see Fig. I.2(a)), but rather stays on the top of the structures touching only a small area of it. This is the Cassie state (see Fig. I.2(b)) [2].

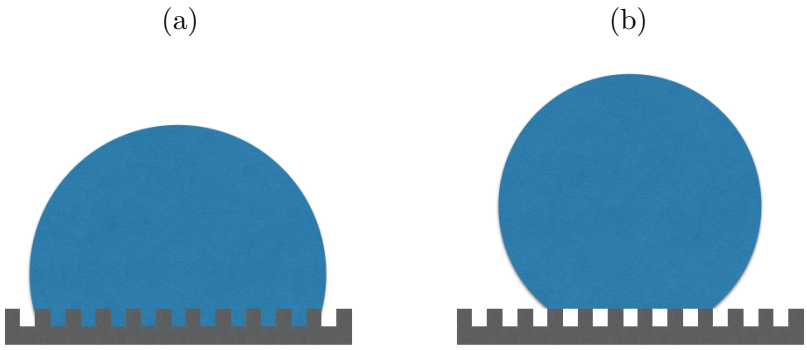

Figure I.2: Schematic representation of (a) the Wenzel state and (b) the Cassie state.

A photography of a drop on a commercial superhydrophobic substrate is shown in Fig. I.3(a). The contact angle in that case is $\Theta = 153°$. This state of the drops over a substrate presents numerous advantages.

The first one is the fact that these drops are almost contactless. Because the drops touch only the top of the structures, they are mostly lying on air, and so the friction they experience is extremely low. That is exactly the reason why drops are so mobile on a lotus leaf [3]. From a more general point of view, the uses of superhydrophobicity are countless in the vegetal world, because the self-cleaning property that is associated with the absence of adhesion is crucial to avoid stagnant water and the development of diseases that goes with it [4]. From the point of view of engineers, the mobility and the quasi-absence of adhesion are key properties that make the manipulation of drops really convenient. Associated to specific microtextures (conic micropillars),

superhydrophobic substrates also feature anti-fogging properties [5].

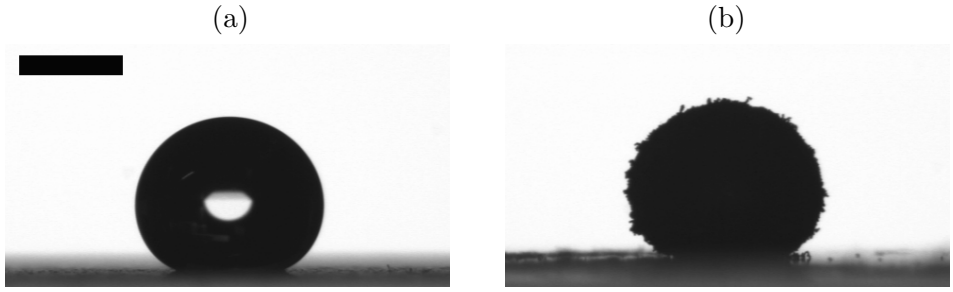

Figure I.3: Photography of (a) a drop on a commercial superhydrophobic substrate, and (b) a liquid marble made of a water drop coated by lycopodium powder. The scale bar represent 1 *mm.*

I.1.2 Superhydrophobicity in a nutshell

The hydrophobicity can also induce a secondary kind of superhydrophobicity. If an hydrophobic microparticle comes into contact with a drop made of water, this particle naturally sticks to the surface of the drop, being more emerged than immersed. Eventually, when you put a drop on an hydrophobic powder, the drop stands on the grains quite like it would do on a superhydrophobic substrate. Then, you can easily put this drop into movement because of the small contact area. And if you do so, the microparticles stick to the surface and coat the drop. The object created, a drop wrapped with hydrophobic particles, is called a liquid marble [6]. A photography of such object is shown in Fig. I.3(b). In that case, the drop of water is coated by lycopodium powder (dry spores of lycopodium plants). The size of the grains is approximately 33 µm, and the object sits on a glass slide. The apparent contact angle is $\Theta = 144°$.

This object present some common features with simple drops on superhydrophobic substrates. Especially, they experience a low friction. This friction can be very different when the drop is large and flattened or small and spherical [7].

I.2 Levitating drops

As interesting as these latter phenomenons can be, they still lack a real absence of contacts. However, several ways exist to help a drop levitate above

a substrate. One could mention the levitation of molten metals using electromagnetic fields [8], the levitation induced by acoustic waves [9], or the levitation over vibrated liquid pools [10]. However, the way we focus on in this thesis is the way of Boerhaave [11], and later, Leidenfrost [12] who gave his name to the phenomenon : the Leidenfrost effect. One century after its discovery, Boutigny, a french pharmacist wrote about this phenomenon the sentence of the prelude to this first chapter [13]. A literal translation could be the following.

> *One is allowed to hope that, sooner or later, the spheroidal state*[1]*, which embraces the Nature in its entirety, from the largest celestial bodies to the infinitely small organized bodies, will be the center of the universal attention.*

To understand what is the Leidenfrost effect, imagine that you are a huge meat lover. So, you want to cook a steak, and cook it well. Then, you remember the precious advices of your grandmother.

> *Before you put your steak in your pan, do not forget to sprinkle a few drops of water in your pan. If they disappear immediately, wait. If they keep a spherical shape and they seem to roll on your pan, you are good.*

Your grandmother had understood more than she knew about the Leidenfrost effect. In that example, the drop almost reaches the pan before experiencing a rapid increase of its evaporation. Under the drop, a vapor film is generated and has to escape to let the drop touch the substrate. An equilibrium can appear between the feeding of this vapor film and its drainage. This leads to a drop sitting on a bed of its own vapor. That vapor layer reduces considerably the heat transfer between the pan and the drop compared to the case of a drop touching the substrate. The drop evaporate relatively slowly because of the insulating layer of vapor, and the mobility of the drop is extremely high because of the absence of any contact. A picture of a Leidenfrost drop levitating above an aluminium substrate is shown in Fig. I.4.

This effect has finally gather a lot of attention for more than ten years, almost as expected by Boutigny. Many studies have been done and may be classified in three kinds whether they are related to (i) the apparition of the Leidenfrost effect, (ii) the mobility and motion of the drops, and (iii) the applications in terms of manipulation, fabrication and deposition assisted by the

[1] This is the name that Boutigny gave to the state of drops experiencing the Leidenfrost effect.

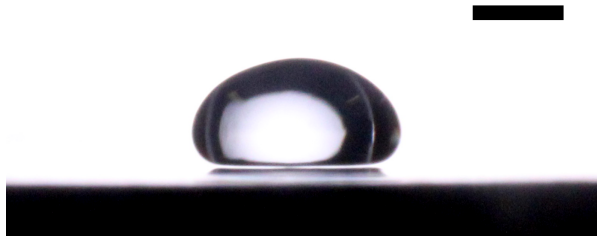

Figure I.4: Photography of a Leidenfrost water drop on an aluminium substrate. The scale bar represent 4 mm.

Leidenfrost effect.

Well before the renewal of interest in the last decade, the studies on the Leidenfrost effect were concentrated on a single problem that leads us to define one of the most important concept of this thesis. In the grandmother parabola, there is key ingredient : if the drop is not in the Leidenfrost state, one has to wait. One has to wait for the pan to be more heated. The Leidenfrost effect appears when the substrate is hot enough. This means that there is a threshold temperature above which the effect appears : this temperature is called the Leidenfrost Point. In Fig. I.5, the lifetime of water drops deposited over a substrate is represented as a function of the temperature of this substrate. The lifetime decreases as the temperature increases until $\sim 120°C$. Then, the lifetime suddenly increases around 150°C. This increase is the signature of the apparition of the Leidenfrost effect. In the following, we note the Leidenfrost Point T_L.

Until the begining of the 21^{st} century, most of the studies were focused on the determination of this temperature. As explained in the review of Bernardin and Mudawar, most of these studies end with empirical laws, and no theory focused on the description of the shape of the drop [15].

Since then, lots of papers focused on the theoretical prediction of shape of the Leidenfrost drops [16–19], and on the experimental determination of this shape [14, 20]. It appears that the understanding of these shapes, and of the mechanism of evaporation of these drops (that relies on the shape), is mandatory to understand what sets the Leidenfrost Point. Nowadays, the idea has emerged that this threshold temperature may be less relevant than a threshold thickness of the vapor layer. The roughness of the substrate [21, 22] and the thermal conductivity of the substrate [23] influence the threshold temperature in a dramatic way. Even the static shapes that are now well known may not be

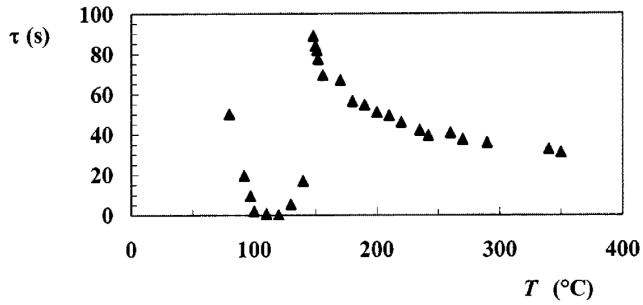

Figure I.5: Lifetime of drops deposited on a substrate as a function of the temperature of this substrate. The lifetime decreases while the temperature increases above the boiling temperature until this lifetime suddenly increases. This is the signature of the apparition of the Leidenfrost effect. Taken from Ref. [14].

sufficient to understand the mechanisms that set the Leidenfrost Point, as the fluctuation of the thickness of the vapor film probably also play a role [20, 24].

The second large interest in the Leidenfrost drops lies in their high mobility. This has been studied extensively in the thesis of Pascal Raux and the influence of the size of the drops compared to the capillary length on the friction has been shown [3]. But the interest in the mobility does not stop at the study of the friction. Indeed, Linke *et al.* showed that these drops propel themselves spontaneously when they are put on substrates with asymetric shapes like sawtooth waves [25]. A few theories have been developed to explain this selfpropulsion. All of them relie on the rectification of the vapour flow inside the grooves of the substrates. The most satisfying ones, for which theory and experiments are in agreement, showed that this vapour induces a viscous entrainment by escaping the grooves. That viscous entrainment pushes the drops down the low slopes [26, 27]. Note that this effect is not limited to Leidenfrost drops but also applies for Leidenfrost solids, *i.e.* solids that sublimate enough to maintain a vapor film when they are deposited over a hot substrate [26], and also on other kinds of asymetric substrates such as ones with herringbone patterns engraved on them [28].

Finally, the third large interest lies in the ability of these drops to consistute reactors for the manipulation of particles from large size structures to molecules without any contact with a solid. On the one hand, these drops can support heavy loaded carts [29]. These carts can even move thanks to the self-propulsion on asymetric substrates. On the other hand, molecules in Leidenfrost drops can undergo chemical reactions and these reactions can

even be facilitated by the Leidenfrost effect [30]. In between these extremes, nanoparticles have been succesfully manipulated in Leidenfrost drops. They can be deposited on substrates [31] or be assembled [32]. Specific types of nanoparticles also form compact shells during the evaporation of the drops [33]. Even molecules can form compact shells, such as surfactants, leading to explosions [34].

In the following of the thesis, we will need a model for the shape and evaporation of Leidenfrost drops. More than a single model, we will use two different ones. To end this chapter, we introduce both models and explain their respective advantages and limitations.

I.2.1 The analytical model

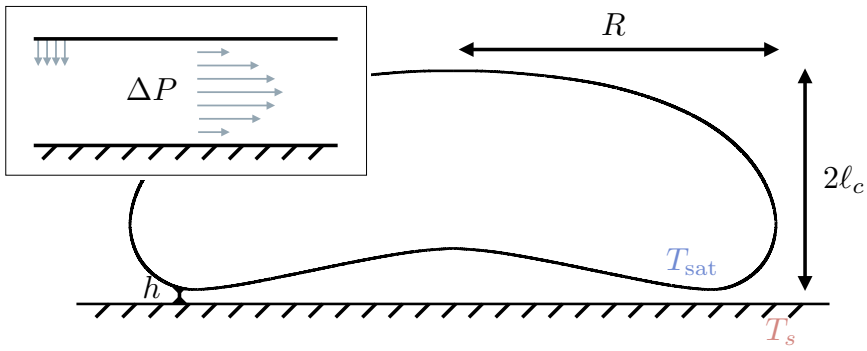

Figure I.6: Schematic view of a Leidenfrost drop larger than the capillary length ℓ_c. The inset is a zoom on the vapor film where the vertical arrows represent the evaporation flux and the horizontal lines represent the Poiseuille flow.

In this first model, called Biance's model in the following [14], drops larger and smaller than the capillary length are considered, but as we will only use this model to describe large drops further, we stick to this part of the model. The large and axysymetric drops that we consider can be thought as a cylinder of height $2\ell_c$ and radius R. A schematic view of such drop is shown in Fig. I.6. The thickness of the vapor film is assumed to be uniform in a so-called "contact region", and is noted h. Burton *et al.* [20] showed that this thickness is not uniform and that a pocket of vapor is always present under Leidenfrost drops. However, this approximation gives good results. The contact region is defined as $S_c = \pi R^2$. The heat transfer through the vapor film, over this contact region, is assumed to be a conductive process. The loss of mass of the drop m through time on a substrate at temperature T_s can thus be expressed by

$$\dot{m} = -\frac{\lambda_v}{\mathcal{L}} \frac{\Delta T}{h} S_c \tag{I.3}$$

where λ_v is the thermal conductivity of the vapor, $\mathcal{L}$ is the latent heat of evaporation of the liquid of the drop, and ΔT is the superheat, which we define as the difference between the temperature of the substrate T_s and the boiling temperature of the drop T_{sat}. This means that the drop is at the boiling temperature, at least locally, at the bottom of the drop, which is a common assumption in the field of the Leidenfrost effect.

The produced vapor has to escape the vapor film. The drop above the film induces an excess of pressure that drives a Poiseuille flow in the film. As the thickness of the vapor film is assumed to be uniform, and as the size of the contact region ($\sim 1 - 10$ mm) is large in comparison with the thickness of the vapor film ($\sim 10{-}100\,\mu$m), the lubrication approximation can be used to describe the flow. Thus, the loss of mass of the vapor film can be expressed by

$$\dot{m} = -\frac{2\pi}{3} \frac{\rho_v}{\eta_v} h^3 \Delta P \tag{I.4}$$

where ρ_v is the density of the vapor, η_v its dynamic viscosity, and ΔP is the excess of pressure imposed by the drop. In the case of large drops, the excess of pressure is dominated by the hydrostatic pressure $\Delta P = \rho_d g 2\ell_c$, $2\ell_c$ being the height of a large Leidenfrost drop and ρ_d the density of the drop. Moreover, when the size of the drop is larger than the capillary length, the radius of the contact region is close to the radius of the drop R. Thus, by combining Eq. (I.3) and Eq. (I.4), one obtains an expression for the thickness of the vapor film

$$h = \left(\frac{3}{4} \frac{\lambda_v \ \eta_v}{\rho_v} \frac{\Delta T}{\mathcal{L} \ \rho_d \ g \ \ell_c} \right)^{1/4} \ R^{1/2} \ . \tag{I.5}$$

Introducing this thickness in Eq. (I.3), and considering that the volume of a large drop is related to its radius by the relation $R = \sqrt{V/2\pi\ell_c}$, one finds that

$$\dot{V} = -\left(\frac{\pi \ \rho_v \ g}{6 \ \eta_v \ \ell_c^2} \right)^{1/4} \left(\frac{\lambda_v \ \Delta T}{\rho_d \ \mathcal{L}} \right)^{3/4} \ V^{3/4} = \ - A \ V^{3/4} \ . \tag{I.6}$$

The resolution of this differential equation gives

$$V(t) = V_0 \left(1 - \frac{t}{\tau_g} \right)^4 \tag{I.7}$$

with V_0 being the initial volume of the large drop, and τ_g its characteristic lifetime. This characteristic lifetime can be expressed as

$$\tau_g = 4 \, \frac{V_0^{1/4}}{A} \, . \tag{I.8}$$

Of course, the assumption that large drops are cylinders of height $2\ell_c$ and radius R is a strong assumption, and of course, the drop also evaporates by its top side even though this top side is not as close to the substrate as the bottom side. However, we will see later that this model is a very good tool to explain experiments, beginning with the basic experiment of a drop evaporating on a flat substrate, described in the paper of the model [14].

I.2.2 The numerical model

However, the bottom of a Leidenfrost drop is never flat as observed by Burton *et al.* [20]. Instead, a pocket of vapor forms at its center. Thus, the vapor film has a high thickness at its center and a small thickness at a radial coordinate that we call the neck. Moreover, the top of a drop is not flat either even though this top side gets flatter when the size of the drop increases.

To overcome these limitations, our collaborators in Université Libre de Bruxelles built a new model that describes accurately the shape of the drop and of the vapor film [19]. The improvements brought by this model are necessary to understand some key effects and establish a base for a model that is developed later. In this model, an axisymetric drop is still supposed to levitate over a flat substrate.

The idea behind the description of shape of the drop is to divide this shape into two different parts : the outer drop region and the vapor layer region. This is illustrated in Fig. I.7. The interface of the outer drop region, $z(r)$, is the same as the shape of a drop on a superhydrophobic substrate : the hydrostatic pressure $\rho_d g(z_{\text{top}} - z)$ balances the capillary pressure $\gamma_d \kappa$ with κ the curvature of the interface of the drop. In a dimensionless form, where lenghts are made dimensionless with the capillary length of the liquid of the drop, one obtains

$$\tilde{\kappa} + (\tilde{z}_{\text{top}} - \tilde{z}) = \tilde{\kappa}_{\text{top}} \tag{I.9}$$

where $\tilde{\kappa}_{\text{top}}$ is the dimensionless curvature at the top of the drop and is used as a free parameter controlling the size of the drop. This solution is assumed to be valid up to a patching point between the intersection with the substrate and the radius of the drop R. Past this patching point, the effect of the vapor

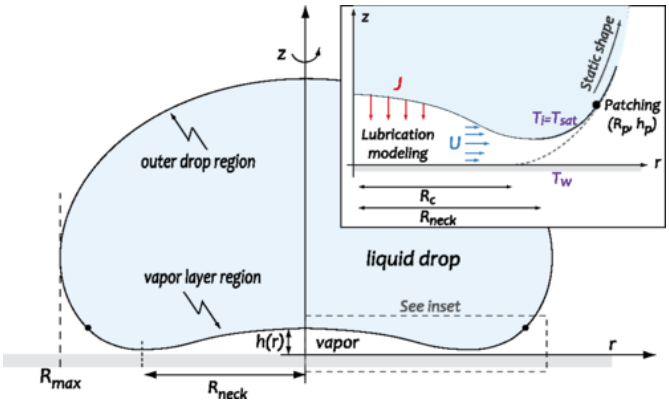

Figure I.7: Schematic view of a Leidenfrost drop. The drop is divided in two different regions, and the vapor film has a non-uniform thickness $h(r)$. Taken from Ref. [19].

flow needs to be accounted for : this is the vapor layer region.

In the vapor layer region, we can express the excess of pressure in the vapor film as the sum of the hydro-static pressure and the capillary pressure $P_v = -(\rho_d g h + \gamma\kappa)$, up to a constant. This excess of pressure drives a Stokes flow with a volumetric flux

$$\vec{q}_v = \frac{h^3}{12}\vec{\nabla}P_v \ . \tag{I.10}$$

As previously said, in the Leidenfrost effect, there is a quasi-equilibrium between the drainage of the vapor and the production of vapor. That is the cause of the levitation. The production of vapor is assumed to be only driven by a conductive heat transfer into the vapor film, similarly as in Biance's model, thus given by

$$\mathcal{J} = \frac{\lambda_v}{\mathcal{L}}\frac{\Delta T}{h} \ . \tag{I.11}$$

Using the incompressibility of vapor, the conservation of the vapor mass and the lubrication approximation, we get $\vec{\nabla}\cdot\vec{q}_v - \mathcal{J}/\rho_v = 0$. Combining this equation with Eq. (I.10) and Eq. (I.11), and using the capillary length to make every length dimensionless, one obtains

$$\frac{1}{12}\frac{1}{\tilde{r}}\frac{\partial}{\partial\tilde{r}}\left(\tilde{r}\tilde{h}^3\left(\tilde{h}+\tilde{\kappa}\right)\right) - \frac{\tilde{\mathcal{E}}}{\tilde{h}} = 0 \tag{I.12}$$

with $\tilde{\mathcal{E}}$ being called the evaporation number. The evaporation number encompasses all the physical parameters of our problem, and is given by

$$\tilde{\mathcal{E}} = \frac{\lambda_v \ \eta_v}{\rho_v \ \mathcal{L}} \left(\frac{\rho_d \ g}{\gamma^3} \right)^{1/2} \Delta T \ . \tag{I.13}$$

This model gives a much better description of the situation than Biance's model. The biggest advantage is maybe the accurate description of the shape of the vapor layer. However, one cannot extract analytical results that can be exploited easily. Moreover, the results of the numerical resolution of this model concerning the evaporation of the drops are really close from those of Biance's model.

I.3 Outline

We saw in this introduction that three large categories of problems are under investigation in the world of the Leidenfrost effect. In this thesis, we will mostly be located in the first field : we improve the understanding of the shapes, the evaporation of Leidenfrost drops, and their impact on the Leidenfrost Point. However, walls between categories are made to be put down. In dynamic situations where the movement of the drops is significant, as well as in a typical situation of the micromanipulation by drops, the questions on their shape, evaporation and the associated Leidenfrost Point subsist.

In the second chapter, we investigate a model situation where we can introduce in a practical case the base elements of the Leidenfrost effect, one by one : Leidenfrost drops in hypergravity. The hypergravity is set by studying our drops in the Large Diameter Centrifuge, a device of the European Space Agency. Through this experiment, we show that the hypergravity is a way to decrease the significance of any capillary driven regime in the shapes and evaporation. However, the main goal is much more ambitious : we show that the Leidenfrost Point depends on the gravity level. Through that, we also show that the Leidenfrost Point is linked to a threshold thickness of the vapor layer.

In the third chapter, based on this observation that the thickness of the vapor film is the key of the Leidenfrost Point, and on the prediction of Sobac's model that the Leidenfrost effect should exist as soon as the superheat is positive on perfectly smooth substrate, we investigate a promising system to lower the Leidenfrost Point : a drop on a hot liquid substrate. And indeed, we see that drops can experience the Leidenfrost effect for very small superheats. We

also take the opportunity to investigate the shapes of the drops and the deformation of the pool. To describe these shapes, we developped a model adapted from Sobac's model that is indeed developed in collaboration with Sobac and our collaborators in Bruxelles. We finally see that not only the substrate has an effect of the drop, but the drop also has an effect on the substrate that goes much beyond its deformation : flows inside the pool are analysed using a particle tracking technique.

In the fourth chapter, we finally make the drop move. We look at a variation of a situation that happens everytime a drop is deposited on a hot substrate. The drop impact in a Leidenfrost situation is rather well known, but repeated impacts offer some strange dynamics and interesting features. We study the bouncing of drops on a vibrated hot substrate. This pushes us on a road to non-linear physics and we observe classical features of this kind of physics : bifurcations. Indeed, when the amplitude of the movement of the substrate is increased, the bouncing of the drop goes through various bouncing modes. Still, we show that some of the features of a single bounce are conserved in the case of repeated bounces.

In the fifth chapter, we explore the dynamic version of the situation of the third chapter. Indeed, the same questions that appear when a drop is deposited on a solid substrate appear also on liquid substrate... And much more ! We investigate the influence of the speed of the impact, the temperature, and other key parameters on the impacts. The goal is to see if a drop impacting a hot liquid substrate always lead to the situation of a Leidenfrost drops, *i.e.* if the Leidenfrost Point varies with these parameters. However, many different behaviors are observed and some links between many classical studies about impacts and about Leidenfrost drops are made.

Finally, in the sixth chapter, we come to the last category of interests that we described in the introduction, and walk on the line between fluids and grains. We look at the organisation of microparticles in Leidenfrost drops. We show that, based on the properties of the liquid and particles used, the way the drop manipulates the particles may be very different. Especially, in some particular situations, the particles can be highly organised at the surface of the drops. These particles also have an impact on the shape, the evaporation and can also supress the Leidenfrost effect... The basic considerations on the Leidenfrost effect are never far away.

References

[1] R. N. Wenzel. *Resistance of solid surfaces to wetting by water.* Ind. Eng. Chem., 28:988–994, 1936.

[2] A. B. D. Cassie and S. Baxter. *Wettability of porous surfaces.* Trans. Faraday Soc., 40:546–551, 1944.

[3] P. Raux. *Interfaces mobiles : friction en mouillage nul et dynamiques de fronts.* PhD thesis, École Polytechnique de Palaiseau, 2013.

[4] K. Koch and W. Barthlott. *Superhydrophobic and superhydrophilic plant surfaces: an inspiration for biomimetic materials.* Philos. T. Roy. Soc. A, 367:1487–1509, 2009.

[5] T. Mouterde and P. Bourrianne. *Seminar at the GRASP lab*, 2016.

[6] P. Aussillous and D. Quéré. *Liquid marbles.* Nature, 411:924–927, 2001.

[7] P. Aussillous and D. Quéré. *Properties of liquid marbles.* Proc. R. Soc. London A, 462:973–999, 2006.

[8] E. C. Okress, D. M. Wroughton, G. Comenetz, P. H. Brace, and J. C. R. Kelly. *Electromagnetic levitation of solid and molten metals.* J. Appl. Phys., 23:545–552, 1952.

[9] A. R. Hanson, E. G. Domich, and H. S. Adams. *Acoustical liquid drop holder.* Rev. Sci. Instrum., 35:1031–1034, 1964.

[10] Y. Couder, E. Fort, C.-H. Gautier, and A. Boudaoud. *From bouncing to floating: noncoalescence of drops on a fluid bath.* Phys. Rev. Lett., 94:177801, 2005.

[11] Boerhaave H. *Elementae chemiae.* Lugduni Batavorum, Leiden, 1732.

[12] J. G. Leidenfrost. *De aquae communis nonnullis qualitatibus tractatus.* Ovenius, Duisburg, 1756.

[13] P. H. Boutigny. *Nouvelle branche de physique: ou, Études sur les corps à l'état sphéroïdal.* Librairie Scientifique-Industrielle de L. Mathias, 1847.

[14] A.-L. Biance, C. Clanet, and D. Quéré. *Leidenfrost drops.* Phys. Fluids, 15:1632–1637, 2003.

[15] J. D. Bernardin and I. Mudawar. *The Leidenfrost point: experimental study and assessment of existing models.* J. Heat Transf., 121:894–903, 1999.

[16] T. G. Myers and J. P. F. Charpin. *A mathematical model of the Leidenfrost effect on an axisymmetric droplet.* Phys. Fluids, 21:063101, 2009.

[17] J. H. Snoeijer, P. Brunet, and J. Eggers. *Maximum size of drops levitated by an air cushion.* Phys. Rev. E, 79:036307, 2009.

[18] Y. Pomeau, M. Le Berre, F. Celestini, and T. Frisch. *The Leidenfrost effect: From quasi-spherical droplets to puddles.* C. R. Mecanique, 340:867–881, 2012.

[19] B. Sobac, A. Rednikov, S. Dorbolo, and P. Colinet. *Leidenfrost effect: Accurate drop shape modeling and refined scaling laws.* Phys. Rev. E, 90:053011, 2014.

[20] J. C. Burton, A. L. Sharpe, R. C. A. van der Veen, A. Franco, and S. R. Nagel. *Geometry of the vapor layer under a Leidenfrost drop.* Phys. Rev. Lett., 109:074301, 2012.

[21] H. Kim, B. Truong, J. Buongiorno, and L.-W. Hu. *On the effect of surface roughness height, wettability, and nanoporosity on Leidenfrost phenomena.* Appl. Phys. Lett., 98:083121, 2011.

[22] C. Kruse, T. Anderson, C. Wilson, C. Zuhlke, D. Alexander, G. Gogos, and S. Ndao. *Extraordinary shifts of the Leidenfrost temperature from multiscale micro/nanostructured surfaces.* Langmuir, 29:9798–9806, 2013.

[23] M. A. J. van Limbeek, M. Shirota, P. Sleutel, C. Sun, A. Prosperetti, and D. Lohse. *Vapour cooling of poorly conducting hot substrates increases the dynamic Leidenfrost temperature.* Int. J. Heat Mass Tran., 97:101–109, 2016.

[24] P. Bourrianne. *Non-mouillant et température.* PhD thesis, École Polytechnique de Palaiseau, 2016.

[25] H. Linke, B. J. Alemán, L. D. Melling, M. J. Taormina, M. J. Francis, C. C. Dow-Hygelund, V. Narayanan, R. P. Taylor, and A. Stout. *Self-propelled Leidenfrost droplets.* Phys. Rev. lett., 96:154502, 2006.

[26] G. Dupeux, M. Le Merrer, G. Lagubeau, C. Clanet, S. Hardt, and D. Quéré. *Viscous mechanism for Leidenfrost propulsion on a ratchet.* Europhys. Lett., 96:58001, 2011.

[27] A. G. Marin, D. A. del Cerro, G. R. B. E. Römer, B. Pathiraj, and D. Lohse. *Capillary droplets on Leidenfrost micro-ratchets.* Phys. Fluids, 24:122001, 2012.

[28] D. Soto, G. Lagubeau, C. Clanet, and D. Quéré. *Surfing on a herringbone.* Phys. Rev. Fluids, 1:013902, 2016.

[29] A. Hashmi, Y. Xu, B. Coder, P. A. Osborne, J. Spafford, G. E. Michael, G. Yu, and J. Xu. *Leidenfrost levitation: beyond droplets.* Sci. Rep., 2:797, 2012.

[30] R. M. Bain, C. J. Pulliam, F. Thery, and R. G. Cooks. *Accelerated Chemical Reactions and Organic Synthesis in Leidenfrost Droplets.* Angew. Chem. Int. Ed., 55:10478–10482, 2016.

[31] M. Elbahri, D. Paretkar, K. Hirmas, S. Jebril, and R. Adelung. *Anti-lotus effect for nanostructuring at the Leidenfrost temperature.* Adv. Mater., 19:1262, 2007.

[32] R. Abdelaziz, D. Disci-Zayed, M. K. Hedayati, J.-H. Pöhls, A. U. Zillohu, B. Erkartal, V. S. K. Chakravadhanula, V. Duppel, L. Kienle, and M. Elbahri. *Green chemistry and nanofabrication in a levitated Leidenfrost drop.* Nat. Commun., 4, 2013.

[33] N. Tsapis, E. R. Dufresne, S. S. Sinha, C. S. Riera, J. W. Hutchinson, L. Mahadevan, and D. A. Weitz. *Onset of buckling in drying droplets of colloidal suspensions.* Phys. Rev. Lett., 94:018302, 2005.

[34] F. Moreau, P. Colinet, and S. Dorbolo. *Leidenfrost explosions.* Phys. Fluids, 25:091111–091111, 2013.

II

Leidenfrost drops in hypergravity

Squeezing drops to death

II.1 Introduction

In the general introduction, we saw that the understanding of the Leidenfrost phenomenon has to begin with the study of its shape and evaporation. Here, we make typical measurements used in the field, apply them on a real model experiment, and confront the results to the theories we have exposed in the introduction.

To explore the limit between theories, one convenient way is to vary an experimental condition that is thought to be immutable and see if the theory still holds. And what a better immutable experimental factor than the acceleration of the gravity, g ? Ways to change the immutable exist, and in the present case, we choose to increase g [1]. We saw earlier that the acceleration of the gravity is highly important in the Leidenfrost effect because of its influence on the capillary length that sets the maximal height of a drop, and its influence on the evaporation as expressed by the evaporation number (see Eq. (I.13)).

How do we characterize the size of the drops, their evaporation ? What is the Leidenfrost Point in this situation, and what does it tells about the essence

of the Leidenfrost drops ?

II.2 Experimental details

The setup can be divided into three parts : the hypergravity device, the typical Leidenfrost system and the acquisition and control system.

Spin it ! Contrary to microgravity, hypergravity is not human-compliant, and it requires large devices to reach gravities higher than g. We used the Large Diameter Centrifuge (LDC), located at the ESTEC center of the European Spatial Agency. A schematic illustration is presented in Fig. II.1. The device is composed of a central trunk with a control box (used to transfer all recordings to a control room) and four arms of approximately 4 m. At the end of each arm, a gondola is suspended. These gondolas are free to move around the axis perpendicular to the plane defined by the arm and the direction of the acceleration of the gravity.

The whole device spins with a pulsation $\vec{\omega}$. The apparent acceleration of the gravity inside the gondolas is then given by $\vec{g^\star} = \vec{g} + \omega^2 R_g \vec{e_r}$ where R_g is the distance between the point of interest inside the gondola and the center of the centrifuge, and $\vec{e_r}$ is the unit radial vector. Note that $g^\star$ is measured by an accelerometer located in the gondola. We define here the reduced gravity as $\Gamma = g^\star/g$. The LDC can go from $\Gamma = 1$ to $\Gamma = 20$.

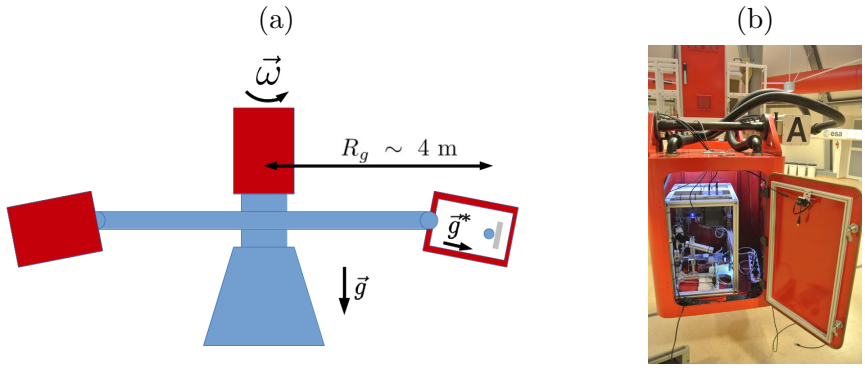

Figure II.1: (a) Schematic representation of the Large Diameter Centrifuge used to achieve apparent gravities $g^\star$ higher than g. (b) Photography of the whole setup loaded inside one of the gondolas of the LDC.

Heat the drop ! In order to produce a Leidenfrost drop, we need a heated substrate. In this situation, we chose an aluminium substrate with two cartridge heaters inside. A thermocouple measured the temperature at the surface of the substrate and a PID controller regulated the current injected in the heaters to reach the desired temperature with an uncertainty of $\sim 1°C$. The PID controller is a program that analyse the signal coming from the thermocouple, as well as its derivative and its integral, and act on the cartridge heaters in order to reach smoothly the desired temperature T_s.

To make drops, a syringe pump was used. The end of the pipe was located ~ 50 mm above the substrate. The volume injected for the main experiment was 153 μL with around 5% of relative uncertainty. For each set of Γ and T_s, three drops were made.

Due to the high mobility of the Leidenfrost drops, a horizontal confinement is needed to keep in an area where they can be observed. Initially, in this project, an infrared camera was tracking the position of the drop, and its position was sent to a retroaction loop that was guiding servo-motors to adjust the inclination of the substrate to keep the drop in the center of the substrate. However, even though the system worked well in earth gravity, problems occured in hypergravity. Thus, we kept the substrate horizontal and used the good old confinement used in the field of the Leidenfrost effect : a metallic ring on the substrate. This ring, being heated by the substrate, was almost at the same temperature (tipically, less than 5°C below). So, drops that would come into contact with the ring did not due to the Leidenfrost effect. The ring had an internal diameter of 75 mm, much larger than the radius of drops to avoid too much heating by the side of the drops, a height of 30 mm, larger than the height of drops, and a thickness of 10 mm to prevent a local cooling of the ring.

Acquire and control The acquisition system consisted in a USB camera recording at 25 frame per second that was located above the substrate. A thermocouple was connected to a DAQ. All the data were collected by a computer in the central gondola that was remotely controlled from another room.

II.3 Lifetimes : a basic concern

As the Leidenfrost is intrinsically a matter of evaporation, one of the most useful measurement in the field of the Leidenfrost effect is the measurement of this evaporation. This usually takes two different forms : on the one hand, the study of the lifetime of the drops, *i.e.* the time between the deposition of

the drops and their total evaporation, and on the other hand, the study of the decrease of the volume or of the radius of the drops over the time.

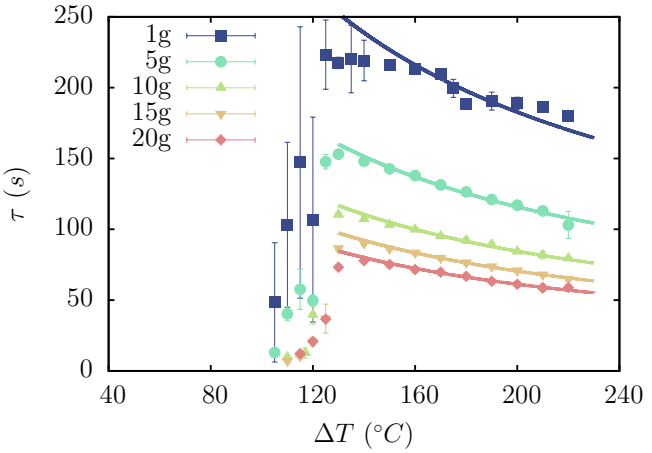

Figure II.2: Mean lifetimes of three drops of initial volume $V_0 = 153\ \mu L$ as a function of the superheat ΔT for five different reduced gravities Γ between 1 and 20. The lines are fits of the data above $\Delta T = 140°C$ using Eq. (I.8).

In Fig. II.2, we plot the mean lifetimes of three different drops as a function of the superheat ΔT for five different reduced gravities $\Gamma = 1$, 5, 10, 15, and 20. Let us first describe the data for $\Gamma = 1$. The lifetime of a drop on a substrate decreases when the temperature of the substrate T_s is increased until a certain point (not shown here). At this point, the lifetime begins to increase quite sharply (here above 100°C). Just below this sudden increase, the lifetime is of the order of 1 s. Above $\sim$ 125°C, the lifetime decreases again. In this last part, the drops are in the Leidenfrost state during their whole evaporation, and their lifetime is of the order of 100 s.

When the gravity is increased, two effects can clearly be noticed here. First, at equal superheats, the lifetime always decreases. For the drops that are in the Leidenfrost state, Eq. (I.8) can be rewritten by replacing g by Γg as

$$\tau_g = 4 \left(\frac{6\eta_v \gamma}{\pi \rho_v g^2} \right)^{1/4} \left(\frac{\rho_l \mathcal{L}}{\lambda_v \Delta T} \right)^{3/4} \Gamma^{-1/2}\ {V_0}^{1/4}\ . \qquad \text{(II.1)}$$

We see that the characteristic lifetime of drops scales as $\tau_g \propto \Delta T^{-3/4}$. Fits using this scaling law are indicated in Fig. II.2 by the continuous lines. Only the data where the drops are clearly in the Leidenfrost state are used

to make the fits. Note that for the data corresponding to $\Gamma = 1$, the fit is less accurate. This is due to the fact that we approximate the lifetime of the drops with the characteristic lifetime of large drops. Indeed, as said at the beginning of Sec. I.2.1, when the drops become smaller than the capillary length, a new regime of evaporation takes place. However, the agreement without taking into account this regime is really good for the data for higher reduced gravities. This is due to the fact that the capillary length is much smaller when the reduced gravity is increased. When $\Gamma = 1$, ℓ_c equals 2.4 mm and when $\Gamma = 5$, ℓ_c only equals 1.1 mm. Starting from the same volume, when $\Gamma = 5$, the drops spend a much larger proportion of their lifetime evaporating in the large drop regime than in the small drop regime, and the approximation $\tau = \tau_g$ becomes more and more valid for high reduced gravities.

The complementary way to look at the evaporation of the drops is to look at the decrease of their radius. Indeed, the lifetime is an integrated measurement of the evaporation, and thus, there is a loss of information. In Fig. II.3, we report the evolution of the radius R of five drops at the same reduced gravities as in Fig. II.2. The measurements were performed at $\Delta T = 200°\text{C}$. Two elements can clearly be noticed on this graph. First, the higher the gravity, the faster is the decrease of the radii. Second, the higher the gravity, the larger is the initial radius. This latter fact is simply the sign that we work

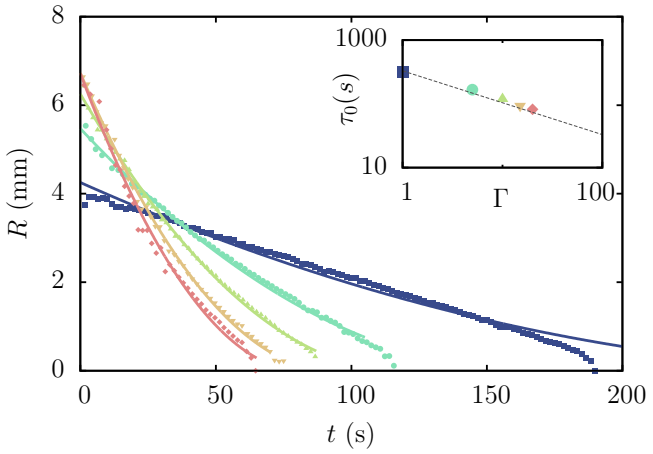

Figure II.3: Radius of drops R as a function of time t for the same five reduce gravities at $\Delta T = 200°C$. The continuous lines are fits using Eq. (II.1). The inset represents the variation of the characteristic lifetimes obtained from the fits as a function of the reduced gravity. The dashed line indicate a power law with an exponent $-1/2$.

at a constant initial volume, and that for large drops, we still have the relation $R = \sqrt{V/2\pi\ell_c}$. Using this relation, we can transform Eq. (I.7) into

$$R(t) = R_0 \left(1 - \frac{t}{\tau_g}\right)^2 \tag{II.2}$$

where R_0 is the initial radius of the drop. This relation is used to fit the data of Fig. II.3. From the five fits, we extract the characteristic lifetime τ_g. The inset presents the variation of τ_g with the reduced gravity Γ, showing that the scaling $\tau_g \propto \Gamma^{-1/2}$ predicted by Eq. (II.1) is in very good agreement with our observations.

II.4 The Leidenfrost Point : the unsolved question

This experiment also shows another key characteristic of the Leidenfrost effect. As we saw, the curve of the lifetime as a function of the superheat is quite singular. In Sec. II.3, we focused on the drops that were in the Leidenfrost regime, but the transition from the boiling regime to the Leidenfrost regime is also interesting. The understanding of the temperature at which this transition occurs has been a subject of debate for many years, as pointed by the work of Bernardin *et al.* [2], and the prediction of this threshold temperature is still nowadays an unsolved question.

Actually, even the definition of the Leidenfrost Point (LFP), *i.e.* the threshold temperature above which the effect takes place, is even not that well settled. We can distinguish two main definitions. First, the dynamic one : the Leidenfrost Point is the temperature above which no nucleate boiling is observed when a drop is deposited on a substrate [3]. Second, the static one : the Leidenfrost Point is the temperature corresponding to the local maximum in the curve of the lifetime as a function of the temperature [4]. These two definitions should coincide. Indeed, when there is no nucleate boiling, the heat transfer is only accomplished by conduction in a vapor film, and is then lower than when there is nucleate boiling, leading to longer lifetimes. Practically, both definitions correspond to two different ways to measure the LFP. In this experiment, we focus on the second one.

Thus, Fig. II.2 allows to determine the Leidenfrost Point for each reduced gravity. In Fig. II.4, we report this evolution of T_L as a function of Γ. The data indicate a slight increase as the reduced gravity increases. However, drawing a quantitative conclusion on this matter is difficult. Indeed, the step of 5°C between each of our experiments induces large uncertainties on the measure-

ment of the LFP.

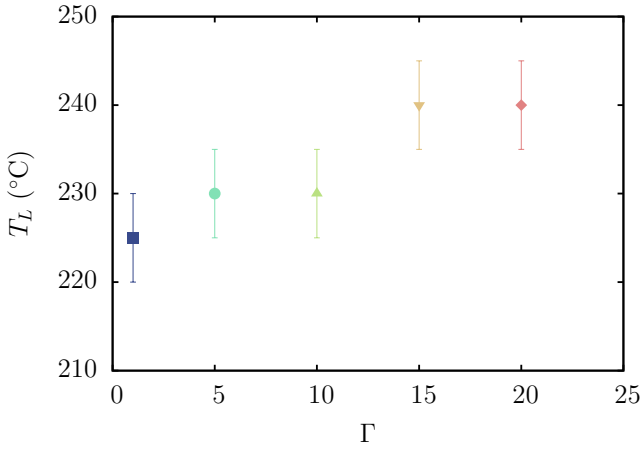

Figure II.4: The Leidenfrost Point T_L as a function of the reduced gravity Γ.

However, a qualitative reasonning is possible and shows very well the limitations of Biance's model and the need for a more accurate model. Indeed, for quite a few years now, the idea that the temperature is less the key parameter than the thickness of the vapor layer has arisen [6]. If the vapor layer is too thin, contacts may be induced with the substrate and suppress the Leidenfrost effect. From Eq. (I.5), if we assume that the thickness when the drop is deposited is the significant parameter (because the perturbations due to an initial contact would induce more perturbations and more contacts), we can deduce

$$h = \left(\frac{3\ \lambda_v\ \Delta T\ \eta_v\ V_0}{8\ \pi\ \mathcal{L}\ \rho_v\ \gamma} \right)^{1/4} \tag{II.3}$$

where no dependence of the reduced gravity is involved. Thus, as the thickness of the vapor film does not depend on the gravity level for a given volume, this model does not seem to bring any insight on the increase of the threshold temperature that we observe in Fig. II.4. As the model from Sobac *et al.* [5] brings a complete description of the shape of the vapor film, this model seems to be more appropriate.

In Fig. II.5, we show the shapes of Leidenfrost drops given by Sobac's model for a drop of 10 μL at $\Delta T = 200$°C. We clearly observe the effect of the gravity, squeezing the drop. To see the effect of the gravity on the

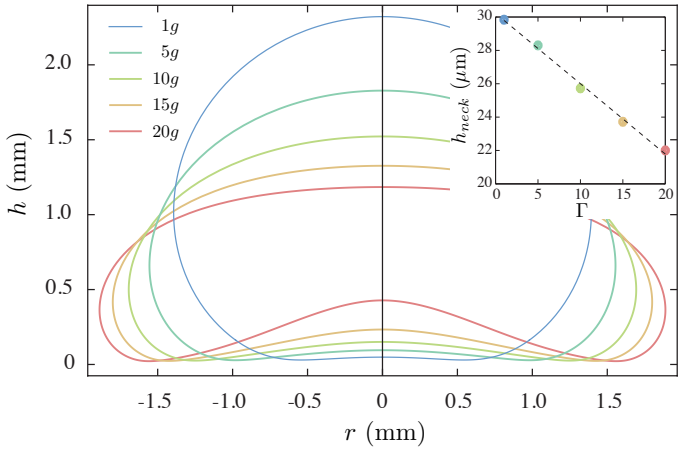

Figure II.5: Shapes of Leidenfrost drops of the same volume (10 μL) submitted to the five different reduced gravities used in the experiments. The shapes are calculated with the model of Sobac et al. [5]. The inset presents the variation of the thickness of the vapor film at the neck with respect to the reduced gravity.

thickness of the vapor layer, we plot in the inset the minimal thickness of this layer h_{neck} for each of the reduced gravity Γ. There is a decrease of h_{neck} that is non-negligible at all, from 30 µm at $\Gamma = 1$ to 22 µm at $\Gamma = 20$. The dashed line is just a guide for the eye. From a qualitative point of view, this supports the idea that an increase of the gravity should be compensated by a higher temperature to stay above a thickness of the vapor layer where contacts between the drop and the substrate are promoted.

II.5 Supersize the drops !

The two models used here consider drops that are axisymetric and none of them give good results when the pocket of vapor that we see in Fig. II.5 becomes too large. Indeed, multiple papers showed that when a Leidenfrost drop becomes too large, the size of the vapor pocket, and especially the thickness of the vapor pocket at the center of the drop, increases dramatically up to the time when the bottom interface reaches the top interface [4, 7]. This phenomenon forms the so-called chimneys.

These chimneys can be interpreted as the result of a Rayleigh-Taylor-like instability [8]. Doing a perturbation analysis on the films, Biance *et al.* showed that the instability occurs when the radius of the drop is larger than

$R_c = 3.84\ell_c$ [4]. Snoeijer *et al.* [7] studied the very similar case of a drop levitated over an air cushion blown from below and found a critical radius $R_c = 3.95\ell_c$ above which the same instability occurs.

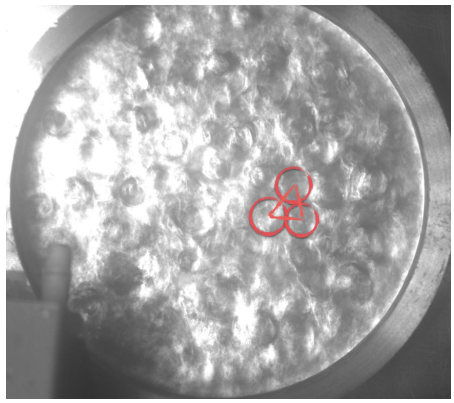

Figure II.6: Typical image obtained from very large bubbles ($R = 32.5$ mm) at $\Gamma = 5$, showing many chimneys. The circles highlight three adjacent chimneys, and the segments show the distance between them.

We took the opportunity of these experiments to drop large quantities of water inside our rings to look at the distance between the numerous chimneys that can form in a drop of $R = 32.5$ mm. With the same kind of images taken from above as in the previous sections, we were able to extract the distance between two adjacent chimneys from center to center D_{ch}. An example is given in Fig. II.6. For each Γ, we measured D_{ch} for approximately a hundred couples of chimneys. The cumulative distribution function is plotted in Fig. II.7(a). Note that we have no data for the largest reduced gravity ($\Gamma = 20$) because the images were recorded with a camera at 25 frames per second and the apparition and disparition of the chimneys was too fast at this reduced gravity to be observed clearly with our setup. In our case, the CDF corresponds to a gaussian distribution of D_{ch} from which we extract the mean and the standard deviation.

In Fig. II.7(b), we plot the mean distance between adjacent chimneys D_{ch} as a function of the reduced gravity. This distance is found to decrease with the reduced gravity with a power law $D_{ch} = 7.89\ell_c \propto \Gamma^{-1/2}$. Although this distance is not the critical size for the apparition of the chimneys R_c, we find it to be slightly above twice the values of R_c found in experiments and theory [4, 5, 7].

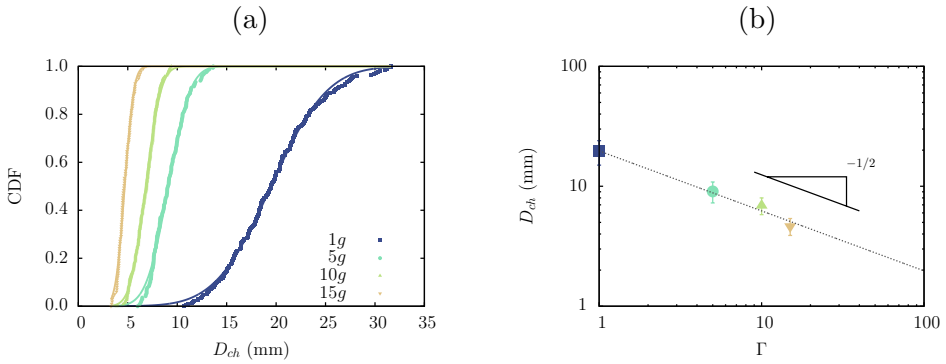

Figure II.7: (a) Cumulative Distribution Function of the distance between two adjacent chimneys D_{ch} in large drops for four reduced gravities. (b) The mean distance D_{ch} as a function of the reduced gravity Γ. The dashed line is a fit by a power law $D_{ch} \propto \Gamma^{-1/2}$.

II.6 Conclusions

In this chapter, we introduced tools that will be useful for the rest of this thesis, *i.e.* the measure of the evolution of the radius with time, the lifetime as a function of the superheat, and a clear definition of the Leidenfrost Point. But we did more...

The hypergravity, at the opposite of the microgravity, appears to be a convenient way to emphasize the role of the large drops regime ($R > \ell_c$). This way, the lifetime of drops as a function of the superheat appears to be well fitted by a power law $\tau \propto \Delta T^{-3/4}$.

Moreover, we were able to show that the gravity has a small but significant impact on the Leidenfrost Point. This is consistent with the idea that the Leidenfrost Point originates from a threshold thickness of the vapor layer below which contacts are promoted and nucleate boiling appears. This feature cannot be explained by a simple model that considers a uniform thickness of the vapor layer (Biance's model), and we need to take into account a model in which the vapor layer comprises a vapor pocket and an annular neck (Sobac's model).

References

[1] L. Maquet, M. Brandenbourger, B. Sobac, A.-L. Biance, P. Colinet, and S. Dorbolo. *Leidenfrost drops: Effect of gravity.* Europhys. Lett., 110:24001, 2015.

[2] J. D. Bernardin and I. Mudawar. *The Leidenfrost point: experimental study and assessment of existing models.* J. Heat Trans., 121:894–903, 1999.

[3] T. Tran, H. J. J. Staat, A. Prosperetti, C. Sun, and D. Lohse. *Drop impact on superheated surfaces.* Phys. Rev. Lett., 108:036101, 2012.

[4] A.-L. Biance, C. Clanet, and D. Quéré. *Leidenfrost drops.* Phys. Fluids, 15:1632–1637, 2003.

[5] B. Sobac, A. Rednikov, S. Dorbolo, and P. Colinet. *Leidenfrost effect: Accurate drop shape modeling and refined scaling laws.* Phys. Rev. E, 90:053011, 2014.

[6] P. Bourrianne. *Non-mouillant et température.* PhD thesis, École Polytechnique de Palaiseau, 2016.

[7] J. H. Snoeijer, P. Brunet, and J. Eggers. *Maximum size of drops levitated by an air cushion.* Phys. Rev. E, 79:036307, 2009.

[8] A.-L. Biance. *Gouttes inertielles : de la caléfaction à l'étalement.* PhD thesis, Paris VI, 2004.

III

Liquid pool

The ideal substrate

III.1 Preamble

In the previous chapter, we demonstrated that the prediction of the Leidenfrost Point is a major issue, and not everything has been understood. However, not everything remains unclear. Kim *et al.* demonstrated that the roughness of the substrate is a key parameter for the establishment of the LFP [1]. Moreover, Kwon *et al.* shown that the mechanism behind the increase of the LFP on microstructured surfaces is relying on a promotion of the wetting via capillary wicking on the structures. This phenomenon is even more accentuated when the roughness is multi-scale [2]. Kruse and coworkers also manufactured various surface patterns, using a femto-laser processing to induce multi-scale roughness on hydrophilic substrates and observed high shifts of the LFP towards higher temperatures [3]. Still, in all these studies, the substrates considered were hydrophilic. However, as stated in the PhD thesis of Bourriane [4], not every roughness leads to this kind of behavior. As a matter of fact, superhydrophobic substrates shows more than extraordinary shifts of the LFP towards low temperatures. On these substrates, the threshold temperature is eliminated : no transition can be seen in the plots of the lifetime as a function of the temperature. Instead, a monotonic decrease of the lifetime with the temperature is observed [4].

Thus, the studies cited above [1–3] indicate that a reduction of the roughness generally reduces the LFP. In the labs, we can find two types of substrates that are smooth at a molecular scale. The first one is already widely used among experimental physicists who work on the Leidenfrost effect : silicon wafers and other cleaved substrates. However, no reduction of the Leidenfrost have been reported on these substrates compared to usual substrates like aluminium substrates... At least, no reduction as drastic as one could want. The second type of smooth substrate has already been used among people working on the Leidenfrost effect. However, nobody tackled the issue of the Leidenfrost Point on these substrates until now : liquid substrates.

Indeed, we find in the literature that liquid substrates have been identified as a good candidate to support Leidenfrost drops. Le Merrer *et al.* studied the friction of Leidenfrost drops made of liquid nitrogen on liquid pools [5]. They showed that this friction was much higher than the friction on solid substrates due to wave resistance. But one of the main reference is probably the work of Snezhko *et al.* [6]. Again, they worked with liquid nitrogen, but they focused on the pulsating behavior of large drops, leading to star-shaped drops. They also investigated the gliding behavior of smaller drops, showing that smaller drops glide faster than large drops. More recentely, a study investigated the analogous case of liquid drops at room temperature on a pool of liquid nitrogen [7]. They focused on the conditions in size and density of these drops to float and on the duration over which the so-called inverse Leidenfrost was sustained, *i.e.* the duration over which the drop was sufficiently hot to be in levitation above the pool due to a film of nitrogen vapor. In that paper, they were limited by the phase transition happening in the drop. Indeed, the drop of liquid that floats above the liquid nitrogen pool experiences freezing while cooling down. Thus, the same kind of limitations that happens in the case of a solid substrate happens when the drop freezes, and the Leidenfrost effect only exists until the surface of the drop becomes solid. After that, nucleate boiling ends quickly the cooling of the drop [7].

This list is not exhaustive, but still, no one seems to investigate the secrets of the Leidenfrost Point on liquid substrates. Moreover, nobody seems to have ever try to heat a liquid substrate to allow drops to be in the Leidenfrost state above it. This is precisely the subject of this chapter. At the opposite of all studies made on the subject until now, we use substrates and drops at temperatures that are more or less slightly above room temperature, which allow us to avoid the use of cryogenic liquids as liquid nitrogen or liquid oxygen. That allows us to have a precise control on the temperatures involved in our

experiment.

The first part of this chapter is devoted to the description of the setup used, the limitations associated, and the experimental subtleties. The second part describes in details the aspects related to the Leidenfrost Point, from its description to its measurement. The third part focuses on the evaporation and points out differences with the case of solid substrates. The fourth part explains some of the aspects of the evaporation by describing notably the shape of the drop and of the substrate using a model extended from Sobac's model *et al.* [8]. Finally, in the last part, one of the possible limitations to our understanding of our system is investigated : the flows inside the pool and their implications are described.

(a) (b)

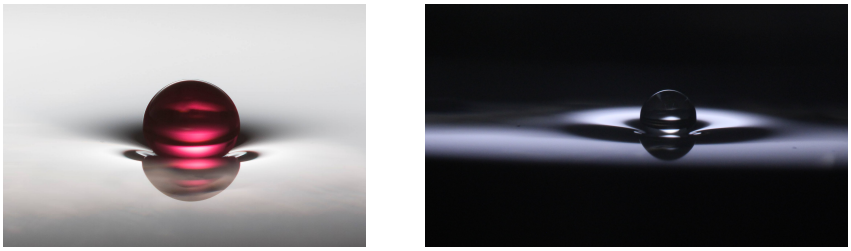

Figure III.1: Ethanol drops on liquid substrates made of silicone oil V20. (a) Erythrosine is used to color the drop. (Image credit : Florence Cavagnon)

III.2 How to sail on an oil sea

Basically, our system was composed of a heated liquid drop and a pool of a heated liquid. However, some subtleties concerning the liquids used and the procedure to make Leidenfrost drops have to be explained.

III.2.1 The liquid of the substrate

To enable the Leidenfrost effect to appear, the major restriction on the liquid used is that its boiling point has to be higher than the boiling point of the liquid of the drop that levitates. In practice, the choice of the liquid that can be used for the pool is not that wide. Most of the liquids commonly found in a laboratory of fluid mechanics boil around 100°C. The main liquid that is stable when heated is the oil. For a better control on the properties of the

pool, we used exclusively silicone oil.

Silicone oil have the distinctive feature that the length of the chains of polymers that compose the oil can be adjustated through its fabrication. The length of these chains has a significant impact on the viscosity of the oil that can vary from $\nu = 0.65$ cSt to $\nu = 10^6$ cSt (at 25°C). Different kinds of oils can be found. In our experiments, we used those that are named V1.5, V5, V10, V20, V50 and V100. The number is approximately the kinematic viscosity of the oil at 25°C.

Silicone oil also presents some other interesting features. Its boiling point depends on the type of oil, but for the V5 and above, the boiling point is above 200°C. However, most of its other properties other than the viscosity are not strongly dependent on the length of the polymer chains. Some of these properties that are useful hereafter are listed in Table III.1. These properties were measured at 80°C.

Silicone oil	T_{sat} (°C)	ρ (kg/m^3)	γ (mN/m)	η (mPa · s)	ℓ_c (mm)
V1.5	194	808	16	0.62	1.40
V5	> 200	828	17	1.68	1.44
V10	> 200	899	19	4.1	1.46
V20	> 200	925	20	8.3	1.49
V50	> 200	913	19	21	1.45
V100	> 200	924	19	36	1.46

Table III.1: Physical properties of the oil used in the experiments: boiling point T_{sat} at 1 atm, density ρ, surface tension γ and dynamic viscosity η. The latter three are considered at 80° C.

III.2.2 The liquid of the drop

As said above, to have a Leidenfrost drop, we have to release a drop made of a liquid with a boiling point lower than the temperature of the substrate. We controled the temperature of our pool of silicone between 25°C and 180°C. Thus, the best liquid that we could imagine considering this was a liquid that boils just above 25°C. Diethyl ether was the best candidate we used ($T_{\text{sat}} = 35$°C). We also used several other liquids including ethanol, HFE–7100, isopropanol and chloroform. The properties of these liquids are listed in Table III.2. The properties are taken at the boiling point of these liquids.

Liquid	T_{sat} (°C)	ρ (kg/m^3)	γ (mN/m)	ℓ_c (mm)	$\mathcal{L}$ (kJ/kg)
Diethyl Ether	34.6	696	16	1.53	377
HFE–7100	58.5	1425	14	0.997	125
Chloroform	61.2	1411	22	1.26	247
Ethanol	78.4	728	17	1.54	846
Isopropanol	82.6	725	16	1.50	779

Table III.2: Physical properties of the liquid used for the drops in the experiments: boiling point T_{sat} at 1 atm, density ρ, surface tension γ and the latent heat of evaporation $\mathcal{L}$. The latter three are at the boiling point of the corresponding liquids.

III.2.3 Experimental procedure

A stainless steel Petri dish was used as a container for the oil. This Petri dish stands over a heating plate. To control the heating of this plate, we used a PID controller. This controller measured the temperature of the oil close to the surface of the pool with a thermocouple (K-type). Indeed, the temperature in a pool of oil tended to be difficult to stabilize and homogenize with our PID controller and our heating system, especially when this oil was very viscous (less recirculation and lower thermal conductivity). The temperature in the pool during a measurement had thus an uncertainty that is around 5°C for the silicone oil V100. However, the temperature that was interesting for us was not the temperature in the bulk, but the temperature of the surface. By placing the thermocouple very close to the surface of the pool, the uncertainty related to the local and temporal variations of the temperature of the substrate was around 1°C. The uncertainty of the PID controller was equal to 1°C. Thus, the uncertainty on the measurement of the temperature was 2°C.

The drops were deposited gently with syringes that were manipulated either by hand or with a syringe pump. The syringe pump allowed to inject liquid at a very low rate, and thus to inflate very slowly a drop after its creation over the substrate. This process improved the stability of large drops during their creation.

As explained in section III.5.1, Leidenfrost drops are highly mobile due to the vapor layer beneath them. Small drops and drops made of liquids that evaporate quickly are especially mobile. This is consistent with the observations of Snezhko *et al.* [6]. To make their observation easy, a way to confine the drops was needed. Therefore, we placed a metalic ring of 20 mm of inner diameter inside the Petri dish. Meniscii on the edges of the ring induced the

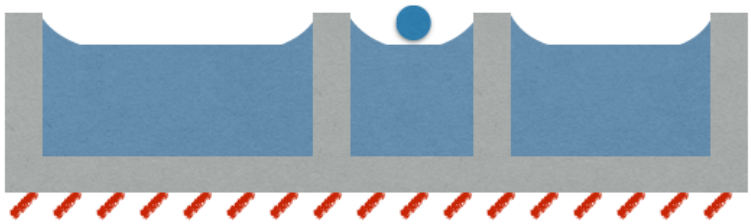

Figure III.2: Schematic side view of the metalic Petri dish, filed with oil and heated from below. Inside the pool, a smaller ring is used to create meniscii that confine a drop.

confinment of the drops. A schematic view is given in Fig. III.2.

III.3 About the Leidenfrost Point

To describe Leidenfrost drops, Sobac's model considers a 2D axisymetric drop evaporating through its lower part through a lubrication film [8]. In this model, the evaporation exists as soon as the superheat ΔT is positive. And as soon as there is evaporation under the drop, there should be a lubrication film applying a force on the drop. Considering that, the smaller is the thickness of the film, the larger is the evaporation, and there should always exist an equilibrium value of the thickness where the pressure in the lubrication film compensate exactly for the weight of the drop... And it should be like this no matter how positive is the superheat. The Leidenfrost Point should be equal to the boiling temperature of the liquid of the drop.

Unfortunately, on solid substrates, this is not the case. Three things can play a role to set the critical temperature. First, if the drop comes very close to the substrate (typically 100 nm), new forces that are not considered in the model come into play : the van der Waals forces. These forces are attractive forces between the interface of the drop and the substrate. They can then induce contacts that suppress the Leidenfrost effect.

Second, the thermal conductivity of the material of the substrate is finite. As the energy is pumped by the drop, the substrate underneath cools down. This effect cannot suppress the Leidenfrost effect just by itself. Indeed, the heat transfer becomes less effective as the substrate cools down, and so the

cooling becomes less effective too, until becoming as effective as the diffusion of heat from the heating system to the surface of the substrate. However, this process tends to promote the role of the van der Waals forces.

Finally, third, the model considers a perfectly flat substrate. Nevertheless, a solid substrate is never perfectly flat. Usual roughnesses for a silicon wafer or a polished aluminium plate are about 10 nm and 1 µm (resp.). The structures related can induce contact points in the vapor layer where bursts of evaporation occur. This effect has been extensively studied by Kim and coworkers [1]. They showed that the addition of micropillars on a surface pushes the Leidenfrost Point towards higher temperatures. Note that the pollution of the substrate by dust can also induce an increased roughness.

Then, if one wants to lower the LFP to the lowest temperature possible, getting rid of these effects is mandatory. Unfortunately, acting on the van der Waals forces is not very convenient, and the thermal conductivity of usual substrates, coupled to the high mobility of the drops, is sufficiently high to reduce the cooling of the substrate down to a few degrees in worst cases. Thus, to lower the LFP, the best way seems to be the lowering of the roughness of the substrate. And what substrate can possibly be smoother than a liquid substrate...

III.3.1 Measurement of the LFP

With drops on a liquid pool, we cannot visualize directly the vapor film due to the curvature of the liquid substrate (see Fig. III.1). Thus, the definition of the Leidenfrost Point that we use here is the same as the one in the second chapter. The LFP is the temperature that corresponds to a local maximum in the lifetime above the boiling point of the drop.

Figure III.3 shows the lifetime of drops on a pool of silicone oil V20 as a function of the superheat. Two different liquids were used for these drops : ethanol (blue squares) and diethyl ether (red dots). The first thing we notice is that, in both cases, there is a dispersion of the values. The maximum lifetime of these drops for each superheat is quite reproducible. This maximum corresponds most of the time to a complete evaporation of the drops. However, at low superheats, below 30°C, the lifetime of the drop generally ends when the drop touches the pool. The reproducibility of the maximum values means that this contact is due to a deterministic process. We expect this process to be linked to different phenomenons such as a local cooling of the liquid pool. Unconfined drops have less time to cool down the substrate localy because of

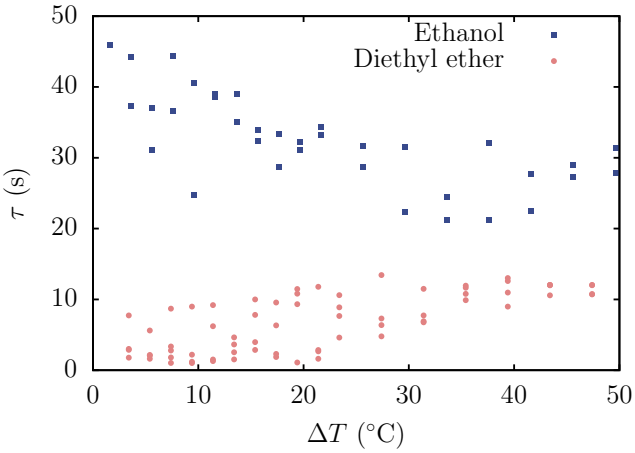

Figure III.3: Lifetime of drops τ as a function of the superheat ΔT. The substrate is made of silicone oil V20. Drops are made from ethanol (blue squares) and diethyl ether (red dots).

their movement and showed slightly larger lifetimes. However, especially at low superheats, the dispersion is due to external perturbations and not to the Leidenfrost effect itself. Still, even for the smallest superheat we investigated, unperturbed drops levitate for times that are of the order of 10 s. That is a feat that is never observed on a solid substrate.

The second thing we observed was that the diethyl ether drops evaporated faster than ethanol drops. The origin of this is multiple, but one of the main reasons is that its latent heat of vaporization is about 377 kJ/kg whereas the one of ethanol is 846 kJ/kg.

We can plot this lifetime as a function of the superheat for different liquids for the drops and the substrates. This gives a measurement of the LFP for these different couples of liquids, *i.e.* the temperature at which the lifetime is the maximum. In Fig. III.4, we show the Leidenfrost Point, T_L, of ethanol and diethyl ether drops as a function of the dynamic viscosity of the oil η_p. The continuous and dashed lines indicate the corresponding boiling temperature and Leidenfrost Point on an aluminium substrate. The dynamic viscosity of the type of oil used decreases when the temperature is increased, so this viscosity is measured at the LFP. The hatched zone at low viscosities is the zone where one can hardly find liquids at such viscosities. For ethanol, we observe that the Leidenfrost state is always achieved as soon as the superheat

is positive, in the range of superheats explored. However, for diethyl ether, the results are more spread. No clear behavior can be extracted. Still, for any investigated viscosity, the LFP is much lower than the LFP on an aluminium substrate.

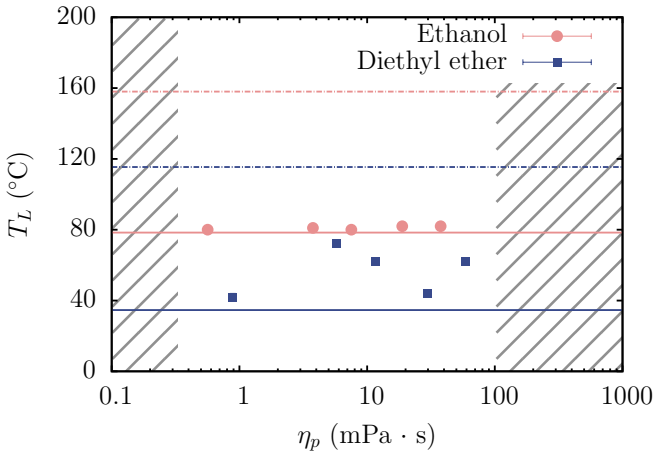

Figure III.4: Leidenfrost Point as a function of the dynamic viscosity of a silicone oil substrate. Drops are made of ethanol (blue squares) and diethyl ether (red dots). The continuous lines represent the boiling temperature and the dashed lines represent the Leidenfrost Point on an aluminium substrate.

Concluding on the origin of the drastic reduction of the Leidenfrost Point over the range of couples of liquids used is not an easy step. This origin may be multiple. The first hypothesis is the reduction of the roughness of the substrate that we already mentionned. However, cleaved substrates should also exhibit very low LFP if the roughness was the only origin. Another possible origin is the existence of Marangoni flows in the pool that can entrain air in the vapor film and helps the levitation [10]. This possibility is ruled out in Sec. III.6. Another phenomenon that can play a role in the reduction of the LFP is the "adaptibility" of the substrate to the variations of the thickness of the neck of the vapor layer that are observed on Leidenfrost drops [11].

Addtionally, keeping a drop in the Leidenfrost state on silicone oil V300 or higher appears to be much harder than on substrates at lower viscosities. Actually, the only way to achieve this is by pre-heating the liquid of the drop close to its boiling point before depositing the drop. And still, a large superheat is needed (about 50°C). This is why the zone of Fig. III.4 above $\eta_p = 100$

mPa.s is hatched. This influence of the viscosity of the substrate may indicate that the problem is linked to flows in the pool. Indeed, being cooler than the substrate, a drop always cools down the substrate below it. Then, buoyancy induces a flow downward just below the drop, making the heavy oil sink. This flow homogenizes the temperature in the pool, which helps to avoid excessive cooling of the surface under the drop. And the higher is the viscosity, the lower is the flow rate, the lower is the homogenization, and the substrate cools down more. That could be one reason that makes difficult the existence of a Leidenfrost drop over such a substrate. Moreover, this difficulty to observe Leidenfrost drops on highly viscous substrate is also in agreement with the origin of the reduction of the LFP being related to the adaptability of the substrate to variations of the thickness of the vapor layer as the viscosity increases the time for the substrate to react on a local fluctuation of the pressure in the vapor film.

III.4 Evaporation

A look at Fig. III.3 shows that the lifetime of ethanol Leidenfrost drops slightly decreases while the superheat increases. However, no information is given about how they evaporate. Indeed, the lifetime is the time between the creation of the drop and its disappearance, either by complete evaporation or by contact with the pool (which induces a partial dilution in the pool and a rapid evaporation). So the lifetime may not be the best indicator on how much the drop evaporates. The first step to understand the evaporation, as made before in the case of solid substrates [12], is to plot the evolution of the radius of Leidenfrost drops over time.

Figure III.5 shows the evolution of the radius with time for ethanol drops for small drops (a) and for large drops (b), *i.e.* drops smaller or larger than the capillary length of the drop. This evolution is shown in both cases for different superheat ΔT. We immediately see that the larger is the superheat, the faster the drops evaporate. This is quite intuitive and similar to what happens in the solid case. However, what is less intuitive is that, in both the case of a small and the case of a large drop, the radius of these drops decreases linearly with time. In the case solid of a solid substrate, many models have captured the essence of the evaporation of Leidenfrost drops [8, 12, 13] : the drop experiences a change of its geometry and of the associated scalings from a small drop to a large drop. This change of geometry induces a change in the evaporation regime. Biance *et al.* have extracted analytical scalings that describe how the drops evaporate with a simple model [12].

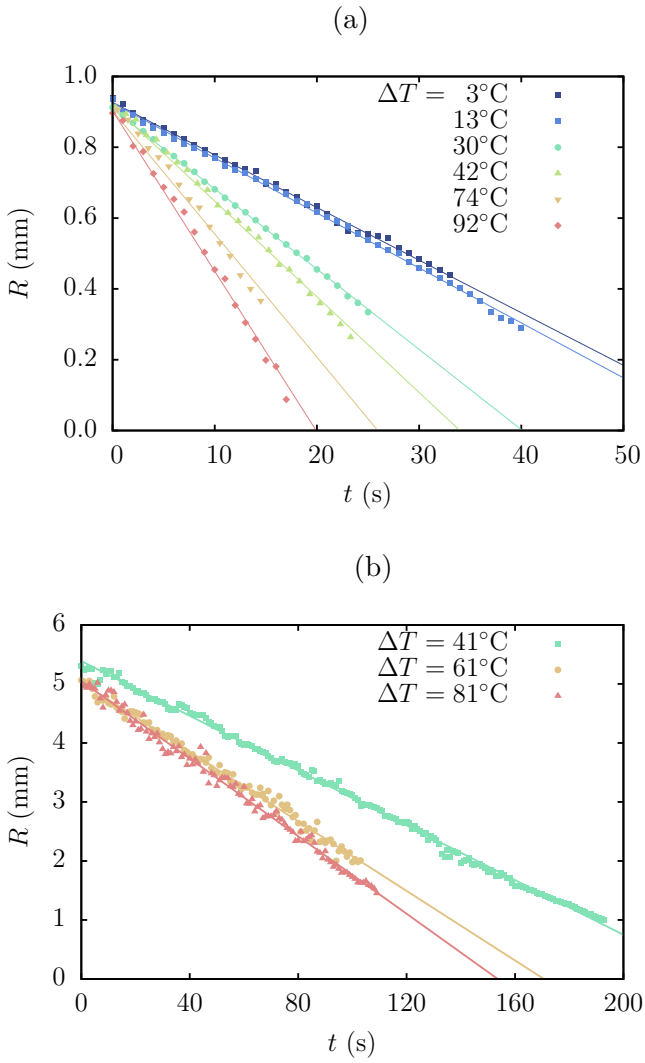

Figure III.5: Radius of an ethanol drop as a function of time on a pool of silicone oil V20 at different superheats. Plots (a) and (b) differ by the initial drop radius.

$$R(t) = R_0 \left(1 - \frac{t}{\tau}\right)^{\alpha} \tag{III.1}$$

In this equation, τ is a characteristic time that is different in the case of a small drop (that remains almost spherical) and the case of a large drop (which flattens and forms a puddle). The exponent α is also different, switching from

1/2 in the first case to 2 in the latter. In Fig. III.5, the continuous lines shows linear fits for each superheat. It clearly appears that in our case, Eq. III.1 is still valid, but α is always equal to 1.

Now that we see that the time evolution of the radius is linear in all investigated cases, we can extract a more interesting value : the reduced time of evaporation. This ratio is the characteristic time for a drop to evaporate completely, τ, divided by its initial radius, R_0. We plot this rate as a function of the superheat for ethanol drops (red dots) and HFE–7100 drops (blue squares) in Fig. III.6. Note that the drops used for this plot had various initial radii between 0.9 mm and 6 mm. For both ethanol and HFE–7100, the reduced time of evaporation follows a law

$$\tau \; R_0^{-1} \propto \Delta T^{-4/5} \tag{III.2}$$

above $\Delta T = 30°\text{C}$, and saturates highly for smaller superheats. This behavior is explained in Sec. III.5.2.

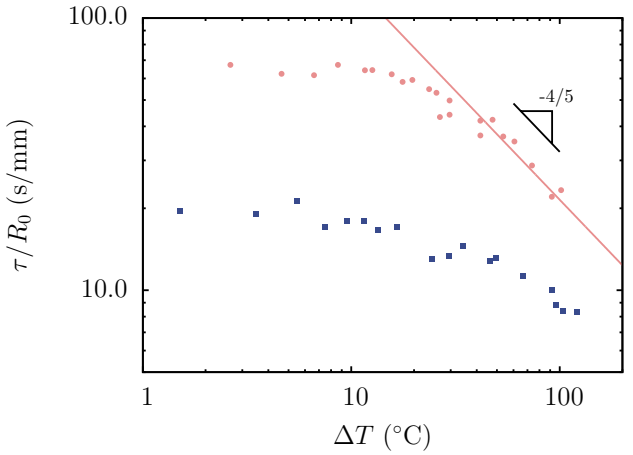

Figure III.6: Reduced time of evaporation for Leidenfrost drops of various initial radii as a function of the superheat ΔT. The drops are made of ethanol (red dots) and HFE–7100 (blue squares) on a pool of silicone oil V20. The continuous lines is a fit of the data over $\Delta T = 30° C$ by the scaling law $\tau/R_0 \propto \Delta T^{-4/5}$.

One can of course ask why such a big difference between the case of a solid substrate and the case of a liquid substrate exists. Obviously, by essence, a solid is a material that is not much deformable at the opposite of a liquid.

And indeed, this is the whole point. The liquid substrate above which you place a Leidenfrost drop deforms under its weight as seen on Fig. III.1.

III.5 Geometry of the problem and its link to the evaporation

To fully understand the origin of the difference between the case of a solid substrate and the case of a liquid substrate, a model was developped with our coworkers at ULB [9]. We do not enter here in the details of this model that is based on Sobac's one [8].

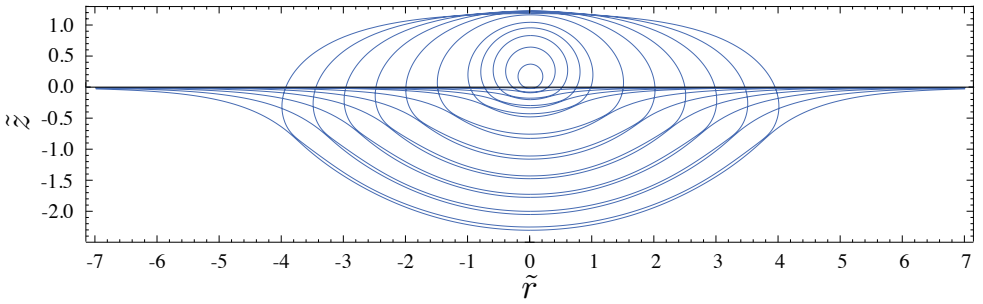

Figure III.7: Numerically determined shapes of ethanol Leidenfrost drops and of the liquid substrates associated (made of silicone oil V20) for a superheat $\Delta T = 40°C$ (which corresponds for ethanol to $T_p = 118°C$).

Figure III.7 shows the geometry of our situation for drops of ethanol on a pool of silicone oil V20 at a temperature $T_p = 118°$C which is equivalent to a superheat $\Delta T = 40°$C. The axis are made dimensionless by dividing the coordinates by the capillary length of the liquid of the drop, $\ell_{c_d} = 1.54$ mm. Many things have to be noticed on this plot.

- The drop deforms the substrate. We could already see that in Fig. III.1, but we see now clearly that all the substrate is deformed. This is the key for a long-range attraction as in the Cheerios effect [14].

- In the case of a Leidenfrost drop on a solid substrate, the drop tends to be flattened by the gravity when the drop becomes larger than the capillary length. Its height saturates at two times its capillary length. Here, as far as studied ($R_{\max} = 4\ell_{c_d}$), the height does not saturate, and the bigger the drop is, the deeper the drop penetrates the pool. This

feature lets us imagine that the relation between the volume V and the maximal radius of the drop $R_{\max}$ does not turn to $V = 2\ell_{c_d}\pi R_{\max}^2$ for big drops as in the case of a solid substrate.

- Another remarkable feature lies in the position of the top of the drop. We observe that that position does not increase monotonically with $R_{\max}$. Indeed, above $R_{\max} = 2.5\ell_{c_d}$, that position slightly decreases as the maximal radius increases. That means that, at a point, very large drops tend to sink. Of course, this tendency depends on the parameters, but we will come back to this in Sec III.5.1.

III.5.1 Deformation of the substrate

In this section, we analyse experimentally the deformation of the surface of the pool by the drop. We measure this deformation by looking just below the interface of the pool with a telecentric lens, as shown in Fig. III.8(a). The pool is made of silicone oil V20 ($\ell_{c_p} = 1.2\,\text{mm}$) while the drop is made of ethanol ($\ell_{c_d} = 1.5\,\text{mm}$). The pool is at a temperature $T_p = 118°\text{C}$. The liquid density ratio is $\rho_p/\rho_d = 1.16$ and the drop radius $R = 0.8\ell_{c_d}$. From the image on the left, we extract a profile that is represent by the dashed curve on the right. Note that the axis are made dimensionless using the capillary length of the drop, ℓ_{c_d}. Figure III.8(b) also shows the prediction of the model for the same parameters. A small discrepancy is observed and could be due to the movement of the drop on the substrate that could also explain the small asymetry observed in Fig. III.8(a).

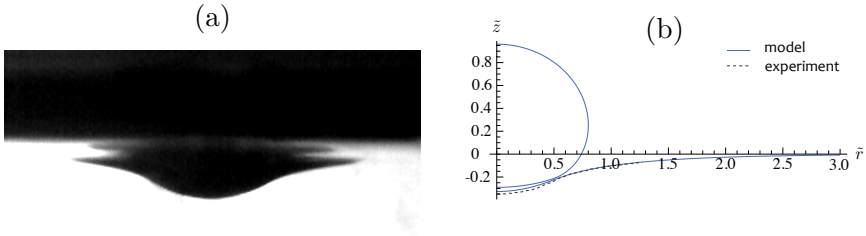

Figure III.8: (a) Experimental determination of the profile of the interface of the pool with a Leidenfrost drop on it. (b) Comparison between the model and the experiment. This experiment corresponds to an ethanol drop on a silicone oil pool at a temperature $T_p = 118°C$. The drop radius $R = 0.8\ell_{c_d}$.

Such a deformation, as said above is crucial, for the Cheerios effect [14]. This effect is responsible for the attraction and repulsion of objects floating at the surface of a liquid and their attraction or repulsion by the walls of the con-

tainer. Indeed, two objects (or parts of objects) that induce a curvature of the same signs on the liquid surface will attract each other, and those that induce curvature of opposite signs will repel each other. Two different drops induces of course two curvatures with the same sign, that is negative away from the drop. Unlike solid objects [15], this effect can not lead to the self-assembly of drops because the attraction ends with the coalescence of the drops.

Fortunately, most solid surfaces are oleophilic. Thus, the walls of our container induces a positive curvature, repel the drops, and prevent the contact between the drops and the walls. This is a useful way to confine the drop without acting directly on them. These two interactions between meniscii are illustrated in Fig. III.9.

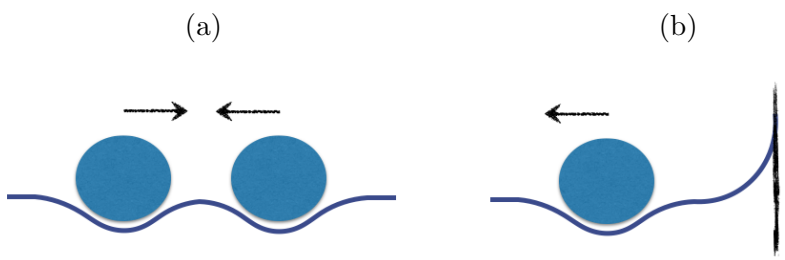

Figure III.9: (a) Two drops in a Leidenfrost state on a liquid pool experience a cheerios effect, attracting each other. (b) An oleophilic wall induces a curvature opposite to the one induced by a drop, and thus repels the drop.

One useful quantity that can be extracted from the profile of the interface is the maximal depth of the interface e_{center}. That quantity is plotted as a function of the radius of the drop in Fig. III.10. The theory and the experiments are in good agreement and we observe a monotonic increase of this depth with the radius of the drop. Looking at these pictures, a question arises: is there a theoretical limit to the size of the drops that can be maintained in the Leidenfrost state, and do we observe this limit in the experiments ?

To answer this question, we can vary two parameters that appear in the equations of the shape of the substrate [9]:

$$\tilde{\rho} = \frac{\rho_p}{\rho_d} \qquad \text{and} \qquad \tilde{\gamma} = \frac{\gamma_p}{\gamma_d} \,. \tag{III.3}$$

The effect of these ratios is illustrated in Fig. III.11. On the right, the ratio of surface tensions is constant, and on the left, the ratio of densities is

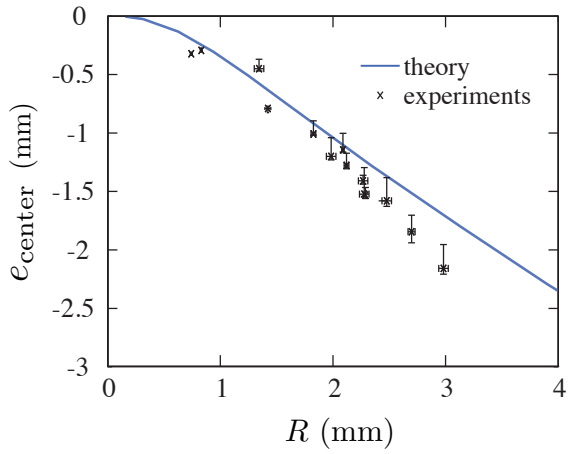

Figure III.10: Depth of the interface (silicone oil V20 at $T_p = 118°C$) below the center of etanol drops, e_{center}, as a function of the radius of the drop, R. Comparison between theory (blue line) and experiments (black crosses).

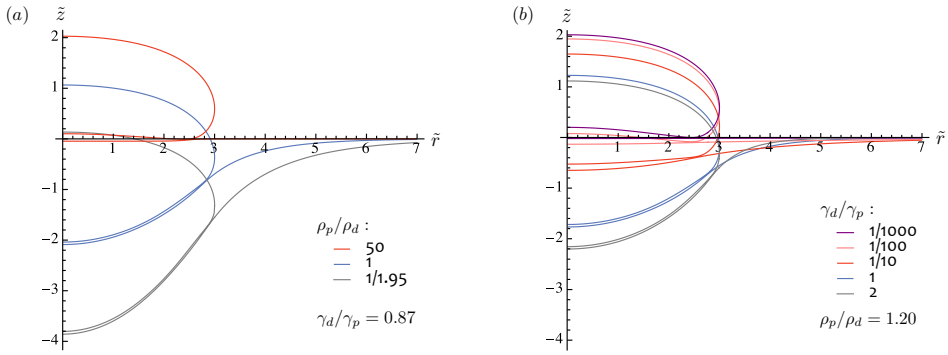

Figure III.11: Shape of the surface of the pool with a drop of radius $R = 3\ell_{c_d}$ for various ratios of tension surface and of densities. (a) The ratio of the densities is kept constant. (b) The ratio of the surface tensions is kept constant.

constant. We see that high values of these ratios tends to make the situation closer to the case of a solid substrate. However, we see that this situation is only reached for extreme values of these ratios. Practically, these extreme values are not encountered in the nature. At the opposite, we see that for low ratios, the drop tends to sink more. For example, for this size of drops ($R = 3\ell_{c_d}$), no stable shape is found for $\tilde{\gamma} = 0.87$ for a ratio $\tilde{\rho} < 1/1.95$. For this threshold value, we observe that the top of the drop reaches the level of

the free surface of the pool. This case is not that far from the case of a drop of ethanol on a pool of silicone oil V20 at a temperature $T_p = 118°C$. Another interesting case is the one of HFE–7100 on the same pool , for which $\tilde{\gamma}^{-1} = 0.7$ for a ratio $\tilde{\rho} = 0.65$. This case is very close to the limiting case in Fig. III.3(a). This explain why we do not succeed to create large drops of HFE–7100 in a Leidenfrost state. For ethanol drops, the largest drops we succeeded to stabilize experimentally was a drop of radius $R = 8$ mm or $R = 5.2\ell_{c_d}$.

In the situations where $\rho_p >> \rho_d$ or where $\gamma_p >> \gamma_d$, the situation can theoretically reach a situation close to the case of a solid substrate. In these limit cases, nothing really differs from the case of a solid from the point of view of the evaporation. In such a situation, we should find the same law of evaporation as in the solid case, *i.e.* Eq. III.1 with $\alpha = 2$ for drops larger than ℓ_{c_d}, and $\alpha = 0.5$ for drops smaller than ℓ_{c_d}. *A contrario*, when the drop sinks more than in the case of a drop of ethanol on silicone oil, *e.g.* a drop of HFE–7100 on the same substrate, the law of evaporation should also be affected. However, the deviation observed for HFE–7100 is negligible. In a good approximation, the exponent of Eq. III.1 remains $\alpha = 1$.

III.5.2 The ingredients for a linear decrease of the radius

As we previously said, the strangest feature of the curves $R(t)$ is the fact that we do not observe two different regimes (for small and large drops) as we do in the case of a solid substrate (see Fig. III.5 and Fig. II.3). Some intuition of this curious fact can be obtained by studying some of the results of the model. In Fig. III.12, we plot the radius of an ethanol drop on a silicone oil pool as a function of its volume, computed with our model. A continuous line indicates the scaling law $R \propto V^{1/3}$. The agreement between this scaling law and the data is good despite a slight deviation for very large drops (that we do not observe in the experiments). This is completely different of the case of a solid substrate for which two regimes are observed : small drops are spherical ($R \propto V^{1/3}$) and large drops turn to puddles ($R \propto V^{1/2}$). This element alone does not imply by itself that there should be only one regime of evaporation but gives the intuition that the capillary length is not anymore a key length for changes concerning the shape of the drops and the evaporation.

Then, in order to extract the evaporation rate and explain the linear scaling for the decrease of the radius with time, we have to integrate the local evaporation flux $\mathcal{J}$ over the vapor film. The details are presented in the paper [9]. Here, we simply show in Fig. III.13 the dependency of the evaporation

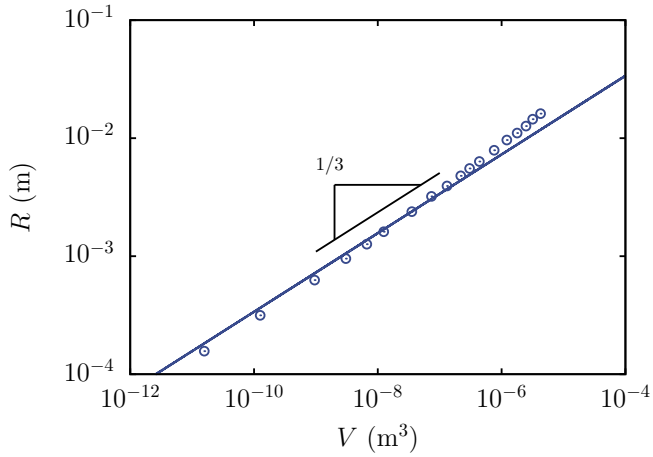

Figure III.12: Predicted radius of an ethanol drop in a Leidenfrost state on pool as a function of its volume. The line indicates a scaling law $R \propto V^{1/3}$.

rate of ethanol drops with respect to their volume (at a fixed temperature of the pool $T_p = 118°\text{C}$), and with respect to the superheat (for drops of radius $R = 1$ mm). In both cases, we can extract scaling laws and combine them to find a differential equation for the evaporation rate.

$$-\frac{\mathrm{d}V}{\mathrm{dt}} \propto V^{2/3}\Delta T^{4/5} \tag{III.4}$$

This equation can be solved and leads to

$$V^{1/3} = V_0^{1/3} - C\Delta T^{4/5}\ t \tag{III.5}$$

with V_0 and C being constants of integration. Considering the relation between the volume and the radius of the drops, we find

$$R(t) = R_0\left(1 - \frac{C'\Delta T^{4/5}}{R_0}t\right) \tag{III.6}$$

with R_0 being the initial radius, and C' a modified constant of integration. We can express $\tau = R_0\Delta T^{-4/5}/C'$ and obtain Eq. (III.1) with $\alpha = 1$ as found in the experiments. Moreover, we see that the reduced lifetime of the drops scales as $\tau/R_0 \propto \Delta T^{-4/5}$ as observed in Fig. III.6.

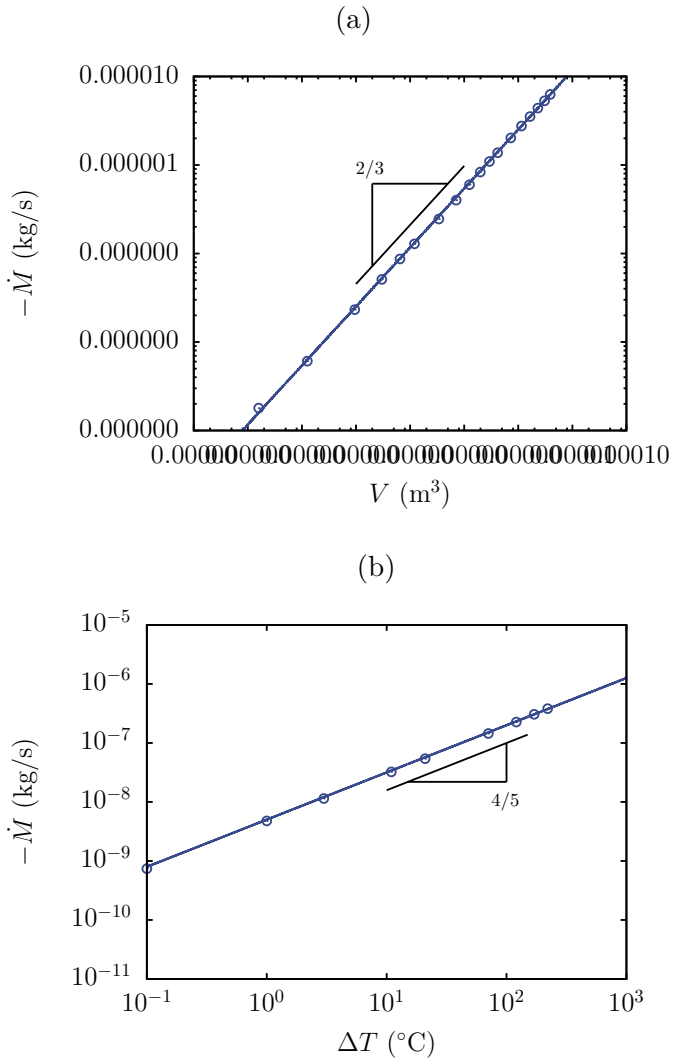

Figure III.13: Evaporation rates of drops of ethanol as a function of (a) their volume (at $T_p = 118°C$), and (b) the superheat (for a drop of radius $R = 1$ mm).

Note that this model does not reproduce the saturation of the reduced lifetime at low superheats that is observed experimentaly. The limitation of this model at low superheats is that the only source of evaporation considered is the conductive transfer through the vapor film. However, a drop already evaporates in an environment at the temperature of the air above the hot pool. In Fig. III.14(a), we show the reduced lifetime of drops suspended at the tip

of a fiber, approximately 1 mm above the surface of the pool. This lifetime seems to be quite independent on the superheat, at least for low superheats. This is consistent with the idea that the drop evaporation in a hot environment depends on the absolute temperature. The continuous line is a fit by a constant. The value of that constant is 125 s.mm^{-1}. This value is higher than the value at which the evaporation rate of Leidenfrost drops made of ethanol saturates, *i.e.* 80 s.mm^{-1}. Indeed, the temperature above the pool is expected to strongly decrease with the distance to the surface of the pool, and the drop is 1 mm above the pool.

The addition of a source of evaporation that is independent on the superheat to the evaporation due to the Leidenfrost effect itself can be written as

$$\dot{R} = C' \Delta T^{4/5} + \mathcal{C} \tag{III.7}$$

which then leads to a reduced lifetime

$$\frac{\tau}{R_0} = \frac{1}{C' \Delta T^{4/5} + \mathcal{C}} \ . \tag{III.8}$$

In Fig. III.14(b), we show on the data of the reduced lifetime as a function the superheat what would be the impact of this source of evaporation on the evaporation of our drops. The blue dotted line is Eq. (III.8) with $\mathcal{C} = 1/80$ mm/s and the coefficient C'_{ste} being the same as in the fit of the experimental data at high superheats. $\mathcal{C}$ represents the evaporation of a drop in the hot environment that exists just above the pool without taking into account the conductive heat transfer from the pool to the drop. The agreement between the data and the curve is good at low and very high superheats but the transition between the two regimes is sharper in the case of the experimental data.

III.6 Convection in the pool

Up to now, no mention has been made of what happens below the surface of the pool. We just considered a deformable surface whose deformation is described by the Young-Laplace equation. The model even considers the surface as static, which leads to a specific prefactor in the lubrication equation that describes the Poiseuille flow in the vapor film under the drop. However, nothing indicates us *a priori* that the surface of the drop and the surface of the pool is static. Still, the impact of flows in the pool and variations of the boundary conditions is of the second order in our problem. The purpose of this section is to investigate how the pool is impacted by the presence of the

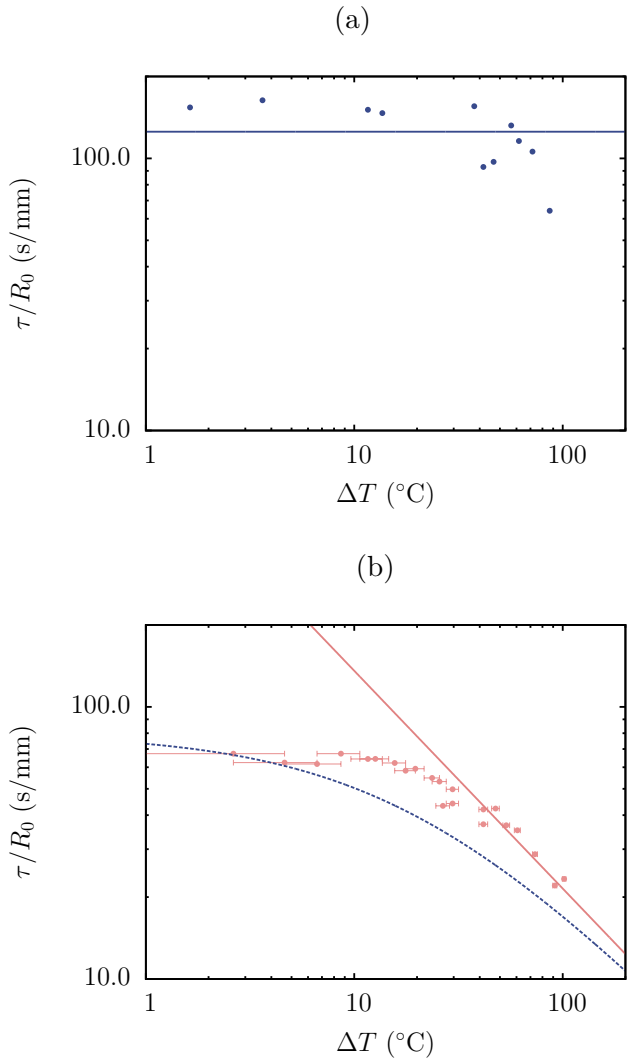

Figure III.14: Reduced lifetimes of drops of ethanol as a function of the superheat (a) for drops suspended on a fiber, approximately 1 mm above the pool, and (b) in the Leidenfrost state over the same pool. The radius of the drops is $R = 1$ mm. The blue line is a fit by Eq. (III.8). The red line indicates the scaling $\tau/R_0 \propto \Delta T^{-4/5}$.

presence of a drop above it, and to study the infuence of what happens in the pool on the Leidenfrost effect.

The first thing that one has to notice about the situation depicted in any

Leidenfrost levitation problem is that there is a heat transfer. This transfer occurs between the substrate and the drop. In the different models used, the transfer is always considered as being driven by conduction. This implies that, in order to evaporate the drop, heat is provided by the substrate. Usually, the Leidenfrost is considered to occur on a metallic substrate, and the conduction in the substrate is much more important than the conduction in the vapor film. This metallic substrate ensures that the temperature of the substrate remains uniform in the substrate and at its surface. However, liquids in general and silicone oil especially have a poor thermal conductivity ($\kappa \simeq 0.15$ W/m.K) compared to aluminium for instance ($\kappa \simeq 200$ W/m.K).

The three orders of magnitude between these conductivities impose to be careful about the homogeneity of the temperature and the convection in the pool. Indeed, a few degrees of difference between the point just under the drop and the bottom of our container can induce free convection and the appearance of rolls. Moreover, the natural convection is not the only convection that can be induced in the pool due to inhomogeneities in the temperature of the pool. More precisely, the surface tension of a liquid does depend on its temperature. Thus, if the drop cools down the surface of the pool, a gradient of surface tension is created and induces a Marangoni flow at the surface. This Marangoni flow can even be responsible for the levitation of drops [10]. A schematic view of these two phenomenons is given in Fig. III.15.

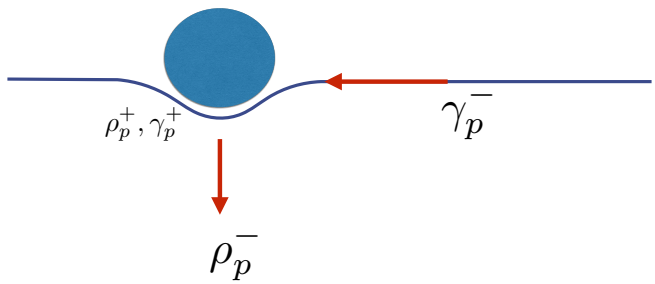

Figure III.15: Schematic view of the production of flows by Marangoni effect at the surface of the pool and by buoyancy in the bulk.

In our case, we see that there is at least two processes that can induce some convection in the pool. Both processes always induce a flow that would be directed towards the drop close to the surface. But a third phenomenon can enter the competition, and run in the opposite direction. The Leidenfrost drop above the substrate produces a flow of vapor just above the surface. This flow

of vapor can entrain the liquid at the surface of the pool. The flow induced by this viscous entrainment follows the direction of the flow of vapor as shown in the schematic of Fig. III.16.

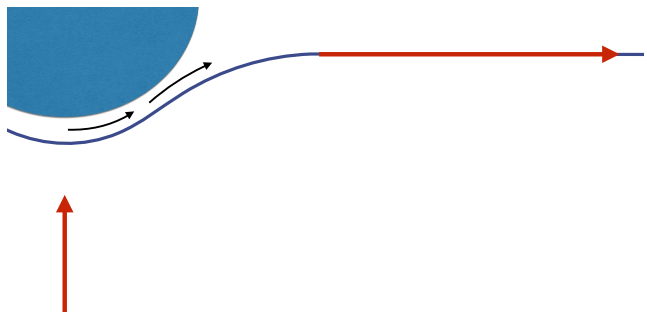

Figure III.16: Schematic view of the viscous entrainment of the oil at the surface of the pool by the vapor flow under the drop.

To understand what processes takes place in our experiment, we performed some experiments using the so-called "particle image velocimetry" technique with a specific setup. This technique will be called PIV in the following. The last part of this chapter will be devoted to that experiment and will try to depict implications for the Leidenfrost drops on liquid pools.

III.6.1 The PIV setup

To visualize the flows in the pool under the drop, the PIV technique uses tracers that are disseminated in the liquid. In our case, these particles were consituted of a polymer shell surrounding a rhodamine core. Their diameter was 15 µm and their density was 1100 kg/m^3. These properties are sufficient for the particles to follow reasonnably well the flows of the silicone oil and to avoid sedimentation to occur on the time scale of an experiment. The drawback of these particles is the fact that the polymer shell tends to melt when the temperature goes above 150°C.

To visualize these small particles, we used a pulsed laser emitting at 532 nm. The beam of the laser was transformed in plane sheet. This laser was synchronized with the acquisition of an high-speed camera whose line of sight was normal to the plane of the laser sheet and focused on it. The field of view was 53 mm large and 38 mm high.

The silicone oil was contained in a parallelepiped aquarium with its sides in the direction of the laser sheet and parralel to it. The oil was heated via a heating plate of 2 cm of height, 12 cm of length, and 8 cm of width made of aluminium. Two cartridge heaters were inserted in it. The heating plate was placed in the aquarium, 3 cm above its bottom. Oil was pourred to reach an height of 4 cm above the top of the heating piece. With this setup, we observed a difference of temperature of 3°C to 5°C between the top surface of the heating plate and the top of the oil pool.

To this setup, we added a syringe pump that created drops above the pool, in the plane of the laser sheet. After the creation of the drop, the pumping stopped and the tip of the syringe kept the drop static in the plane of the laser sheet. The camera then acquired images during 0.88 s at a rate of 1000 fps. This ensured that the size of the drop remained approximately constant, and that we had a sufficient amount of images to average the PIV data.

We performed experiments with ethanol and HFE–7100 for the liquid of the drop, and silicone oil V20 and V100 for the pool.

III.6.2 Qualitative analysis

A convenient way to visualize the flows is to superimpose two plots : one is a heat map showing the intensity of the flow at a location, the other is a map of vectors pointing in the direction of the flow with a size proportionnal to the intensity of the flow. In Fig. III.17, we show two exemples. On the left, an ethanol drop stands on a silicone oil V20 pool with a surface temperature of $T_p = 104$°C. On the right, a drop of HFE–7100 stands on a pool of silicone oil V20 with $T_p = 64$°C. $y = 0$ mm represent the surface of the pool and $x = 0$ mm represent the horizontal position of the center of mass of the drop. Note that on the left part, close to the surface, the laser sheet is intercepted by the drop and no data can be extracted in this region.

A few differences can be easily noted between both graphs :

- In the case of the ethanol drop, at the surface of the pool, the flow goes towards the drop, and under the drop, towards the bottom of the pool. Considering the discussion above, this indicates that in this case, either the buoyancy or the Marangoni effect dominates the viscous entrainment. This is just the opposite for the case of HFE–7100 where the viscous entrainment seems to be the driving mechanism of the flows.
- The positions of the centers of the vortices also differs from one case to

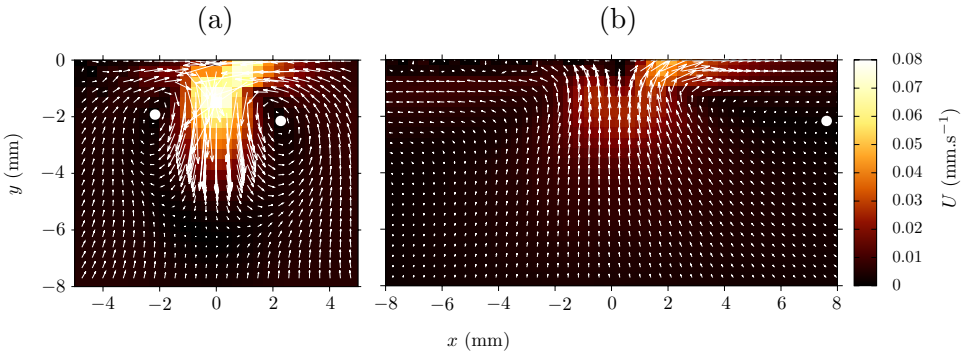

Figure III.17: PIV maps for (a) a drop of ethanol on a pool of silicone oil V20 with $T_p = 104°C$ and (b) a drop of HFE–7100 on a pool of silicone oil V20 with $T_p = 64°C$. The centers of the vortices that are in the field of view are indicated by white dots. The directions of the flow in (a) is the opposite than those in (b).

the other. Indeed, the vortices are much more far from the drop in the case of the HFE–7100 drop (around 10 mm) compared to the case of the ethanol drop (around 2 mm).

III.6.3 Quantitative analysis

New observables These plots contain a lot of information. To understand the phenomenon, we have to refine them and to choose carefully a few observables. Among many choices, we define U_u as the maximum of the projection of the velocity of the fluid along the vertical axis under the center of the drop, and U_s as the maximum of the projection of the velocity of the fluid along the

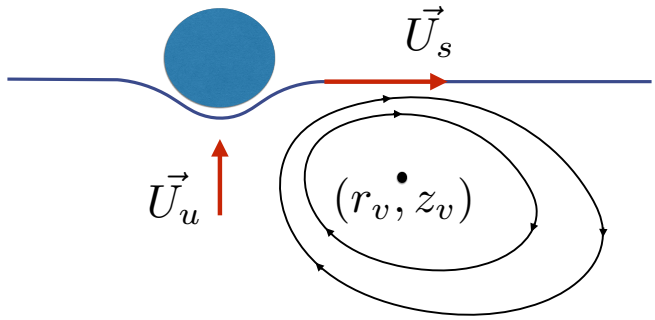

Figure III.18: Choice and definition of observables needed to analyse the results of PIV measurements.

horizontal axis at the surface of the pool. We also note r_v the radial and z_v the vertical position of the center of the vortices, *i.e.* the points where the velocity of the fluid is nul. A representation of these quantities is given in Fig. III.18.

The case of ethanol drops Let us first focus on the velocity of the fluid under the drops, and especially under ethanol drops. In Fig. III.19, we plot this velocity as a function the superheat for drops with radii $R = 1.28$ mm (with 7% of relative uncertainty on the radius). We observe a monotonic increase of the velocity as the superheat increases.

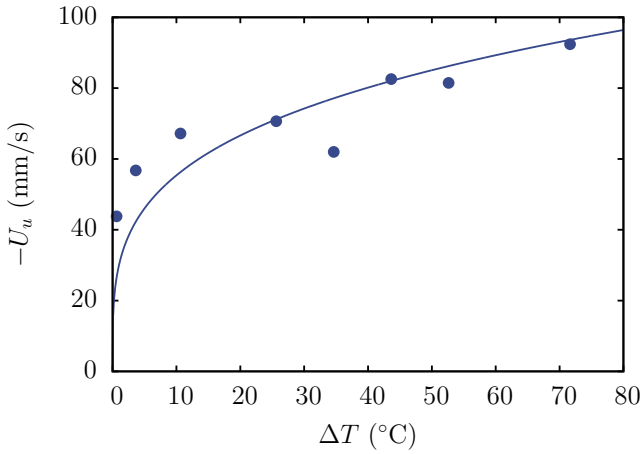

Figure III.19: Maximum of the projection of the velocity of the fluid along the vertical axis under the center of the drop U_u as a function of the superheat ΔT for drops of radii $R = 1.28$ mm. The line is a fit using Eq. (III.14).

To explain this increase, we first determine whether Marangoni or natural convection dominates, we can take a look at the dimensionless numbers that characterize these phenomenons. The Marangoni number Ma and the Rayleigh number Ra, for the Marangoni convection and the natural convection respectively, can be written as

$$\begin{cases} \mathrm{Ma} = \dfrac{\mathrm{d}\gamma_p}{\mathrm{d}T} \dfrac{(T_b - T_t)\ L}{\alpha_p\ \eta_p} & \text{(III.9)} \\ \mathrm{Ra} = \dfrac{\rho_p\ g\ \beta\ L^3\ (T_b - T_t)}{\alpha_p\ \eta_p} & \text{(III.10)} \end{cases}$$

where L is the depth of the oil pool, α_p is the thermal diffusivity of the oil, T_b is temperature of the heating plate, T_t is the temperature at the top of the pool, under the drop, and β is the thermal expansion coefficient. With these numbers, we can then make another one that compares both phenomenons. This one is called the Bond number. Even though the name is the same as the first dimensionless number introduced in this thesis, this Bond number is of course different from the number that compares the effect of gravity and surface tension in drops. Its expression is

$$\mathrm{Bo}^* \;=\; \frac{\mathrm{Ra}}{\mathrm{Ma}} \;=\; \frac{\rho_p \; g \; \beta \; L^2}{\frac{\mathrm{d}\gamma_p}{\mathrm{d}T}} \; . \tag{III.11}$$

We can easily compute the value of this Bond number, Bo^*, knowing that for all oils used, $\beta = 10^{-3}$ K^{-1} and $\mathrm{d}\gamma_p/\mathrm{d}T = 5.10^{-5}$ N.m^{-1}.K^{-1}. The density of the oils used can vary a little bit with the temperature and between the different kinds used, but always stays around 900 kg.m^{-3}. Thus, Bo $\simeq 282$ and we can see that the natural convection dominates Marangoni convection.

To estimate the vertical velocity of the oil flowing under the drop, we can note that the situation is completely similar to the situation depicted in the paper of Dorbolo *et al.* where a bloc of ice cools down the surface of a liquid pool [16]. The velocity of the fluid is then

$$U_u \;=\; \left(\frac{\beta \; g \; \dot{M} \; \mathcal{L}}{z \; \rho_P \; c_{\mathrm{p,p}}} \right)^{1/3} \tag{III.12}$$

where z is the vertical position under the surface of the pool, under the drop. $\dot{M}\mathcal{L}$ is the heat flux between the pool and the drop, and $c_{\mathrm{p,p}}$ is the specific heat capacity of the silicone oil. Moreover, we know from the theory of Sec. III.4 that the heat flux scales as

$$\dot{M}\mathcal{L} \;\propto\; R^2 \; \Delta T^{4/5} \; . \tag{III.13}$$

Thus, combining the two last equations, we find that the velocity U_u scales as

$$U_u \;\propto\; z^{-1/3} \; R^{2/3} \; \Delta T^{4/15} \; . \tag{III.14}$$

Note that we emphasized the dependency of this velocity with z. Indeed, this expression for U_u diverges right at the surface under the drop. However, this scaling law is used to fit the data of Fig. III.19 and we observe a good agreement showing that the vortices under ethanol drops are driven by the buoyancy.

The case of drops of HFE–7100 For drops of HFE–7100, we saw that the oil at the surface of the pool flows away from the drop, which means that viscous entrainment dominates natural convection (and *a fortiori* the Marangoni convection). This viscous entrainment can be quantified using the continuity of the stresses across the interface.

$$\eta_p \frac{\partial V_{\mathrm{t,p}}}{\partial n} = \eta_v \frac{\partial V_{\mathrm{t,v}}}{\partial n} \tag{III.15}$$

In this equation, n is the coordinate normal to the interface, and $V_{\mathrm{t,p}}$ and $V_{\mathrm{t,v}}$ are the tangential velocities of the oil and of the vapor at the interface between the pool and the vapor film. To compute an order of magnitude for the velocity of the fluid induced in the pool by this continuity of the stresses, we can make the strong approximation that the interface is horizontal and that the velocity of the oil decreases linearly between the surface of the pool and the center of the vortex.

$$\eta_p \frac{U_s}{z_v} = \eta_v \frac{\partial V_{\mathrm{t,v}}}{\partial n} \tag{III.16}$$

As the velocity of the oil at the surface of the pool is negligible compared to the velocity of the vapor at the middle of the thickness of the film, V_{neck}, we can go even further

$$\eta_p \frac{U_s}{z_v} \sim \eta_v \frac{V_{\mathrm{neck}}}{h_{\mathrm{neck}}/2} \tag{III.17}$$

where we make the assumption that the viscous entrainment is induced by the part of the vapor film where the stress in the vapor is the more important, *i.e.* in the neck. Using the model presented in Sec. III.5, we can compute the values for V_{neck} and h_{neck}, and then calculate the stress at the surface of the pool in the vapor film. In Fig. III.20, we compare the stresses calculated in the vapor phase with the model (in blue), and those measured in the silicone oil using PIV. The values found are comprised between 0.1 Pa and 1 Pa for the range of superheat explored (ΔT going from 1°C to 100°C) for both stresses.

Considering the strong approximations made in the reasonning (assuming a linear velocity profile between the surface of the pool and the center of the vortex), and the experimental difficulties to obtain symmetrical vortices, and the possible influence of flows that are not generated by the presence of the drop, and the effect of the buoyancy-driven convection, both stresses are in a reasonable agreement showing that the vortices under drops made of HFE-7100 are driven by the viscous entrainment.

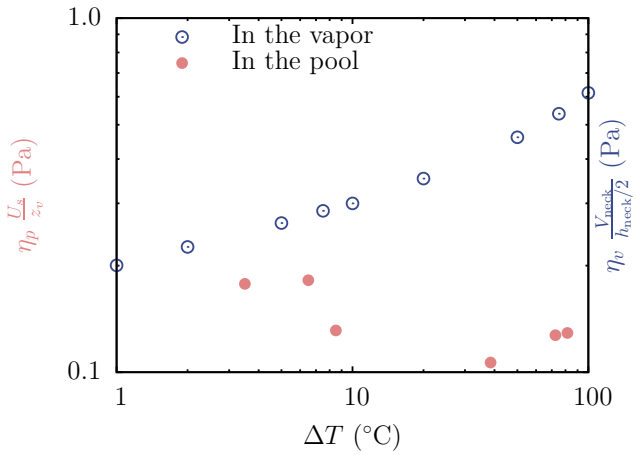

Figure III.20: Stresses at the surface of the pool as a function of the superheat. In blue: stresses calculated with the values of $V_{\rm neck}$ and $h_{\rm neck}$ extracted from the model described in Sec. III.5. In red: stresses calculated with the values of U_s and z_v measured using PIV.

III.7 Conclusions

We studied Leidenfrost drops on heated liquid pools made of silicone oil. This is a typical example of an experiment on the Leidenfrost effect that looks simple, but still, it reveals a high complexity and elegance.

And indeed... For the first time, we showed that the Leidenfrost effect can be triggered as soon as the substrate is hotter than the boiling point of the liquid of the drop when this substrate is made of silicone oil. At least for ethanol. Diethyl ether has shown to be a little bit harder to put in a Leidenfrost state, but still, it appears that its Leidenfrost Point is less than 40°C above its boiling point on any substrate we used, which is far lower than its Leidenfrost Point on a metallic substrate. However, we were unable to hold Leidenfrost drops on substrates with viscosities above 0.1 Pa.s.

We also looked at the shapes of our drops and to the deformation of the liquid substrates below them. A model has been developed on the basis of Sobac's model to rationnalize these experiments. Of course, the evaporation has been investigated, and we observed that the radius of the drops decreases linearly with time, whatever the radius of the drops. That points out the fact that the capillary length is much less significant in the case of liquid substrates than in the case of solid substrates.

Finally, inspired by our ineffectualness to stabilize drops on high viscosity pools, we investigated what was happening in the pool, under the drop, and discovered a new world. The presence of a Leidenfrost drop induces a torroidal vortex all around the drop. However, this vortex is very different depending on the liquid of the drop. For ethanol drops, the vortex are driven by buoyancy : the oil sinks under the drop and recirculate to come back at the surface of the pool, coming from the side of the drop towards its center. For HFE–7100 drops, the oil flows in the opposite direction in a vortex with similar characteristics. The flow is then driven by viscous entrainment: the flow of vapor in the vapor layer between the drop and the pool induces a high stress at the surface of the pool and entrains oil from the center of the drop to its side.

References

[1] H. Kim, B. Truong, J. Buongiorno, and L.-W. Hu. *On the effect of surface roughness height, wettability, and nanoporosity on Leidenfrost phenomena.* Appl. Phys. Lett., 98:083121, 2011.

[2] H.-M. Kwon, J. C. Bird, and K. K. Varanasi. *Increasing Leidenfrost point using micro-nano hierarchical surface structures.* Appl. Phys. Lett., 103:201601, 2013.

[3] C. Kruse, T. Anderson, C. Wilson, C. Zuhlke, D. Alexander, G. Gogos, and S. Ndao. *Extraordinary shifts of the Leidenfrost temperature from multiscale micro/nanostructured surfaces.* Langmuir, 29:9798–9806, 2013.

[4] Bourrianne P. *Non-mouillant et température.* PhD thesis, École Polytechnique de Palaiseau, 2016.

[5] M. Le Merrer, C. Clanet, D. Quéré, É. Raphaël, and F. Chevy. *Wave drag on floating bodies.* Proc. Natl. Acad. Sci., 108:15064–15068, 2011.

[6] A. Snezhko, E. Ben Jacob, and I. S. Aranson. *Pulsating–gliding transition in the dynamics of levitating liquid nitrogen droplets.* New J. Phys., 10:043034, 2008.

[7] M. Adda-Bedia, S. Kumar, F. Lechenault, S. Moulinet, M. Schillaci, and D. Vella. *Inverse Leidenfrost Effect: Levitating Drops on Liquid Nitrogen.* Langmuir, 32:4179–4188, 2016.

[8] B. Sobac, A. Rednikov, S. Dorbolo, and P. Colinet. *Leidenfrost effect: Accurate drop shape modeling and refined scaling laws.* Phys. Rev. E, 90:053011, 2014.

[9] L. Maquet, B. Sobac, B. Darbois-Texier, A. Duchesne, M. Brandenbourger, A. Rednikov, P. Colinet, and S. Dorbolo. *Leidenfrost drops: liquid substrate.* Phys. Rev. Fluids, 110:24001, 2015.

[10] R. Savino, D. Paterna, and M. Lappa. *Marangoni flotation of liquid droplets.* J. Fluid Mech., 479:307–326, 2003.

[11] J. C. Burton, A. L. Sharpe, R. C. A. van der Veen, A. Franco, and S. R. Nagel. *Geometry of the vapor layer under a Leidenfrost drop.* Phys. Rev. Lett., 109:074301, 2012.

[12] A.-L. Biance, C. Clanet, and D. Quéré. *Leidenfrost drops.* Phys. Fluids, 15:1632–1637, 2003.

[13] X. Xu and T. Qian. *Hydrodynamics of Leidenfrost droplets in one-component fluids.* Phys. Rev. E, 87(4):043013, 2013.

[14] D. Vella and L. Mahadevan. *The cheerios effect.* Am. J. Phys., 73:817–825, 2005.

[15] M. Poty, G. Lumay, and N. Vandewalle. *Customizing mesoscale self-assembly with three-dimensional printing.* New J. Phys., 16:023013, 2014.

[16] S. Dorbolo, N. Adami, C. Dubois, H. Caps, N. Vandewalle, and B. Darbois-Texier. *Rotation of melting ice disks due to melt fluid flow.* Phys. Rev. E, 93:033112, 2016.

IV

Shaken drops

Repeated impacts on a solid substrate

IV.1 Preamble

Inevitably, when it comes to the deposition of a drop over a substrate, whether this substrate is hot or not, the way the drop is deposited is often important for the experiment. For instance, one may remember an old measurement of the contact angle of a drop on a substrate, made with too little care while he or she was still a young researcher... The scattering of the results may be catastrophic. As another example, in chapter III, this deposition was also quite critical in some case, and the choice made was to deposit the drops gently on the meniscii of the substrate.

In general, in the Leidenfrost effect, this deposition is not seen as critical. However, studies have shown that the way the drop are deposited have a strong influence on the Leidenfrost Point [1]. This temperature was defined there as the temperature of the transition between impacts with and without any nucleation boiling. The Leidenfrost Point increased strongly while the speed of the impacting drops U_0 was increasing.

Moreover, the impact dynamic in itself is interesting. And this fact is a very general feature of drops. Their impacts can lead to many different be-

haviors and have an... Impact ! on different domains from the transmission of diseases in agriculture [2] to inkjet printing [3]. On superhydrophobic substrates [4], just as on hot substrates [5], the drops have shown one important common feature. The impact time τ_i scales as the capillary time, $\sqrt{M_d/\gamma_d}$, where M_d is the mass of the drop.

However, it is well known that an impact is not the end of the story. When a first impact leads to second one, then to a third one, and to many more, this is a highway to non-linearity. Though, if one just drop an object on a substrate, this will not lead to an infinite amount of impacts, because a part of the impact energy is dissipated during the impact. To reach a state where any impact is followed by another one, energy must be injected in the system.

A very convenient way to inject this energy is to work with an electromagnetic shaker. This device allows to oscillate a substrate with a well defined amplitude A and frequency ν. The most classical study on this system, *i.e.* the problem of the bouncing ball, has been studied for quite a long time due to its interest as a model system for studying transitions to chaos [6, 7], and still, nowadays, variations of this system are still studied like the bouncing of a ball on a spherical vibrated plate [8].

In this chapter, we revisit the problem of the bouncing ball using the Leidenfrost effect, and study the movements of Leidenfrost drops bouncing on a vibrated substrate. This system is analogous in some aspects to the well-known case of the bouncing drops, *i.e.* drops bouncing on vibrated liquid substrates thanks to a renewal of the air film between the drop and the substrate at each bounce [9, 10]. Recently, our system has received a little attention and vibrations of the substrate have been shown to be efficient at removing the Leidenfrost effect [11]. This study was focused on relatively high frequencies of vibrations ($\sim 10^2$ Hz). In our study, we focus on lower frequencies to get closer from the inverse of the capillary time. By doing so, we avoid the suppression of the Leidenfrost effect and we are able to study the dynamics of bouncing drops with a stable vapor layer.

IV.2 Experimental setup

To vibrate the substrate, an electro-magnetic shaker was used. To pilot its movement, we used a low-frequency generator that generates a sinusoidal signal with a frequency ν and an amplitude $\mathcal{A}$. This signal was sent to the shaker through an amplifier. The substrate then oscillated with an amplitude A. We define the pulsation of the signal $\omega = 2\pi\nu$ and the reduced accelera-

tion $\Gamma = A\omega^2/g$. An accelerometer mesured the acceleration of the substrate, giving a oscillating signal. The peak-to-peak value of the signal given by the accelerometer was proportionnal to the reduced acceleration.

The substrate was a thick plate of aluminium of $100 \times 100 \times 30$ mm^3 in which two cartridge heaters were inserted. The top side of this piece was slightly curved in order to maintain a confinment for the bouncing Leidenfrost drops just as in the study of Chastaing *et al.* for the bouncing ball [8]. A thermocouple measured the temperature of the substrate and a PID controler set the heating of the cartridge heaters. In all the experiments of this chapter, as we focused on the dynamics of the Leidenfrost drops, the temperature is set to 300°C, well above the Leidenfrost Point of water on polished aluminium (~ 220°C).

The drops were deposited with a micropipette as close as possible to the substrate. To avoid any effect due to the deposition, the data were acquired ten seconds after the deposition when the bouncing is stable through time.

The drops were filmed from a side view with a slight angle (less than 5^circ) in order to be able to extract their vertical movement. The acquisition was made with a high-speed camera, and the acquisition rate was adapted to ν to have at least 10 images per bounce when possible.

IV.3 First measurements

In Fig. IV.1(a), a typical image sequence is shown. Images are separated by 4 ms and the scale bar represent 2 mm. The oscillations of the substrate are characterized by $\nu = 28$ Hz and $\Gamma = 0.4$ and the radius of the drop is $V_d = 10$ μl. The movement of the substrate is barely distinguishable, so we emphasized this movement tracing a the blue line. We see a first impact followed by the take-off of the drop an parabolic trajectory. From this side view, we could easily detect the center of mass of the drop, its top, and its bottom. The position of the substrate was also detected, but with a shift that can be determined from the moments when the drops impacts it.

In Fig. IV.1(b), we plot the vertical position of a drop ($R = 1.25$ mm) as a function of time (red area), the position of its center of mass (yellow line) and the position of the substrate (blue line). A small drift can be noticed in the vertical position of the drop. This is an artifact due to the movement of the drop in the direction of the line of view of the camera. This drift is neglected in the following.

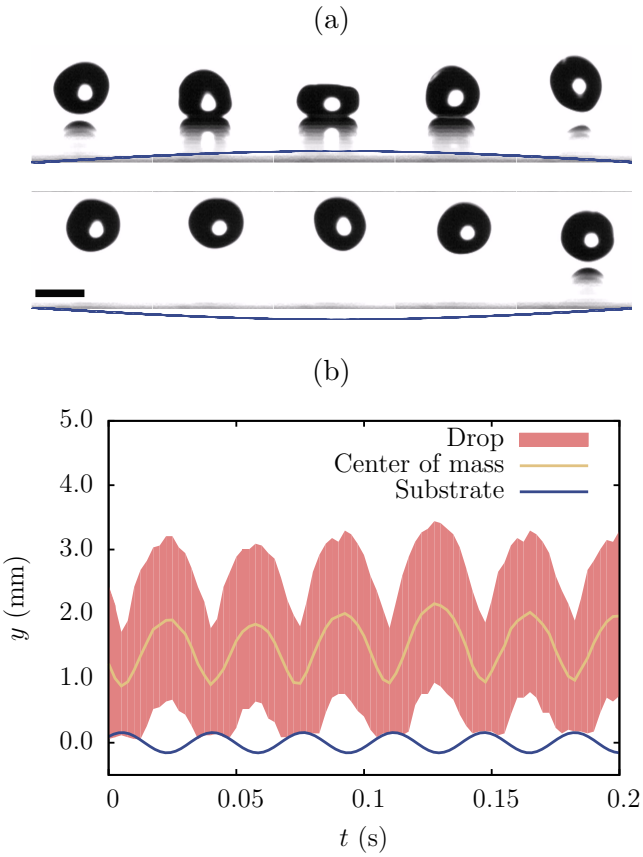

Figure IV.1: (a) A drop bouncing on a substrate oscillating with $\nu = 28$ *Hz and* $\Gamma = 0.4$. *The drop has a radius* $R = 0.75$ *mm. The scale bar represent* 1.5 *mm and the time step* 4 *ms. The blue line emphasizes the movement of the substrate. (b) Vertical position of a drop* ($R = 1.25$ *mm) as a function of time and position of its center of mass* y_{CM}. *The position of the substrate is also indicated.*

From these data, we extracted some observables. The instant at the impact n, $t_{i,n}$, at the take-off n, $t_{t,n}$, from which we can deduce the time between two successive impacts $\Delta t_{i,n} = t_{i,n} - t_{i,n-1}$. In the following, for more clarity, we use the notation Δt_i for this quantity as we never focus on one of the $\Delta t_{i,n}$, but rather plot all their values to have a statistical view on them.

If we consider that the first impact takes place before the first take-off, we can also define the contact time $\tau_{c,n} = t_{t,n} - t_{i,n}$, and the flight time

$\tau_{f,n} = t_{i,n} - t_{t,n-1}$. Just as for the time between successive impacts and take-offs, we use the notation τ_c and τ_f.

Note that we evoke here impacts, take-offs, contacts and flights as if there was a real contact at a time between the substrate and the drop. Of course, our drops are still in the Leidenfrost state and there is no contact. However, we define here that there is a contact when the thickness of the vapor film is lower than it would be in a static case. Experimentally, with our setup, determining this instant precisely is impossible, but as the drop impacts and take-offs quickly from the substrates, it is easy to determine the time with the time resolution of our acquisition. The uncertainty on our measurements is then directly the time resolution of our acquisition.

To characterize any observable X, to each bounce and value of X, a gaussian function is attributed with a standard deviation that is the uncertainty of the measurement and a unitary height. An example is shown in Fig. IV.2, where each measurement is represented by a gaussian function (in blue). All these gaussians functions are summed and the result is representative of an intensity (red line). Then, the resulting function is normalized by its maximal value, and this normalized intensity is represented by a color scale, from 0 (white) to 1 (black). Compared to a mean and a standard deviation, this visualisation helps to visualize when the observable can take more than one value for one set of parameters.

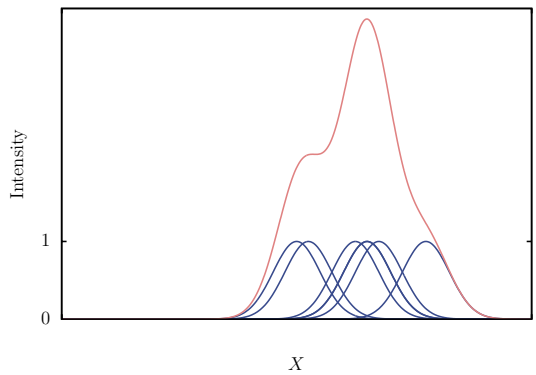

Figure IV.2: Illustration of the method used to analyze data. To each measurement, a gaussian function is attributed (blue curves). The sum of these gaussian functions is representative of an intensity (red curve). This intensity is then normalized by the maximal value of this function and transformed in a color scale from 0 *(white) to* 1 *(black).*

IV.4 How to bounce

The first thing that we can characterize with this method is the impact of the drops. In Fig. IV.3, we present the contact times of drops of different radius while bouncing as a function of (a) the reduced acceleration Γ ($R = 0.75$ mm – $\nu = 28$ Hz), (b) the frequency ν ($R = 0.75$ mm – $\Gamma = 0.5$), and (c) the radius R ($\nu = 28$ Hz – $\Gamma = 0.5$).

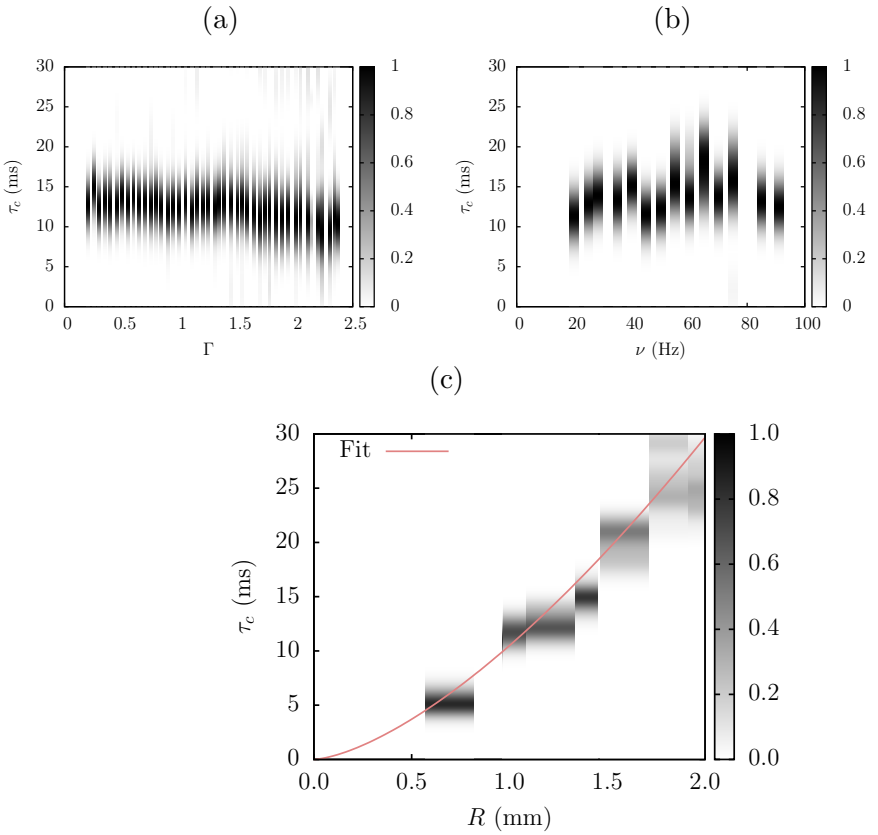

Figure IV.3: Contact time τ_c of Leidenfrost drops as function of (a) the reduced acceleration Γ ($R = 0.75$ mm – $\nu = 28$ Hz), (b) the frequency ν ($R = 0.75$ mm – $\Gamma = 0.5$), and (c) the radius R ($\nu = 28$ Hz – $\Gamma = 0.5$).

We see in Fig. IV.3(a) and (b) that the contact time is independent on the parameters of the oscillation, but dependent on the radius of the drop. A fit of our data leads to the law

$$\tau_c = 2.6 \sqrt{\frac{\rho R^3}{\gamma}} \ . \tag{IV.1}$$

This result is the same as the one found by Biance for Leidenfrost drops impacting static substrates *et al.* [5] and even the prefactor is the same. This time is very close to the time of an oscillation of a free drop in the simplest mode of deformation, *i.e.* the quadrupolar mode where the drop just elongates and flattens. In this time, initially calculated by Rayleigh, the prefactor was $\pi/\sqrt{2} \simeq 2.2$ [12]. The drops are found to have the same contact while on a static substrate and on an oscillating substrate.

Note that in Fig. IV.3(a), we see that for reduced accelerations higher than 1.5, some impacts seem to have a contact time that is around 30 ms. This unexpected and occasional doubling is due to non-linearities induced by the strong deformations of the drops, and is developped further.

IV.5 To bounce or not to bounce

Now that we know how a drop bounces on an oscillating substrate, the question that can come to one's mind is: when does a drop bounces or not ? To express that, we measure the time of flight of drops on a substrate oscillating at $\nu = 28$ Hz. In Fig. IV.4, we plot the time of flight normalized by the period of an oscillation $\tau_f/\tau_{\rm osc}$ as a function of the radius of the drops R for four different values of the reduced acceleration. For the sake of clarity, we do not plot every event as in Sec. IV.4 but rather plot the mean value observed and the standard deviation. We see that the normalized time of flight tends to 1 when the drop radius tends to 0, and that this time decreases quickly with the radius of the drops, whatever is the value of the reduced acceleration Γ for all considered values.

From what we know from Sec. IV.4, the time of flight should be simply $\tau_f = \tau_{\rm osc} - \tau_c$. Thus, using Eq. (IV.1), one obtains

$$\frac{\tau_f}{\tau_{\rm osc}} = 1 - \frac{1}{\tau_{\rm osc}} \frac{2.6\ R^{3/2}}{\ell_c\ \sqrt{g}} \ . \tag{IV.2}$$

This law is plotted without any adjustable parameter in Fig. IV.4. A good agreement with the data is observed. Thus, we can deduce that drops that are too large does not bounce. More precisely, we find the criterium

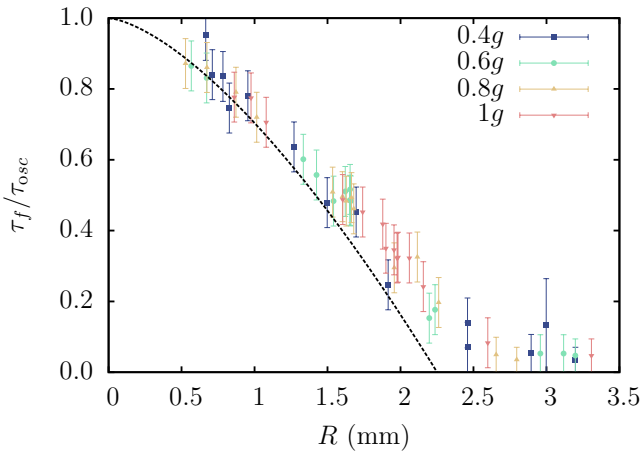

Figure IV.4: Reduced time of flight τ_f/τ_{osc} as a function of the radius of the drop. The frequency of the oscillating substrate is $\nu = 28$ Hz and four different reduced acceleration Γ are represented.

$$R = \left(\ell_c \, \frac{\tau_{\text{osc}} \sqrt{g}}{2.6} \right)^{2/3} . \tag{IV.3}$$

That criterium means that, for higher frequencies, a drop that would be too large cannot perceive the movement of the substrate and does not bounce.

IV.6 The road to non-linearities

In all bouncing systems, as in many other systems in non-linear physics, particular phenomenons tend to appear, among which the phase locking. When a system is submitted to periodic forcing, this system tends to adopt a dynamic that is periodic with a period that is the same than the period of the forcing. This phenomenon is exactly what is observed in Fig. IV.1: the drop bounces one at each oscillation of the substrate. However, it is well known that things are not always as easy. In this kind of systems, when the forcing becomes too high, another phenomenon appears...

In Fig. IV.5, the reduced time between successive impacts $\Delta t_i/\tau_{\text{osc}}$ is presented as a function of the reduced acceleration of the substrate. The frequency of the forcing is set to $\nu = 28$ Hz, and the radius of the drop is $R = 0.75$ mm. For low reduced accelerations, we can see that everything goes quite smoothly; the drop bounces once per oscillation of the substrate. However, things get

a little bit messy between $\Gamma = 1$ and $\Gamma = 1.5$: the dispersion of the Δt_i increases. Above $\Gamma = 1.5$, we see that most of the bounces have a duration of two oscillations. We call these bouncing modes according to number of oscillation of the substrate k and the number of bounces of the drop l occuring in a period of the whole dynamic of the system, and this mode will be noted (k, l). The mode below $\Gamma = 1$ is then the mode $(1, 1)$ and the main mode above $\Gamma = 1.5$ is the mode $(2, 1)$. However, we also that some bounces seem to have a duration of $\sim 1.5\tau_{\text{osc}}$ and $\sim 0.5\tau_{\text{osc}}$. This is a sign that some "big" bounces are followed by "small" bounces. This is the mode $(2, 2)$. What happens between $\Gamma = 1$ and $\Gamma = 1.5$ is a transition between the mode $(1, 1)$ and the modes $(2, 1)$ and $(2, 2)$. This transition is called a "bifurcation".

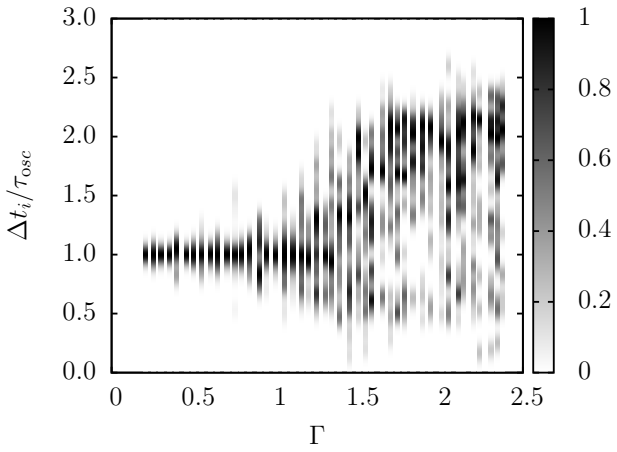

Figure IV.5: Reduced time between successive impacts $\Delta t_i/\tau_{\text{osc}}$ as a function of the reduced acceleration of the substrate with $\nu = 28$ Hz and $R = 0.75$ mm.

Note that, most of the time, a non-linear system like this one finds a mode by phase locking, and then, tends to stay in this mode if it is not perturbed. However, in our case, the contact of the drop with the substrate induces oscillations. At low reduced accelerations, these oscillations simply consist in a quadrupolar mode where the drop flattens, then elongates. However, at higher reduced accelerations, other modes tends to appear as well perturbations. These perturbations are not damped quickly because of the low viscosity of water. As a consequence, the perturbated drop changes constantly its bouncing mode.

A good example of a similar system where the drops are locked in modes

and where perturbations are locked is the system first studied by Couder *et al.* [9]. In this system, there is also a lubrication film under the drop. However, this film is not fed, but renewed at each bounce, and the substrate is not hot but is a liquid pool. In this system, things are very similar to what happens in our system. However, a few differences have to be noticed. First, the substrate deforms at least a little bit. Second, the liquids involved are usualy much more viscous than water. And third, using this viscosity, small drops, and higher frequencies, they are able to keep stable drops at larger reduced accelerations.

Denis Terwagne, during his thesis, measured the reduced time between successive impacts $\Delta t_i/\tau_{\rm osc}$ (noted $\Delta T_{\rm min}/T$) as a function of the reduced acceleration Γ [13]. The result is retranscripted here in Fig. IV.6. Increasing Γ, different bouncing modes are observed... Much more different modes can be identified compared to our system, but we can identify the mode $(1,1)$ and a bifurcation to a mode $(2,2)$ around $\Gamma = 1.5$. However, the mode $(2,1)$ is not seen at these low Γ but only above 2.5. Moreover, due to a high damping of the parasite vibrations of the drop, in one experiment, the drop is locked in a mode that is determined by the initial conditions.

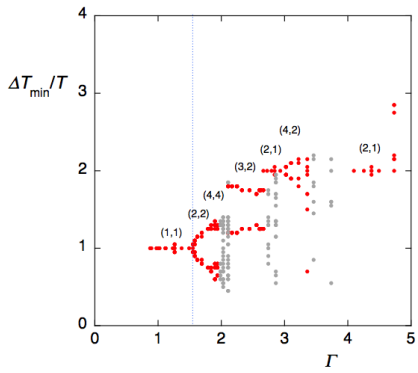

Figure IV.6: Reduced time between successive impacts $\Delta t_i/\tau_{\rm osc}$ as a function of the reduced acceleration of the substrate Γ, with $\nu = 50$ Hz and $R = 0.445$ mm. (Taken from D. Terwagne's thesis [13])

However, for the case of bouncing Leidenfrost drops, the use of viscous liquids is not possible. When they reach their boiling point, liquids tends to always reach viscosities that are of the same order of magnitude as the viscosity of water. To our knowledge, no "viscous Leidenfrost effect" has ever been reported.

IV.7 A way to switch modes

Let us now consider drops of fixed initial radius, $R = 0.75$ mm, and a gentle reduced acceleration, $\Gamma = 0.5$. If one increases the frequency ν, or in other words, decreases $\tau_{\rm osc}$, as the contact time τ_c is constant, there is a moment where the drop will be in contact for more than one period of oscillation. So the drop cannot be in a $(1, 1)$ any longer. In Fig. IV.7, we plot the reduced time between successive impacts $\Delta t_i/\tau_{\rm osc}$ as a function of the frequency ν. For low values of Γ, it appears that the drop bounce in a $(1, 1)$, as expected from what we saw at $\nu = 28$ Hz. However, above $\nu = 40$ Hz, we see a sudden change. Between $\nu = 45$ Hz and $\nu = 80$ Hz, we see that the bouncing as switched to a mode $(2, 1)$. Above $\nu = 80$ Hz, we see that there is again a sudden change. The data are less clear, but it seems that they are still close from $\Delta t_i/\tau_{\rm osc} = 3$, indicating a mode $(3, 1)$.

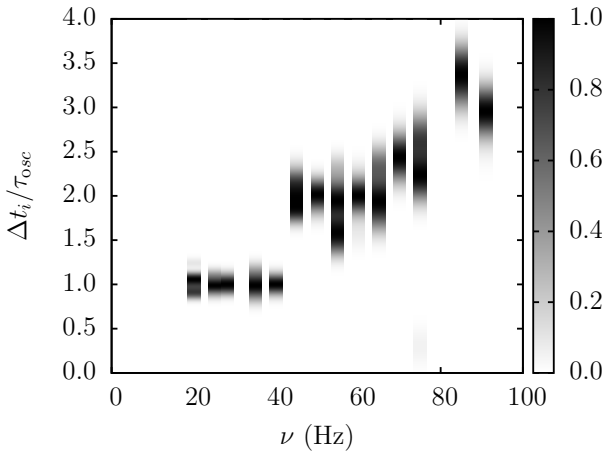

Figure IV.7: Reduced time between successive impacts $\Delta t_i/\tau_{\rm osc}$ as a function of the frequency of the substrate with $\Gamma = 0.5$ Hz and $R = 0.75$ mm. The mean value is also plotted as a guide for the eye.

In this experiment, as said previously, we used drops with a fixed radius $R = 0.75$ mm. Such a drop has a contact time $\tau_c = 13.9$ ms. If we consider the duration of an oscillation of the substrate at $\nu = 40$ Hz and at $\nu = 80$ Hz, we get $\tau_{osc} = 25$ ms and $\tau_{osc} = 12.5$ ms. Then, in our case, when the contact time becomes approximately larger than a half of the duration of an oscillation of substrate, the mode switches, and when it becomes approximately larger than a full period, the mode switches again.

IV.8 Conclusions

In this chapter, we focused on the second field of interest related to Leidenfrost drops : their mobility. We studied repeated impacts of drops on vibrated hot substrates. The experiment is reminiscent of the experiments of the bouncing ball and of the drop bouncing on vibrated liquid pools.

We demonstrated that the impact time is independent on the impact velocity and is close to the natural frequency of a drop oscillating in a quadrupolar mode. This impact time being indenpendent on the parameters of the oscillation of the substrate, we showed that large drops cannot bounce for low forcings if their impact time is larger than the period of the oscillation of the substrate.

Moreover, we showed that an increase of the reduced acceleration of the substrate leads to a bifurcation from a mode of bouncing where the drop bounces once each oscillation of the substrate to more complex behaviors. For reduced accelerations between 1.5 and 2.5, the drop tends to be in a mix between a mode with two different bounces each two oscillations, and a mode with one large bounce each two oscillations.

Finally, it appears that for a fixed volume, increasing the frequency of the oscillations also leads to a change of the bouncing mode where the drop bounces once each oscillation to a mode with one large bounce each two oscillations.

References

[1] T. Tran, H. J. J. Staat, A. Prosperetti, C. Sun, and D. Lohse. *Drop impact on superheated surfaces.* Phys. Rev. Lett., 108:036101, 2012.

[2] T. Gilet and L. Bourouiba. *Rain-induced ejection of pathogens from leaves: revisiting the hypothesis of splash-on-film using high-speed visualization.* Integr. comp. biol., page icu116, 2014.

[3] H. Minemawari, T. Yamada, H. Matsui, J. Tsutsumi, S. Haas, R. Chiba, R. Kumai, and T. Hasegawa. *Inkjet printing of single-crystal films.* Nature, 475:364–367, 2011.

[4] D. Richard, C. Clanet, and D. Quéré. *Surface phenomena: Contact time of a bouncing drop.* Nature, 417:811–811, 2002.

[5] A.-L. Biance, F. Chevy, C. Clanet, G. Lagubeau, and D. Quéré. *On the elasticity of an inertial liquid shock.* J. Fluid Mech., 554:47–66, 2006.

[6] P. Pierański. *Jumping particle model. Period doubling cascade in an experimental system.* J. Phys., 44:573–578, 1983.

[7] R. M. Everson. *Chaotic dynamics of a bouncing ball.* Physica D, 19:355–383, 1986.

[8] J.-Y. Chastaing, E. Bertin, and J.-C. Géminard. *Dynamics of a bouncing ball.* Am. J. Phys., 83:518–524, 2015.

[9] Y. Couder, E. Fort, C.-H. Gautier, and A. Boudaoud. *From bouncing to floating: noncoalescence of drops on a fluid bath.* Phys. Rev. Lett., 94:177801, 2005.

[10] D. Terwagne, N. Vandewalle, and S. Dorbolo. *Lifetime of a bouncing droplet.* Phys. Rev. E, 76:056311, 2007.

[11] B. T. Ng, Y. M. Hung, and M. K. Tan. *Suppression of the Leidenfrost effect via low frequency vibrations.* Soft matter, 11:775–784, 2015.

[12] Lord Rayleigh. *On the capillary phenomena of jets.* In Proc. R. Soc. London, volume 29, pages 71–97, 1879.

[13] D. Terwagne. *Bouncing droplets, the role of deformations.* PhD thesis, Université de Liège, 2012.

V

Impact on a liquid pool

A way to not extinguish an oil fire

V.1 Preamble

In Chapter III, we saw that a drop can be deposited on a liquid substrate at a temperature that is just above the boiling point of the drop and experience a Leidenfrost effect. While explaining the experimental methods, we specified that the drops were deposited "gently". Indeed, when a drop was dropped from a large height, we observed that the impact was not producing a Leidenfrost drop, and the substrates seemed to be unaffected after the stabilization of its interface. The point of this chapter is precisely to explain what happens when the drop is not deposited gently.

The study of impacts on liquid pools (either impacting drops or impacting solids) is an old issue and has seen a lot of improvements over the past century since the pioneering work of Worthington and Cole [1]. The case of superhydrophobic spheres is close from what we imagine at the first thought of the impact of a Leidenfrost drop. Indeed, a Leidenfrost drop is a perfectly non-wetting drop as stressed many times in this manuscript. We can then imagine similar behaviors. Recently, the case of solid sphere impacts has been extensively studied by Duclaux *et al.* and Aristoff *et al.* for constant-speed and decelerating spheres respectively [2, 3]. In both case, the impacts exhib-

ited various morphologies of impacts. The impact of the wetting properties of these spheres by the liquid of the pool has also proved to be significant.

However, as explained, the Leidenfrost drops disappears when the impact height is too high. This means that either the drop evaporates quickly, or the drop merges with the substrate. In both cases, there is a contact between both fluids which means that the Leidenfrost effect is suppressed. The situation is then similar to the one produced by the impact of a drop on another liquid. In this situation, the drop is perfectly wetting the substrate wether there is a quick evaporation or a mix.

Thus, in this chapter, we describe how this transition between a perfectly non-wetting state to a perfectly wetting state happens. We first present the experimental procedure. Then, we describe qualitatively the different behaviors of the drop and of the substrate as the impact velocity of the drop increases. After that, we describe the conditions for reaching the different behavior observed. Finally, we describe quantitatively the different regimes and build models for the description of the regimes themselves and for the transitions between them.

V.2 Experimental details

The base of the setup was the setup used in Chapter III. However, a few differences can be noted. As one of the main control parameters is the velocity of the impacting drop, U_0, we had to control the height at which the drop was released. We used a vertical rail with a millimetric rule printed on and with a syringe attached on the mobile part. Under the syringe, we placed a liquid pool with a depth that was much larger than the depth of interest in our experiments. Practically, the depth of the pool was between 20 mm and 40 mm. Also, in this chapter, as the typical time of an impact was about a tenth of seconds, we used a fast camera with a side view and a frame rate up to 5000 frames per second to capture the dynamics of the impact, either to simply observe and determine the regime of impact, or catch the whole dynamic.

In this chapter, we used the HFE–7100 as the liquid of the drops. This liquid has the advantage to boil at a relatively low temperature ($T_{\text{sat}} = 58.5°\text{C}$), and thus, to allow to explore larger range of temperatures than the ethanol.

As we explored the dynamic of a drop entering an oil pool, we expected strong effects of the viscosity of the oil pool. Thus, we used various viscosities

in these experiments. The oils are named V5, V20, V50 and V100 and their measured viscosities at 25°C were measured in viscometer in a Couette geometry, and were respectively 5.86, 21.2, 50.6 and 90.5 mPa.s. These viscosities evolves with temperature T following the empirical law

$$\eta(T) = \eta(T_0) \exp\left(B\left(\frac{1}{T} - \frac{1}{T_0}\right)\right) \tag{V.1}$$

where T_0 is the temperature of the reference. Temperatures have to be expressed in kelvins. B is an empirical factor and its value is 1683 K. That empirical law is found in the datasheet of the silicone oils Rhodorsil 47 [4], and is in good agreement with our measurements (see Fig. V.1).

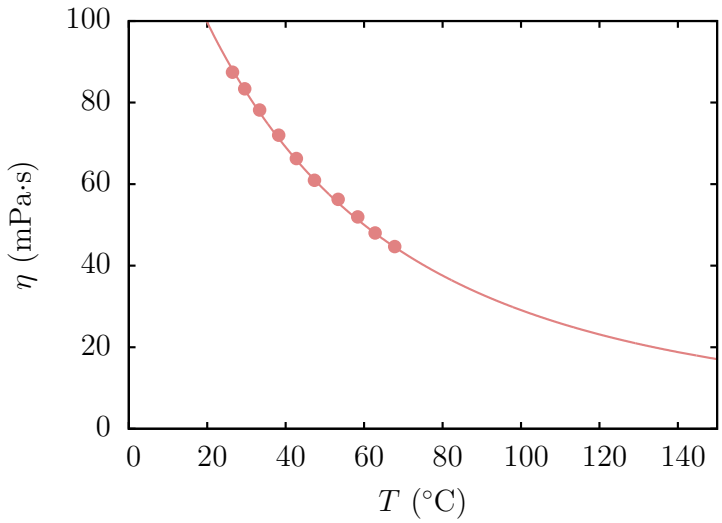

Figure V.1: Variation of the viscosity of one of the oils used (V100) with the temperature. The points represent the measurements and the line is a fit by Eq. (V.1).

V.3 Qualitative observations

Four different regimes of impact can be distinguished. Before anything else, let us describe them by their order of apparition when we increase the velocity of the drop at the impact. In these first example, the experimental conditions are kept constant except for the impact velocity : the radius of the drops is $R = 0.56$ mm, the silicone oil is the V20 and the temperature of the pool is $T_p = 100$°C ($\Delta T = 41.5$°C).

Bouncing This first regime is what happens when you deposit a drop gently on the hot pool to make a Leidenfrost drop like those observed and described in Chapter III. The drop approaches the substrate, begins to deform it, eventually forming a column if the drop penetrates deep enough. Then, the surface tension of the pool tends to diminish the size of the cavity that is formed. That propels the drop that further comes back with less energy because of dissipation. After a few numbers of bounces (typically, one or two), the drop stabilizes as a drop in Leidenfrost on a liquid pool. Figure V.2 shows a top view (a) and a side view (b) of this bouncing phenomenon. The impact velocity is 0.5 m.s^{-1} in both cases, and the interval between the frames is 10 ms in (a) and 4 ms in (b).

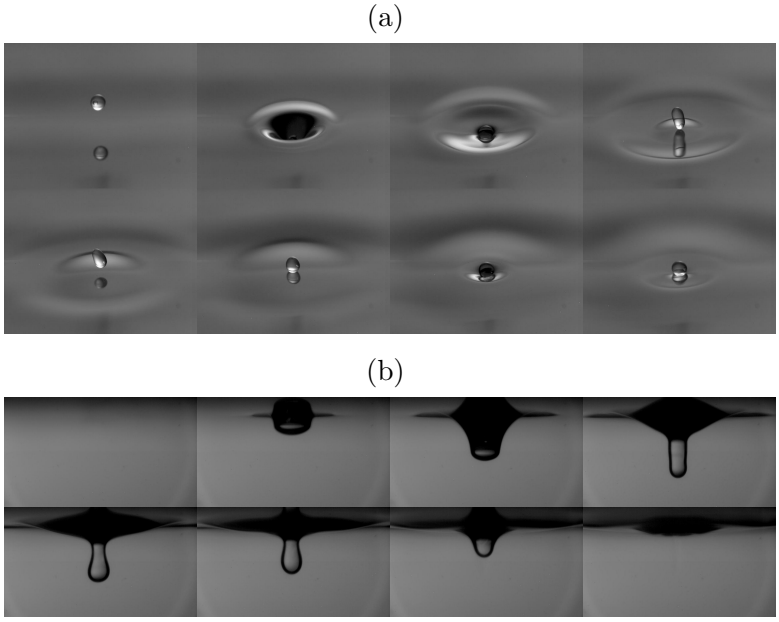

Figure V.2: HFE–7100 drops bouncing on a pool of silicone oil. (a) Top view and (b) side view showing a drop with radius $R = 0.56$ mm impacting a pool of silicone oil V20 at a temperature $T_p = 100°C$. The impact velocity is 0.5 $m.s^{-1}$ and the interval between the frames is 10 ms in (a) and 4 ms in (b).

Antibubble When a similar drop impacts the pool a bit faster, the column formed by the impact of the drop may deform between the drop and the level of the undeformed surface and pinch-off. When this pinch-off occurs, the drop is surrounded by a complete film of vapor that is a mix of some air and some

vapor of HFE–7100. This film is very thin at the beginning (about the typical size of the film under a Leidenfrost drop), but expands quickly due to the evaportation of the drop that is surrounded by the hot oil. Figure V.3 shows a snapshots of a sideview. The impact velocity is larger than in the bouncing regime and is $U_0 = 0.75$ m.s^{-1}.

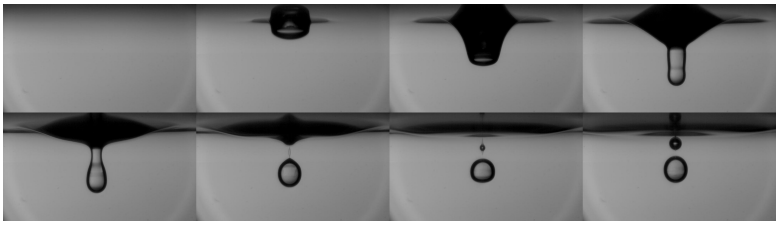

Figure V.3: Side view of a drop of HFE–7100 impacting on a pool of silicone oil and forming a thermal antibubble. The drop has a radius $R = 0.56$ mm and impacts a pool of silicone oil V20 at a temperature $T_p = 100°C$. The impact velocity is 0.75 $m.s^{-1}$ and the interval between the frames is 4 ms.

This phenomenon is reminiscent of the antibubbles first studied by Dorbolo *et al.* [5]. Jets of soapy water entering a pool of the same fluid can entrain some air, form a column that destabilizes at a point. That entraps a liquid drop in a thin layer of air that is itself surrounded by the liquid of the pool. Even though the phenomenon has been studied, there is still some ongoing research about some specificity of the impact of the physico-chemistry of the interfaces of these objects on their lifetime [6]. Indeed, these objects should not last long if you consider that you have a drop falling into a gazeous phase. However, due to the nature of the interfaces between air and soapy water, the drainage takes a long time and the lubrication is able to prevent the coalescence of the drop with the surrounding pool.

In our case, the situation is slightly different. Drainage is much more efficient, but the film under the drop is fed just like in the usual Leidenfrost effect. In a way, we have a kind of a *thermal antibubble*. This thermal antibubble is initially more dense than the liquid of the pool because of the density of the HFE–7100 ($\rho_d = 1400$ kg.m^{-3}). Thus, the antibubble tends to sink. However, as the drop inside the antibubble is evaporating, the global density of the object decreases and the antibubble finally comes back to the top of the pool. The time for such a drop to come back to the surface is typically of the order of a second.

Film breaking The third regime appearing when the impact velocity is even more increased is very similar to the antibubble regime. Indeed, when the pinch-off occurs, a little wave is emitted where the film closes, at the top of the antibubble. When the impact velocity is sufficient, this wave can disrupt the vapour film surrounding the drop. If that happens, the oil wets the drop inside the antibubble, and the drop begins to evaporate quickly and some bubbles appear. However, everything is not clear as a part of the drop seems to sink in the pool without boiling. The impact velocity is larger than for the bouncing and antibubble regimes, and is $U_0 = 0.9$ m.s^{-1}. A snapshot is shown in Fig. V.4 with an interval between the frames of 4 ms.

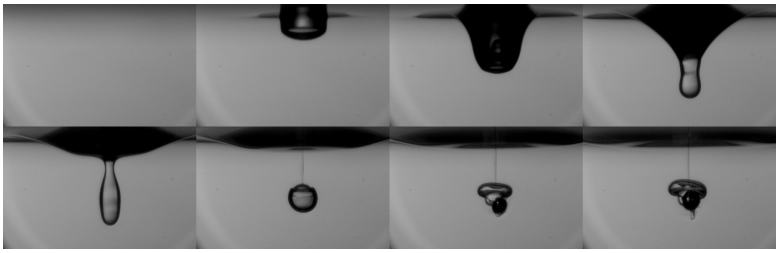

Figure V.4: A thermal antibubble is destroyed by the rupture of the vapor film by a wave emitted at the pinch-off. The drop has a radius $R = 0.56$ mm and impacts a pool of silicone oil V20 at a temperature $T_p = 100°C$. The impact velocity is 1.5 $m.s^{-1}$ and the interval between the frames is 4 ms.

This regime is a transition regime between the antibubble regime, and the last regime (direct contact regime), and has not been extensively studied because of its complexity that requires a deep understanding of the pinch-off mechanism, of the wave generation, and of the geometry of the vapor film in a dynamic situation. This is far beyond the scope of the present thesis.

Direct contact Finally, for the largest velocities, the dynamics is very different. Indeed, when the drop approaches too fast, the drop has no time to generate a vapor film and touches immediately the pool. Doing so, the drop tends to wet the surface of the pool at the same moment when its kinetic energy is released in this surface. The energy release creates a cavity that is almost hemi-spherical and that is completely similar to those created by the explosion of firecrackers at the surface of liquid pools [7]. While this cavity is created, the drop spreads inside. When the cavity finally retracts, the drop leaves a *flower* of liquid HFE–7100 where some bubbles are sometimes created, and that latter sinks to the bottom of the pool. However, just as in the film breaking regime, most of the HFE–7100 that stays in the pool tends to sink.

In Fig. V.5, we show a snapshot of such impact with an interval between the frames of 4 ms and an impact velocity $U_0 = 1.2$ m.s^{-1}.

Note that this phenomenon is really similar to what happens when one tries to extinguish a fire on an oil pool with water. The kinetic energy is such that the water penetrates the pool, leading to rapid evaporation and bubbles of vapor popping at the surface of the pool, ejecting droplets of burning oil.

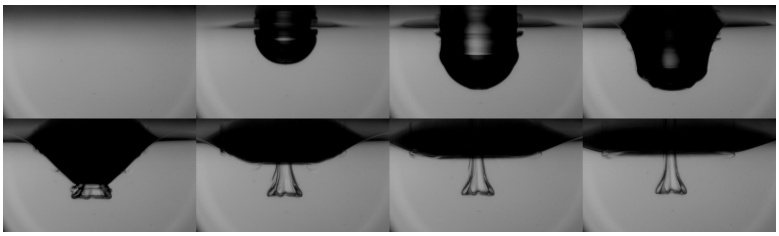

Figure V.5: A drop impacts the pool too fast to allow the creation of a vapor film, and thus directly contacts it. The drop has a radius $R = 0.56$ mm and impacts a pool of silicone oil V20 at a temperature $T_p = 100°C$. The impact velocity is 1.2 $m.s^{-1}$ and the interval between the frames is 4 ms.

Based on that, the following can be divided into three parts. First, we give the range of parameters (superheat and Weber number) in which these phenomenons are observed through phase diagrams. Second, we give the dynamic description of the different regimes, *i.e.* how the drop penetrates, how the cavity expands, how the drop behaves... Third, we explain what are the key elements that leads to the transitions from one regime to another.

V.4 Phase diagrams

In our experiments, the most important dimensionless number that we can build is the Weber number. Indeed, the Weber number compares the kinetic energy of an element of the system to the energy of the deformation of an element of the system. However, the one we use is not the common one. Quite regularly, the Weber number is meant to characterize the deformation of the drop during an impact. In most of the cases we studied, the drops are small and their speed is not sufficient to deform them a lot. The liquid substrate is much more affected by the impact. Thus, what we want to compare is the kinetic energy of the drop $E_k \propto \rho_d R^3 U_0^2$ and the energy associated to the deformation of the pool. This energy, for a deformation of a typical size of R, the radius of the drop impacting, scales as $E_d \propto \gamma_p R^2$. The Weber number

writes

$$\mathrm{We} \;=\; \frac{\rho_d \; R \; U_0^2}{\gamma_p} \;. \tag{V.2}$$

We saw previously that increasing the impact velocity leads to different regime. Thus, we can associate a threshold We for each transition from one regime to the other. However, as the Leidenfrost effect is involved in these impacts, we expect *a priori* that the threshold Weber numbers for the transitions between the different regimes change depending on the temperature. In Fig. V.6, we plot the threshold Weber number above which we observe the antibubble regime (blue dots - We_a), above which the antibubble regime turns into the film breaking regime (green dots - $\mathrm{We}_{\mathrm{f.b.}}$), and above which the direct contact regime takes place (red dots - $\mathrm{We}_{\mathrm{d.c.}}$), as a function of the superheat ΔT.

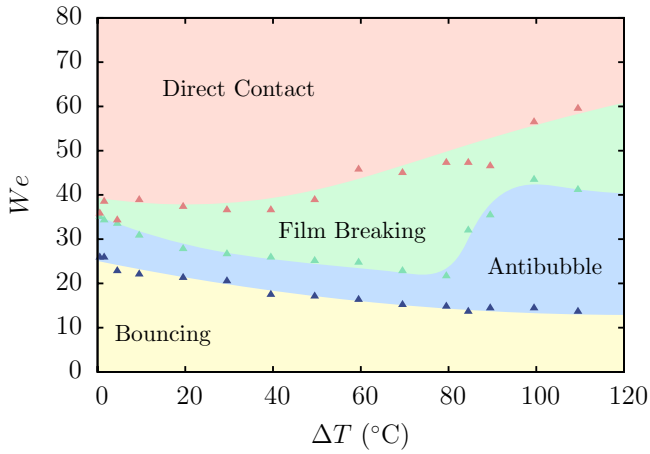

Figure V.6: Threshold Weber numbers associated to the transitions between the four regimes of impact as a function of the superheat ΔT. The drops are made of HFE–7100 and have a radius $R = 0.56$ mm. The pool is made of silicone oil V20.

We see that the higher temperature, the lower is the minimal Weber number to get an antibubble, even though the decrease is quite slow. At the opposite, to have a direct contact between the drop and the pool, the higher is the temperature, the higher needs to be the Weber number.

Although this kind of phase diagrams is very intuitive and gives a good idea of the range of parameters for which the different phenomenons are ob-

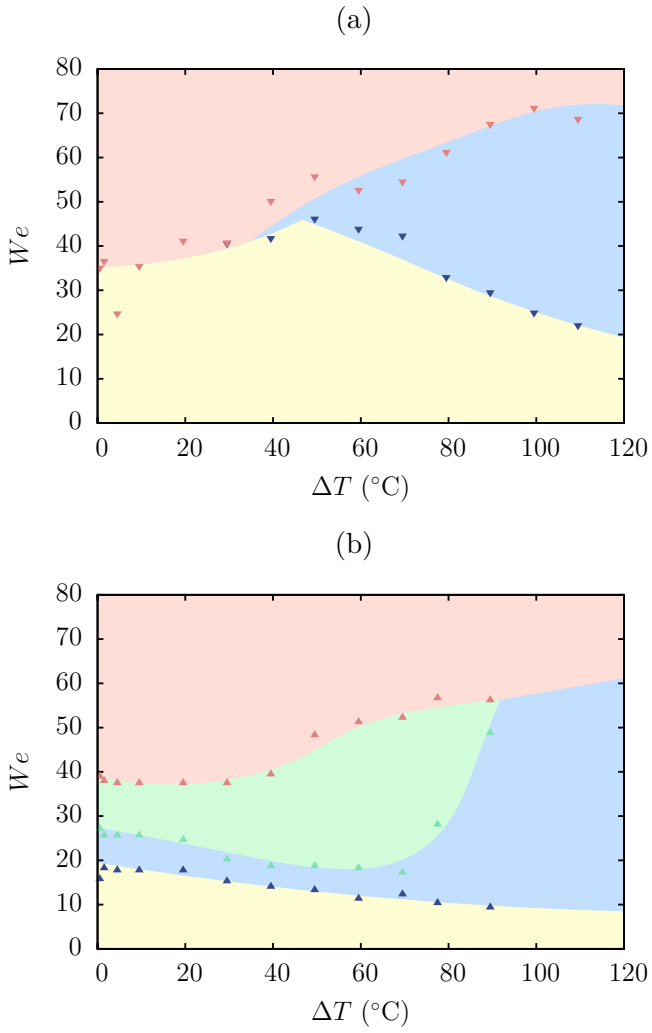

Figure V.7: Threshold Weber numbers associated to the transitions between the four regimes of impact as a function of the superheat ΔT. The drops are made of HFE–7100. (a) Radius of the drop $R = 0.56$ mm and silicone oil V100. (b) Radius of the drop $R = 0.73$ mm and silicone oil V20.

served, they are not universal. If we change the viscosity of the pool, or the radius of the drop, the phase diagram changes quite a lot. Indeed, in Fig. V.7, we plot the same plot as in Fig. V.6 with the same experimental parameters except for the oil of the pool (silicone oil V100) in Fig. V.7(a), and for the radius of the drop ($R = 0.73$ mm) in Fig. V.7(b). The result is clear: the

limits between the different regimes can change drastically, some regimes may even disappear and some are not present at any superheat.

Thus, we see that we cannot handle the mechanisms behind the transitions through phase diagrams, and make the data collapse on single curves for each of these transitions. To understand what are the key ingredients of the transitions, we first have to describe quantitatively the different regimes.

V.5 Description of the regimes and of what drives the transitions

V.5.1 Bouncing on a pool

To understand the interaction between the impacting drop and the pool in the bouncing regime, we have to look at the deformation of the pool. Especially, we are interested in the vertical position of the point of the surface that is just under the drop, where the deformation is the maximal. Following the notations of Chapter III, we note this deformation e_{center}. In Fig. V.8(a), we plot this deformation as a function of time. The oil used is a silicone oil V20 at $T_p = 82°\text{C}$ (equivalent to a superheat $\Delta T = 24°\text{C}$). The radius of the drop is $R = 0.56$ mm and the impacting velocities are included between 0.195 m.s^{-1}

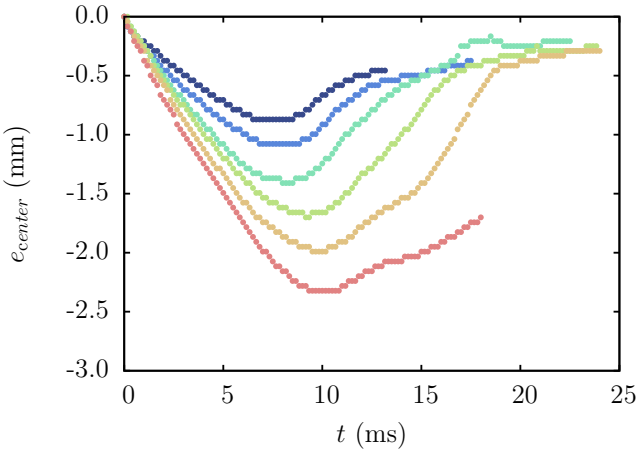

Figure V.8: Position of the surface below the drop during an impact in the bouncing regime. The impact velocities are comprised between 0.195 $m.s^{-1}$ (dark blue) and 0.359 $m.s^{-1}$ (light red), the drop radius is $R = 0.56$ mm, and the pool is made of silicone oil V20 and is at $T_p = 82°C$ (equivalent to $\Delta T = 24°C$).

(dark blue) and 0.359 m.s^{-1} (light red).

From these curves, there are two observables that we can extract: the maximum depth reached by the drop $z_{\max}$ and the time to reach this depth $t_{\max}$. In Fig. V.9, we plot these two quantities as a function of the Weber number of the impact, for impacts on a pool of silicone oil V20 with drops of radius $R = 0.56$ mm. We show that both $z_{\max}$ and $t_{\max}$ increase while the Weber number increases. Moreover, the lines in Fig. V.9(a) are linear fits of the data for the three different temperatures. We then have a correlation $z_{\max} = a + b'$ We. This is coherent with the fact that a drop just above the surface of the pool with an impact velocity $U_0 = 0$ m.s^{-1} still penetrates the pool as shown in Chapter III. Moreover, it appears that $b' = b$ Oh$^{-2/3}$, with $b = 0.019$ mm. The highest is the kinetic energy of the drop, the lowest is the viscosity and the surface tension, the deepest the drop penetrates the pool.

To model the impact of these drops in the Leidenfrost state, we have to make a few assumptions. The drop is assumed to stay spherical during the collision, and the variations of the thickness of the vapor film (that is of the order of 10 µm) are negligible in front of the radius of the drop (of the order of 1 mm). Then, we have simply that the position of the bottom of the drop z_{bot} is equal to the postion of the lowest point of the surface e_{center}, and the center of mass of the drop z_{CM} is the postion of the lowest point of the surface e_{center} plus a shift corresponding to the radius of the drop R. In a very general way, the equation of motion of the interface while the droplet penetrates the pool can be written as

$$(M_d + M_{\text{add}}) \frac{\mathrm{d}^2 z_{\text{bot}}}{\mathrm{dt}^2} = M_d\, g + F_\gamma + F_d + F_b \qquad \text{(V.3)}$$

with M_d and M_{add} being respectively the mass and the added mass of the drop, and the four forces acting on the drop being the weight, the surface tension force that resultates from the deformation of the pool, F_γ, the drag force due to inertial and viscous friction, F_d, and the buoyancy force caused by the formation of a cavity made of air, vapor and the drop, F_b. Let us describe the three last forces. First, the surface tension force generated by the deformation of the pool can be approached with a linear spring model. This leads to a force $F_\gamma = -\gamma_p e_{\text{center}}$. Gilet and Bush showed that this linearity of the force with the displacement of the interface stays valid until a pinch-off in the case of a drop impacting a soap film [8]. Second, the drag force is probably the most complex to describe. This drag force on an object that evolves in a fluid is not as simple as the Stokes force when the object is a fluid object [9]. Here, the situation is even more complex as a drop is surrounded by a thin

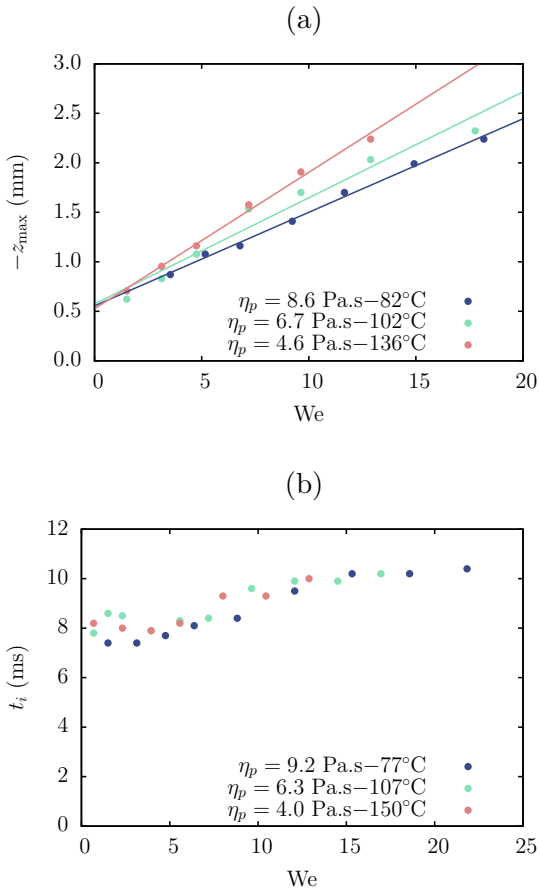

Figure V.9: (a) Maximum depth reached by the drop $z_{\max}$ and (b) time to reach this depth $t_{\max}$ in the bouncing regime on a pool of silicone oil V20 at three different temperatures, for a drop of radius $R = 0.56$ mm as a function of the Weber number. (a) The lines corresponds to linear fits of the data for the three different temperatures.

layer of gas, and the whole object penetrates an interface. However, we can write this force as

$$F_d = -\frac{1}{2}\rho_p \, \pi R^2 \, C_d \, \dot{z_{\text{bot}}} \, |\dot{z_{\text{bot}}}| \tag{V.4}$$

with C_d being the drag coefficient. Generally speaking, this coefficient depends on the Reynolds number $\text{Re} = \rho_p R|\dot{z_{\text{bot}}}|/\eta_p$. However, this dependency is not trivial. Here, we assume that the object that penetrates the pool is a bubble of radius R. This is true in the sense that there is always a gas layer between the drop and the pool in this regime. For such object [9], the drag coefficient

takes the form

$$C_d = \frac{8}{\mathrm{Re}} \left[1 + \left(\frac{4}{\mathrm{Re}} + \frac{1}{2} \left(1 + \frac{2.344}{\sqrt{\mathrm{Re}}} \right) \right)^{-1} \right] . \tag{V.5}$$

The last force is the buoyancy. Assuming that the cavity created is a cylinder of radius R and depth z_{bot}, the buoyancy force can be expressed as $F_b = \rho_p \pi R^2 z_{\mathrm{bot}} g$. Combining all these forces, Eq. (V.3) becomes

$$\begin{aligned} (M_d + M_{\mathrm{add}})\, \ddot{z}_{\mathrm{bot}} = M_d\ g - \gamma_p z_{\mathrm{bot}} \\ - \frac{1}{2} \rho_p \pi R^2\ C_d\ \dot{z_{\mathrm{bot}}} |\dot{z_{\mathrm{bot}}}| + \rho_p\ \pi R^2 g\ z_{\mathrm{bot}}\ . \end{aligned} \tag{V.6}$$

The added mass can be expressed as $M_{\mathrm{add}} = C_m \tilde{\rho} M_d$, with C_m being the added mass coefficient and $\tilde{\rho} = \rho_p / \rho_d$ being the ratio of densities. This coefficient has a value depending on the geometry of the problem. In our case, we follow the case of an hydrophobic sphere entering a water pool, studied by Aristoff and Bush [10]. We then define the ratio between the mass of the drop and the sum of the mass of the drop and its added mass, $C_g = 1/(1 + \tilde{\rho} C_m)$, and the characteristic capillary time of a drop of the liquid of the pool $\tau_p = \sqrt{4\pi R^3 \rho_p / 3\gamma_p}$. Dividing all terms by the factor $M_d + M_{\mathrm{add}}$, we get

$$\ddot{z}_{\mathrm{bot}} = C_g\ g - \frac{\tilde{\rho}\ C_g}{\tau_p^2} z_{\mathrm{bot}} + \frac{3g\tilde{\rho}\ C_g}{4R} z_{\mathrm{bot}} - \frac{3\tilde{\rho}\ C_d\ C_g}{8\ R} \dot{z_{\mathrm{bot}}} |\dot{z_{\mathrm{bot}}}| . \tag{V.7}$$

In this equation, the blue, green, yellow and red terms are respectively the gravity, surface tension, buoyancy, and friction terms.

In Fig. V.10, we show the results of this model compared with experiments for a pool of silicone oil V20 and a drop of radius $R = 0.56$ mm. The lines come from the integration of Eq. (V.7) without any adjustable parameter. As boundary conditions, we use $z(0) = 0$ and $\dot{z}(0) = U_0$, the impact velocity, extracted from linear fits of the early times of experimental data. The agreement is not really satisfactory even though the orders of magnitude of the maximum depth reached by the drop z_{max} and the time to reach this depth t_{max} resulting from the model are the same as the ones found experimentally. Especially in the case of the time to reach the maximum depth, the tendency is not correct. Indeed, this time decreases when the impact velocity increases, in the theory, while we observe an increase in the experiments. This is illustrated in Fig. V.11 where we show (a) $-z_{\mathrm{max}}$ as a function of the impact velocity and (b) t_{max} as a function of the impact velocity. The points represent different experiments. The curves represent the prediction of the model obtained by

integrating numerically Eq. (V.7) for different values of U_0.

If we try to guess where the deviations come from, we have to understand the role of the different terms. The main term is the surface tension term. If this term was the only one, the time $t_{\max}$ would be constant and proportionnal to τ_p. At least, it is the case for a force linear with z_{bot}. However, this force should deviate from this linearity for large deformations of the pool. Our model seems to give better predictions at high impact velocities where the non-linear effects should be the most significant. Thus, the non-linearities of the surface tension do not seem to be our problem. The buoyancy term is also linear in z_{bot}. Thus, taking the buoyancy term into account also gives a constant $t_{\max}$. That value is represented by the dashed line in Fig. V.9(b). We observe that the order of magnitude of this value is in agreement with our measurements.

Nonetheless, the influence of the two other terms (gravity and friction) is to induce a decrease of the time to reach the max depth when the impact velocity is increased. However, their actions are disctinct. At high impact velocities, adding the gravity term does not change the tendancy given by the surface tension and buoyancy terms. However, at low velocities, higher values are found for $t_{\max}$. At the opposite, adding the friction term does change the trend at low impact velocities, but reduces $t_{\max}$ at high impact velocities.

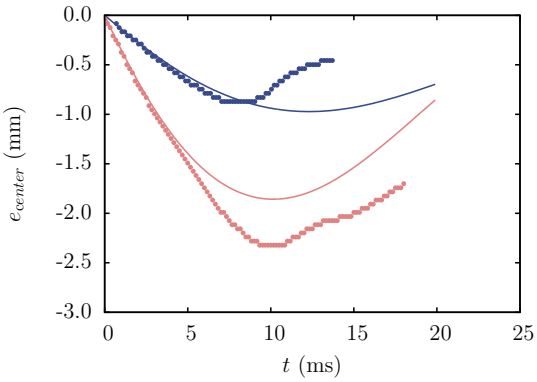

Figure V.10: Position of the surface below the drop during an impact in the bouncing regime. The impact velocities are 0.195 $m.s^{-1}$ *(dark blue) and* 0.359 $m.s^{-1}$ *(light red), the drop radius is* $R = 0.56$ *mm, and the pool is made of silicone oil V20 and is at* $T_p = 82°C$. *The model is represented without any adjustable parameter by the plain curves.*

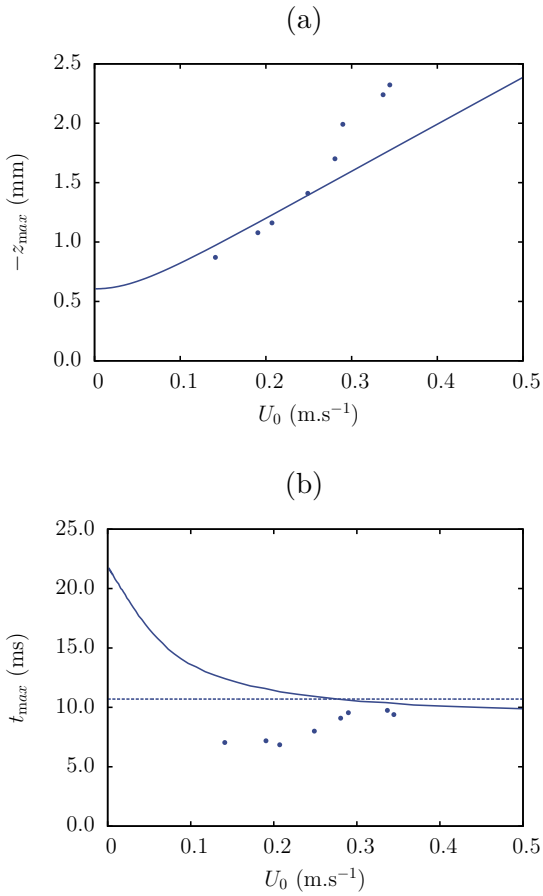

Figure V.11: (a) Maximum depth reached by the drop $z_{\max}$ and (b) time to reach this depth $t_{\max}$ in the bouncing regime on a pool of silicone oil V20 at $T_p = 82°C$, for a drop of radius $R = 0.56$ mm, as a function of the impact velocity. The lines represent the $z_{\max}$ and $t_{\max}$ resulting from the numerical integration of Eq. (V.7) while the points are experimental data.

Thus, none of these terms, as they are written there, can lead to an increase of the time to reach the max depth when the impact velocity increases. The weight term is quite obvious and cannot be modified. The only possibilities that we have are the modification of the buoyancy term to take into account a more complex deformation of the surface, but this can be hardly expressed in terms of analytical functions, and the modification of the drag coefficient to take into account the fact that the drop penetrates an interface and is not a bubble, but a drop surrounded by a vapor layer on its lower front.

V.5.2 A pinch-off for an antibubble

When an antibubble forms, the beginning of the impact is exactly the same as one in the bouncing regime: the drop creates a cavity that has the shape of a column. Of course, such a column is not stable because the surface energy and the potential energy are increased compared to an unperturbed surface of the pool. Moreover, when a long column of a fluid is immersed into another fluid, we can expect that a Rayleigh-Plateau-like instability occurs and destabilizes that column, leading to a pinch-off. In this phenomenon, there is no apparent reason that the temperature should play a role. Typically, in the non-viscous case, only the size of the column determines the wave length of the instability [11]. In this process, the role of the drop is to create the cavity, not to destabilize it.

Here, we assume that the column destabilizes when its height, $z_{\max}$, is above the selected wavelength in the viscous case of the Rayleigh-Plateau instability. The associated wave number has been calculated by Chandrasekhar [12], and is given by

$$k_{\max} \;=\; \frac{1}{R}\,\sqrt{\frac{1}{2+\sqrt{18}\;\mathrm{Oh}}} \tag{V.8}$$

where Oh is the Ohnesorge number, which is defined by $\mathrm{Oh} = \eta_p/\sqrt{\rho_p\gamma_p R}$. This number compares the surface tension effects with the viscous effects. In our case, Oh is always smaller than 1 and the viscous correction in Eq. (V.8) is always small, but non-negligible. As we assume that we have a single wave length between the surface of the pool and the depth of the cavity at which we observe its destabilization. Then, we can identify $k_{\max} = 2\pi/z_{\max}$, and find

$$z_{\max} \;=\; 2\pi\,\sqrt{2}\,R\,\sqrt{1+\frac{3}{\sqrt{2}}\;\mathrm{Oh}}\;. \tag{V.9}$$

In Fig. V.12, we show the maximal depth reached by the surface of the pool $z_{\max}$ as a function of the second term of Eq. (V.9). Data are shown for pools of two different oils (V10 and V20) and for various temperatures T_p. We also represent the data for drops of size $R = 0.74$ mm (large drops) and $R = 0.56$ mm (small drops). We see that the data collapse on one single curve, but the prefactor is half of the expected one. This deviation may have several origins among which the finite size of the column and the fact that the outer

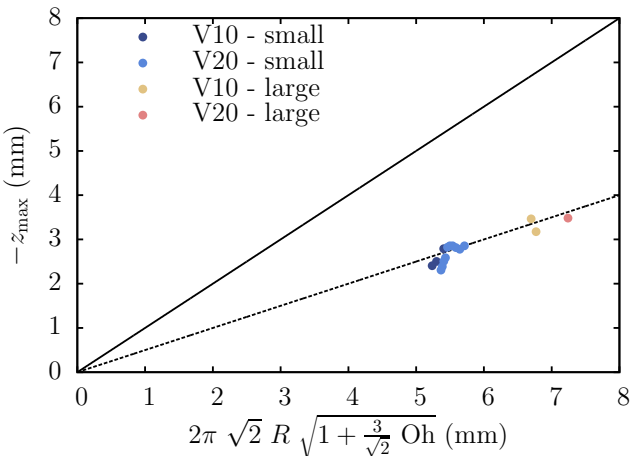

Figure V.12: Threshold depth reached by the surface of the pool before the transition to the antibubble regime, $z_{\max}$, as a function of the radius of the drop R, corrected by a factor coming from the resolution of the Rayleigh-Plateau problem with a viscous filament.

fluid is denser than the inner fluid of the column.

Note that we only did experiments with a small range of sizes of drops (around the capillary length of the liquid) due to the way they were made (using a syringe). Moreover, as the viscous correction in Eq. (V.9) is quite small, the interpretation of the destabilization of the column by a viscous Rayleigh-Plateau instability must be taken with care.

As explained in Sec. V.5.1, in the bouncing regime, we found the experimental correlation

$$-\,z_{\max}\ =\ a\ +\ b\ \mathrm{Oh}^{-2/3}\ \mathrm{We}\ . \tag{V.10}$$

Thus, combining Eq. (V.9) and (V.10), one finds out a semi-empirical law for the threshold value of the Weber number above which the impact of a Leidenfrost drops creates an antibubble.

$$\mathrm{We}\ =\ \frac{\mathrm{Oh}^{2/3}}{b}\ \left[\pi\ \sqrt{2}\ R\ \sqrt{1+\frac{3}{\sqrt{2}}\ \mathrm{Oh}}\ -\ a\right] \tag{V.11}$$

To test this result, in Fig. V.13, we plot the threshold Weber number We_a as a function of the Ohnesorge number of the pool Oh. We show the data for

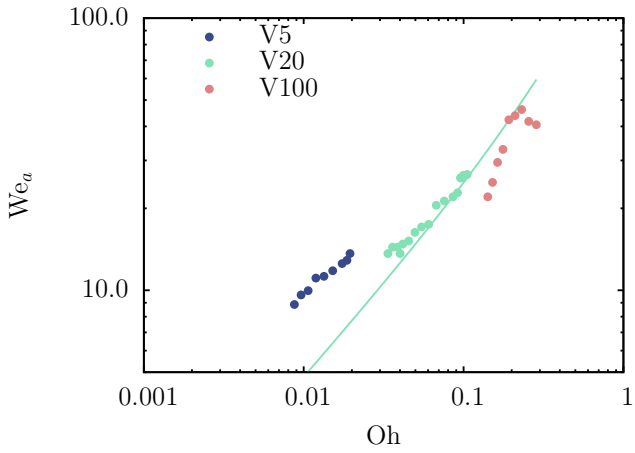

Figure V.13: Threshold Weber number above which antibubbles are created We_a *as a function of the Ohnesorge number of the pool* Oh *for three kinds of oil and various temperatures. The green curve is the plot of Eq. (V.11).*

three different oils (V5, V20, and V100) and for various temperatures between $T_p = 60°\mathrm{C}$ and $T_p = 160°\mathrm{C}$. Additionally, we plot the curve of Eq. (V.11) using the values of a and b found for the case of drops

V.5.3 The life of thermal Antibubbles

In the antibubble regime, the drop spends most of its time encapsulated in a growing bubble of vapor. Because of the high density of the HFE–7100 and the impact velocity, the antibubble tends to first sink. Then, as the antibubble grows and as the global density of the object decreases, the antibubble goes up to the surface. This is represented in Fig. V.14: a drop of $R = 0.56$ mm creates an antibubble in a pool of silicone oil V20 at $T_p = 119°\mathrm{C}$. The first image corresponds to the moment of the pinch-off. The scale bar represent 5 mm and the interval between the frames is 15 ms.

In Fig. V.15, we show the measured vertical trajectories of the center of mass of antibubbles z_{CM}. These antibubbles are created by drops of radius $R = 0.56$ mm, with three different impact velocities (see legend). The pool is made of silicone oil V20 at $T_p = 160°\mathrm{C}$. Note that the temperature is measured at the top of the pool. However, small thermal gradients exist in the pool. Typically, at the lowest point reached by the antibubbles, the temperature may be up to 5°C above the temperature of the top of the pool. In the following analysis, we neglect that small gradient ($\simeq 0.5°\mathrm{C.mm}^{-1}$) that

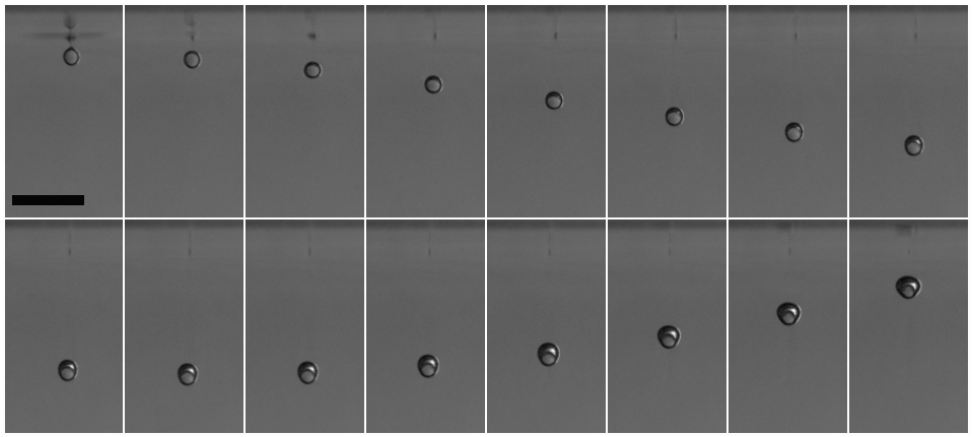

Figure V.14: A snapshot of an antibubble created by impacting a drop of HFE–7100 with radius $R = 0.56$ mm on a pool of silicone oil V20 at $T_p = 130°C$ with an impact velocity $U_0 = 0.48$ $m.s^{-1}$. The scale bar represents 5 mm and the interval between the frames is 15 ms.

induces only small variations of the physical characteristics of the silicone oil. In Fig. V.15, we see that drops impacting with higher velocities reach higher depths. This is due to the fact that the residual velocity that they keep after the pinch-off is higher.

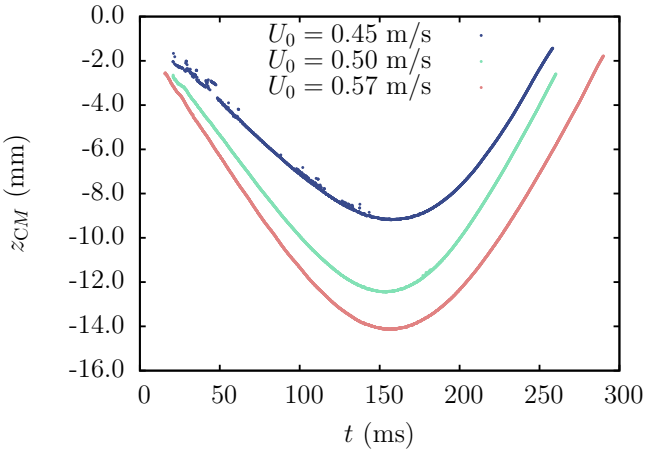

Figure V.15: Experimentally measured vertical trajectories of three thermal antibubbles made drops of radius $R = 0.56$ mm, with three different impact velocities, in a pool of silicone oil V20 at $T_p = 160°C$.

These trajectories are complicated to fully modelize. Indeed, one has to understand how the drop evaporates to know how the buoyancy acts on the antibubble. However, the problem of the evaporation of a thermal antibubble is already complicated because the drop evaporates in an environment saturated in vapor, where the geometry of the heat source is not trivial (the shape of the bubble around the drop evolves with time and is affected by the size of the drop inside and by the velocity of the antibubble in the surrounding fluid). This complicated study is beyond the scope of this thesis.

Even though integrating the evaporation of the drops inside the antibubbles in a model is quite complicated, we can still elaborate a model where the evolution of the volume of the antibubble $V_a(t)$ is not predicted but measured. Assuming that the volume of the drop does not change significantly during the delay time between the impact and the pinch-off, and that the initial vapor layer has a negligible size compared to the radius of the drop, we have $V_a(t_{\text{p.o.}}) = V_0 = 4\pi R^3/3$ at the moment of the pinch-off $t_{\text{p.o.}}$. Thus, by measuring the volume of the antibubble $V_a(t)$, we can deduce the global density of the antibubble at any moment. Indeed, assuming that the mass of the antibubble is conserved (*i.e.* that the vapor of the HFE–7100 does not mixes in the silicone oil), we have

$$\rho_a(t) \;=\; \rho_d \;\frac{V_a(t_{\text{p.o.}})}{V_a(t)} \tag{V.12}$$

and the combination of the buoyancy force and of the weight at any moment can be simply written as

$$F_g \;+\; F_b \;=\; (\rho_a - \rho_p)\;V_a\;g\;. \tag{V.13}$$

To these forces, we still have to add a friction term, just like for the description of the bouncing regime. We take exactly the same force. Finally, the added mass has to be considered. In the case of a bubble rising in a fluid, this added mass has been expressed by Zhang *et al.* [13], and using the same drag force and the same formalism as in the previous section, we have finally the equation

$$(M_d + M_{\text{add}})\,\ddot{z_{\text{CM}}} = (\rho_a - \rho_p)\,V_a\;g - \frac{\pi}{2}R^2\rho_p C_D \dot{z_{\text{CM}}}|\dot{z_{\text{CM}}}| \tag{V.14}$$

that can be developed into

$$(V_0\;\rho_d + C_m\;V_a\;\rho_p)\,\ddot{z_{\text{CM}}} = (V_0\;\rho_d - V_a\;\rho_p)\,g - \frac{\pi}{2}R^2\rho_p C_D \dot{z_{\text{CM}}}|\dot{z_{\text{CM}}}| \tag{V.15}$$

where the added mass coefficient $C_m = 0.5$, and the drag coefficient is the one previously used. Introducing in this equation the values measured for $V_a(t)$ and $R_a(t)$, the volume and the radius of the antibubble (that plays a role in the drag coefficient because of its dependency on the Reynolds number), we can compare the consistency between the measured acceleration of the drop, and the theory. This is shown in Fig. V.16(a) where the red curve represent the experimental data ($R = 0.56$ mm, silicone oil V20 at $T_p = 119$°C), and the blue curve represent the theory: the agreement is quite good. In Fig. V.16(b), we show the detail of the two terms $a_g + a_b$ and a_d, *i.e.* the forces $F_g + F_b$ and F_d divided by $M_d + M_{\text{add}}$, and their sum. We see that when the discrepancy between the model and the theory is the largest, around $t = 350$ ms, the two terms should almost compensate for each other, while they are at their largest values. Considering this, we understand that a slight error in the estimation of one the terms leads to a noticeable deviation.

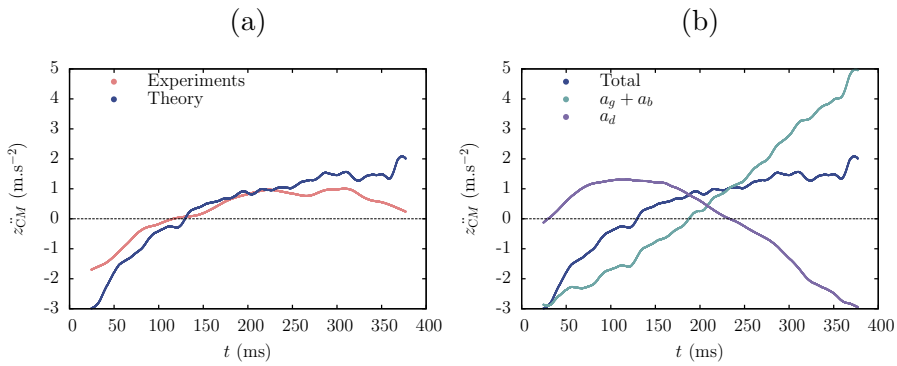

Figure V.16: (a) Comparison between the measured acceleration of an antibubble (in red), and the value predicted by the theory from the measured $V_a(t)$, $R(t)$, and $\dot{z}_{\text{CM}}$ (in blue). (b) Detail of the influence of the weight and buoyancy (in green) and of the drag force (in purple) in the model for the total acceleration of the antibubble (in blue).

The origins of the discrepancies may come from the non-spherical shape of the antibubble. Indeed, the drag force depends on the Weber number associated with its movement ($\text{We} = \rho_p R \dot{z}_{\text{CM}}^2 / \gamma_p$) [9]. However, due to the drop inside the bubble, the theory developed in this paper of Loth *et al.* can hardly be used in our case, because the presence of the drop modifies the shape of the surrounding bubble as shown in Fig. V.14.

V.5.4 Too fast to blow

Finally, the transition towards the direct contact regime is driven by a competition between the production of vapor in the Leidenfrost effect and the impact velocity. Therefore, we expect the property of the pool to play no role at the first order because the evaporation of a Leidenfrost drop is not affected by any of the properties of the substrate except its temperature. In Fig. V.17, we plot the threshold Weber number above which a direct contact between the drop and the pool is observed at the impact, $\mathrm{We}_{\mathrm{d.c.}}$, as a function of the superheat ΔT for three kinds of silicone oil (V5,V20, V100). We observe indeed that the curves are not much affected by the viscosity of the pool. However, for large viscosities of the pool, the threshold Weber number is slightly larger.

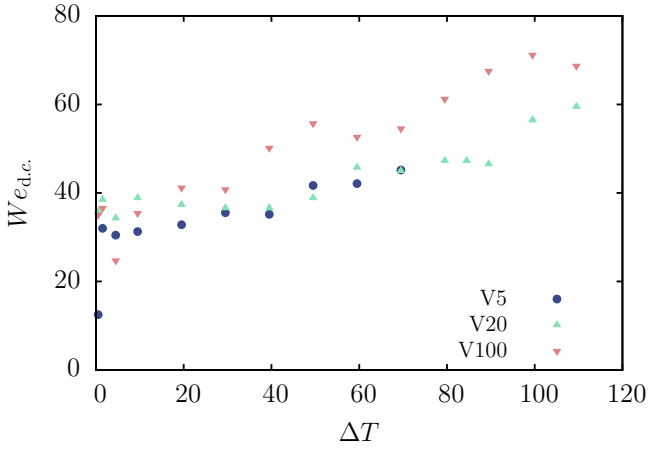

Figure V.17: Threshold Weber number above which a direct contact is observed $\mathrm{We}_{\mathrm{d.c.}}$ *as a function of the superheat for three kinds of oil.*

The question of the understanding of what leads to a direct contact may be formulated in another way: what is the impact of the We number on the Leidenfrost Point. And this question is far from being well understood, even on solid substrates. Contradictory conclusions have been drawn in the literature. Tran *et al.* have shown that the absence of any contact during an impact of a drop on a superheated silicon wafer depends on the temperature [14], while Staat *et al.* (mostly the same team) has shown recently that the Leidenfrost Point depends weakly at most on the Weber number [15]. Both studies as well as the transition showed in Fig. V.17 indicates clearly that the creation of a stable vapor film between an impacting drop and a hot substrate is far from being obvious.

An interesting parameter that controls the evaporation in the Leidenfrost effect is the evaporation number, $\tilde{\mathcal{E}}$, introduced previously in Sobac's model (see Chapter I).

$$\tilde{\mathcal{E}} = \frac{\lambda_v \ \eta_v \ \Delta T}{\gamma \ \rho_v \ \ell_c \ \mathcal{L}} \tag{V.16}$$

In our case, the direct contact occurs when the evaporation is not sufficient to slow down the drop before a contact between the drop and the surface of the pool occurs. We can then plot the threshold Weber number above which a direct contact is observed as a function of the evaporation number. This is done in Fig. V.18 for drops of HFE–7100 ($R = 0.56$ mm - red circles) and drops of ethanol ($R = 0.87$ mm - blue squares) impacting on a pool of silicone oil v20. We see that for each liquid, the threshold Weber number increases with the evaporation number, and two different regimes can be distinguished. The first one follow a scaling law $\mathrm{We}_{\mathrm{d.c.}} \propto \tilde{\mathcal{E}}^{1/8}$. In that regime, the data for the HFE–7100 and the ethanol collapse on a single curve. The second regime does not contain enough data to extract a scaling law.

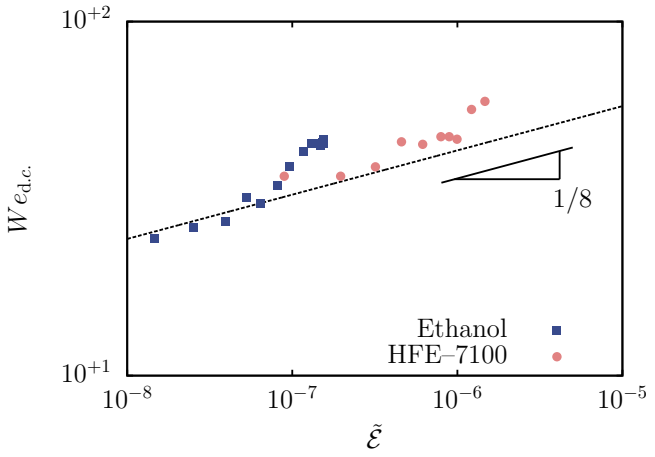

Figure V.18: Threshold Weber number above which a direct contact is observed $\mathrm{We}_{\mathrm{d.c.}}$ *as a function of the superheat for three kinds of oil.*

V.5.5 Cavities in the Direct Contact regime

Thus, when a drop impacts the pool with a velocity that is too high, the vapor film is not created fast enough to prevent contact between the drop and the pool. In that condition, the kinetic energy of the drop is transfered to the

pool. That leads to the formation of an hemispherical cavity. Benusiglio *et al.* studied the formation of similar cavities created by the explosion of firecrackers at the surface of water pools [7]. We believe that the mechanism is similar here: the kinetic energy of the drop is quickly transfered to a point of the surface of the pool.

The Reynolds number associated with the flows in these impacts is typically of the order of 10^2. Thus, the dissipation is dominated by inertia more than by viscosity. Moreover, gravity dominates quickly the surface tension effects as the size of the cavity increases. More precisely, the gravity dominates when the potential energy, $\frac{1}{2}\rho_p g z_{\max}^4$ becomes larger than the capillary energy, $2\gamma z_{\max}^2$, *i.e.* when $z_{\max}$ becomes larger than $\sqrt{2}\ell_{c_p}$. In our case, this condition is always satisfied. The conservation of the energy can then be written as

$$E_k \;=\; \frac{1}{2}\rho_p \; z_{\max}^4 \; g \; . \tag{V.17}$$

where E_k is the kinetic energy of the incoming drop. By replacing E_k by its expression, we obtain an expression for the max depth of the cavity.

$$\frac{1}{2}\rho_d \; \frac{4\pi}{3} R^3 \; U_0^2 \;=\; \frac{1}{2}\rho_p \; z_{\max}^4 \; g \tag{V.18}$$

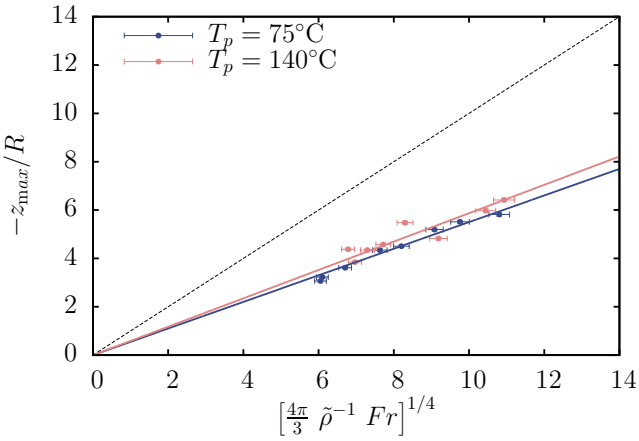

Figure V.19: Maximum depth of the cavities created by impacts of drops of radius $R = 0.56$ mm, normalized by this radius, as a function of $\tilde{\rho}^{-1}$ Fr, up to a factor. The experiment is done on a pool of silicone oil V100 at two different temperatures. The dashed line is a guide for the eye and represent Eq. (V.19).

We can rewrite this equation in a dimensionless form using the Froude number, $\mathrm{Fr} = U_0^2/gR$.

$$\frac{z_{\max}}{R} = \left(\frac{4\pi}{3}\,\tilde{\rho}^{-1}\,\mathrm{Fr}\right)^{1/4} \tag{V.19}$$

In Fig. V.19, we show the first term as a function of the second one for impacts on a pool of silicone oil V100 at two different temperatures ($T_p = 75°\mathrm{C}$ in blue; $T_p = 140°\mathrm{C}$ in red). We see through fits (continuous lines) that the relation is indeed linear. However, the prefactor found by fits is 1.7 times smaller than the one expected.

V.6 Conclusion

In this chapter, we investigated the dynamic limits of the situation depicted in Chapter III. Drops impacting a liquid substrate hotter than the boiling point of the drop does not always lead to the Leidenfrost state: a drop with too much kinetic energy eventually ends evaporating quickly after contacting the hot substrate, which is equivalent to a suppression of the Leidenfrost state.

Moreover, these impacts have shown unexpected behaviors, between the case of bouncing Leidenfrost drop, and the violent evaporation of a drop impacting too fast. A drop that evaporates enough to maintain a vapor layer can form a thermal antibubble if the drop penetrates deep enough in the pool. These thermal antibubbles are composed of a Leidenfrost drop surrounded by its own vapor in the surrounding hot fluid of the pool. These objects are particularly fragile in the first moments of their life when the vapor layer around the drop is thin, and the pinch-off that close the cavity made by the impact can destabilize this vapor layer.

These different regimes (the bouncing regime, the antibubble regime, the film breaking regime and the direct contact regime), when they are present for a set of parameters, always appear in this order as the impact velocity increases. However, when the pool is highly viscous, the film breaking regime tends to disappear, as well as the antibubble regime at low superheats.

We also showed that the movement of the antibubbles in the pool are well described by a semi-empirical model that considers an object of variable density submitted to its weight, buoyancy, and a drag force. The drag coefficient of a spherical bubble in a fluid gives a reasonnable agreement with the ex-

periments. However, the evaporation of such an object reveals itself to be very complex, notably because of the deformation of the vapor pocket by its movement in the surrounding fluid and by the presence of the drop inside.

References

[1] A. M. Worthington and R. S. Cole. *Impact with a liquid surface studied by the aid of instantaneous photography. Paper II.* Phil. Trans. R. Soc. Lond. A, 194:175–199, 1900.

[2] V. Duclaux, F. Caillé, C. Duez, C. Ybert, L. Bocquet, and C. Clanet. *Dynamics of transient cavities.* J. Fluid Mech., 591:1–19, 2007.

[3] J. M. Aristoff, T. T. Truscott, A. H. Techet, and J. W. M. Bush. *The water entry of decelerating spheres.* Phys. Fluids, 22(3):032102, 2010.

[4] Bluestar Silicones. *Rhodorsil Oils 47*, 2016.

[5] Stéphane Dorbolo, Hervé Caps, and Nicolas Vandewalle. *Fluid instabilities in the birth and death of antibubbles.* New Journal of Physics, 5(1):161, 2003.

[6] B. Scheid, S. Dorbolo, L. R. Arriaga, and E. Rio. *Antibubble dynamics: The drainage of an air film with viscous interfaces.* Phys. Rev. Lett., 109:264502, 2012.

[7] A. Benusiglio, D. Quéré, and C. Clanet. *Explosions at the water surface.* J. Fluid Mech., 752:123–139, 2014.

[8] T. Gilet and J. W. M. Bush. *The fluid trampoline: droplets bouncing on a soap film.* J. Fluid Mech., 625:167–203, 2009.

[9] E. Loth. *Quasi-steady shape and drag of deformable bubbles and drops.* Int. J. Multiphase Flow, 34:523–546, 2008.

[10] J. M. Aristoff and J. W. M. Bush. *Water entry of small hydrophobic spheres.* J. Fluid Mech., 619:45–78, 2009.

[11] J. W. Strutt and L. Rayleigh. *On the instability of jets.* Proc. London Math. Soc, 10(4), 1878.

[12] S. Chandrasekhar. *Hydrodynamic and Hydromagnetic Stability.* Dover Publications, Oxford, 1961.

[13] J. Zhang and L.-S. Fan. *On the rise velocity of an interactive bubble in liquids.* Chem. Eng. J., 92:169–176, 2003.

[14] T. Tran, H. J. J. Staat, A. Prosperetti, C. Sun, and D. Lohse. *Drop impact on superheated surfaces.* Phys. Rev. Lett., 108:036101, 2012.

[15] H. J. J. Staat, T. Tran, B. Geerdink, G. Riboux, C. Sun, J. M. Gordillo, and D. Lohse. *Phase diagram for droplet impact on superheated surfaces.* J. fluid mech., 779:R3, 2015.

VI

Interactions with granular material

Wrap a drop

VI.1 Preamble

For decades now, drops are in the highlights for their ability to act as micro-reactors. They are vessels in which many things can happen in a controlled way like mixing [1], chemical reactions [2], or deposition [3]. This latter famous example, the so-called coffee ring effect, and the hundreds of studies that followed about organisation and deposition of particles by evaporating drop [4, 5] have more than numerous implications on the industry (inkjet printing [6], lab-on-a-chip devices and microfluidics, agriculture...). This example indicates that Leidenfrost drops as a huge potential for organizing particles, and in general, interacting with them. Indeed, Leidenfrost drops have a really interesting feature that is not found in others drops: they are contactless. That means that you can avoid some of the contamination that occurs while moving a drop on a substrate. That also means that you have no contact line, which is a key factor in many applications of drops (either with benefits or disadvantages).

However, there is only a few papers that have been written on the subject of the interactions of Leidenfrost drops with micro or nano-particles. But the field seems rich in terms of suprises. For example, Tsapis *et al.* showed that nanoparticles in Leidenfrost drops were able to agregate in shells [7]. The

mechanism behind this specific behavior is the slow diffusion of the particles that are thus unable to homogeneize quick enough in the bulk of the drop while evaporating. The result is an elastic shell that ends up buckling when the drop ends its evaporation. Another surprising effect is the deposition of nanoparticles due to the Leidenfrost effect. Indeed, a drop loaded with nanoparticles moving on a substrate can leave a part of its content on the substrate [8]. Even salts disolved in the drops seems to be able to reach the vapor phase and react on the surface to form nanoparticles [8]. This deposition can result in nanowires that could possibly be functionnalized, *e.g.* to be conductive. These drops have also shown to be very efficient at forming gold nanoparticles, or forming and depositing coper oxyde nanorods or zinc oxyde nanoparticles on grids with a remarquable reproducibility [9].

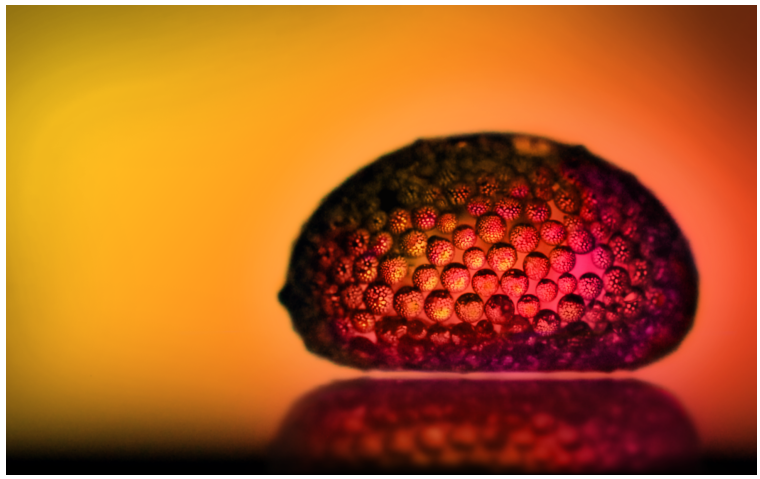

Figure VI.1: A centimetric Leidenfrost drop made of water covered by glass beads of mean radius $R_b = 150\,\mu m$ on a substrate at $T_s = 300°C$. The dots inside the beads are due to the refraction of the light coming from the beads on the other side of the drop.

In the light of all these possibilities, it seems pretty obvious that the best is still to come. However, on the range of all the particles that can be used, only a small part has been used. Up to now, a few salts and a few types of nanoparticles have been used. No particles larger than 100 nm were used. However, the size of usual Leidenfrost drops goes from 1 mm to 10 mm. So what about particles from 100 nm to 100 µm ? In Fig. VI.1, we see a Leidenfrost drop covered by glass particles. In this chapter, we focus on the characterization of these kind objects.

First, we observe how such particles behave when they are put in Leidenfrost drops. When does a form of organization emerge ? Where are the particles located ? Second, we investigate the effect of the presence of particles in the drops on the evaporation of the drops and on their shape ? Finally, we describe the objects resulting from the complete evaporation of the drops.

A large part of these results have been the subject of a publication [10].

VI.2 How to wrap a drop

In this experiment, we use a classical substrate, *i.e.* a polished aluminium plate. This plate was a disc about 100 mm large and 10 mm thick. The substrate that we used was slightly curved in order to confine the drop (radius of curvature ~ 5 m).

The beads that could be used were constrained by a major aspect related to the Leidenfrost effect : the high temperature needed to reach this state. Especially, since we used water, and since the Leidenfrost Point of water is above 200°C on polished aluminium, the beads had to be resistant to these high temperatures. The various types of beads that were used are listed in Table VI.1. The main experiment was done with the types I to III. The type IV has the advantage that the beads are made of basalt, which is opaque and enables a better visualisation of the beads.

	Matter	Density (kg/m^3)	Radii range (µm)	Θ_d
I	Glass	2500	$20-35$	-
II	Glass	2500	$45-75$	$26^\circ \pm 3^\circ$
III	Glass	2500	$100-200$	$31^\circ \pm 9^\circ$
IV	Basalt	2900	$53-62.5$	$30^\circ \pm 3^\circ$

Table VI.1: Physical properties of the different types of beads used in the experiments.

In this table, we also report the contact angle of these beads with bidistilled water. These measurements were done with the visualization of beads floating at the surface of water in a large container. A side view of a basalt bead is shown in Fig. VI.2. Fitting circles on the lower image of the bead and on the higher image (reflection on the surface of the water) allowed to get the contact angle Θ. This method is only possible for small objects, for

which the deformation of the liquid-air interface is negligible [11]. Hereafter, we note Θ_d the angle measured by this direct visualization. However, it was not possible to get the contact angle of the smallest beads with this method even with a microscope. The contact angles we measured for the type II to IV were between 26°C and 31°C. Thus, the beads are hydrophilic even though they are able to float [12].

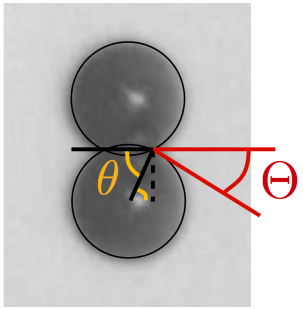

Figure VI.2: A basalt bead ($R_b \simeq 58\,\mu m$) is floating at the surface of bidistilled water. This side view allows to get the contact angle Θ of the water on the surface of the bead.

The experimental procedure of the experiment was the following. First, we created a drop with an initial volume $V_0 \simeq 1$ mL. In this drop, we poured a well know mass of beads M from the top of the drop. These beads were previously weighed with a balance with a precision of 0.1 mg. A few beads could however stick to the funnel used to pour them in the drop because of humidity or fall around the drop. Thus, the uncertainty on the mass of beads inserted in the drops was 0.2 mg. After this step, we let the drop evaporate and followed the evolution of its volume V, surface S and radius R with time.

VI.3 How the drop is wrapped

To obtain a drop like the one in Fig. VI.1, glass beads are introduced in a large water drops in the Leidenfrost state. Quickly, the glass beads accumulate in the bottom of the drop, and form a stripe around the neck region. Then, the beads cover a larger and larger part of the surface as the drop evaporates. However, beads may not only be distributed on the surface. This is not obvious at all that the beads are not located in the bulk of the drop. In this section, we first analyse in which conditions a layer of beads covers the surface of Leidenfrost drops. A few conditions are necessary to obtain a beautiful and

homogeneous monolayer.

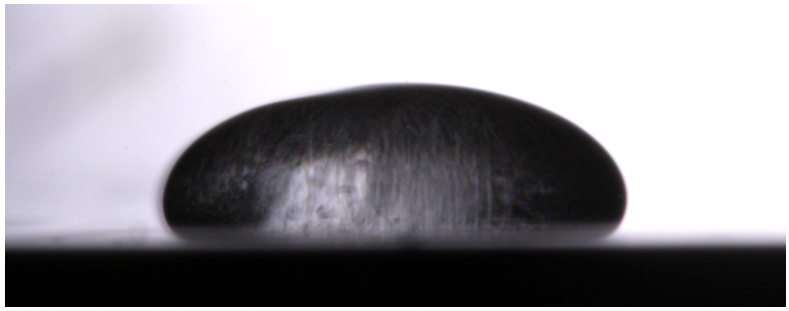

Figure VI.3: An ethanol drop with glass beads (type II) in it. The fast movement of the beads in the bulk of the drop makes them blurred.

First, the liquid of the drop must wet only partially the material of beads. For example, when glass microbeads are poured into ethanol drops, we observe clearly that the beads are located everywhere in the drops, and no wrapped drop is produced. This is illustrated in Fig. VI.3 where the blurred image of the beads (type II) betrays their fast movements in the bulk of the drop. The beads move in the bulk of the liquid, entrained by the inner flows of the drop. A competition between the pinning force of the contact line, the flows in the drop and the buoyancy dictates wether a bead can stay at the surface. The critical point for the stability of a layer is the stability of the beads that lay at the top surface of the drop. In this case, the combination of the weight of the bead and of the buoyancy tends to make the bead sink. The inner flows also tends to bring the bead to the bottom at the center of the drop. Indeed, flows in a Leidenfrost droplet are directed towards the bottom of the drop at the center and towards the top along the borders. The only stabilizing force is then the pinning force of the contact line. For that reason, in the following, we focus our observations on water drops and avoid low surface tension liquids.

Second, the drop must be initially much larger than the volume of the beads V_b, and still smaller than the threshold above which the chimney instability happens. When this instability happens, the beads are mixed in the bulk by the rapid flows induced by the bursts of the chimneys. The instability is triggered when the radius of the drop is above $R_c = 3.84\ell_{c_d}$ [13, 14]. A water drop of 1 mL has a radius $R \simeq 7.5$ mm which is smaller than $R_c = 9.9$ mm for water. However, the condition on the size of the drop is even more restrictive. The surface of the drop S_d must be much larger than the surface that the beads can cover S_b. This surface can be expressed as

$$S_b \;=\; \frac{N_b\ \pi\ R_b^2}{\phi_b} \tag{VI.1}$$

where N_b is the number of beads inserted in the drop, R_b is the mean radius of these beads and ϕ_b is the surface fraction occupied by the beads. N_b can be expressed as the ratio between the mass of the beads inserted M, which is the control variable, and the mean mass of one single bead M_b.

$$N_b \;=\; \frac{M}{M_b} \;=\; \frac{3\ M}{4\ \pi\ R_b^3\ \rho_b} \tag{VI.2}$$

Combining Eq. (VI.1) and Eq. (VI.2) leads to

$$S_b \;=\; \frac{3\ M}{4\ R_b\ \rho_b\ \phi_b}\ . \tag{VI.3}$$

Assuming that a water drop of 1 mL is a puddle, its volume is $V = 2\ell_{c_d}\pi R^2$ and its surface is $S = 2\pi R(R + 2\ell_{c_d})$. Thus, we find that

$$S \;=\; \sqrt{\frac{V\ 2\ \pi}{\ell_{c_d}}}\ \left[\sqrt{\frac{V}{2\ell_{c_d}\ \pi}} + 2\ell_{c_d}\right]\ . \tag{VI.4}$$

Thus, the criterium on the initial conditions is that $S >> S_b$ in order to let the beads self-organize. Practically, for drops of 1 mL, M can reach 30 mg for the type I to 200 mg for the type III. In the case where these criteria are verified, the beads can wrap the drops.

To analyze this monolayer, the first thing that can be done is to understand how the beads are packed at the surface of the drop. To achieve this, we use fluorescein in the drop and the type IV beads, which are opaque. A typical image is shown in Fig. VI.4. This kind of image allows to get the position of the beads assuming that we can neglect the effect of the curvature of the drop by taking a small part of the surface. We can then obtain the surface fraction occupied by the beads ϕ_b. In all observed cases, we find $\phi_b = 0.80 \pm 0.03$. This surface fraction is close to the random close packing of hard disks [15, 16].

We can also define the efficiency of the trapping of the beads by the surface of the drop, E, as the ratio between the surface of the drop at the moment when it becomes fully covered, S_c, and the surface that the beads can cover, S_b.

$$E \;=\; S_c\ \frac{4\ R_b\ \rho_b\ \phi_b}{3\ M} \tag{VI.5}$$

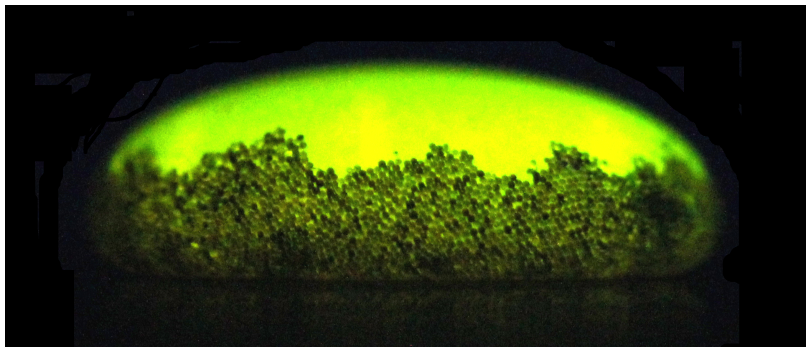

Figure VI.4: A water drop with fluorescein in it and basalt beads ($R_b \simeq 58\,\mu m$) at its surface.

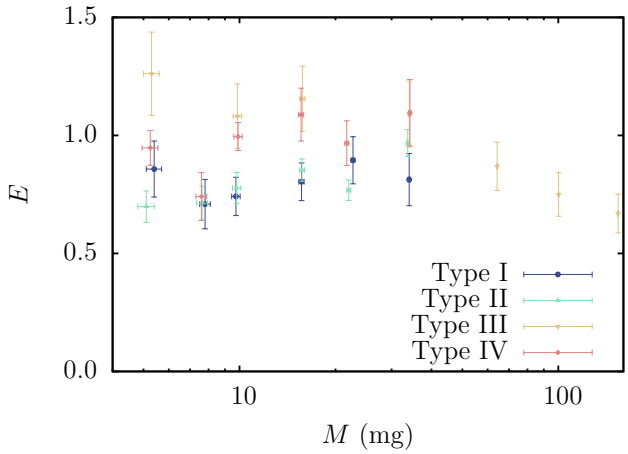

Figure VI.5: Efficiency of the trapping of the beads by the surface of the drops, E, for different type of beads, as a function of the mass of beads inserted, M.

By measuring S_c, we can then calculate this efficiency of trapping. In Fig. VI.5, we plot this efficiency as a function of the mass of the beads inserted in the drop M, for the first four kinds of beads. We see that for any kind of beads, this efficiency is above 0.7. A large part of the beads inserted are trapped by the surface of the drop. For the largest beads used in the experiment (type III), some efficiencies are above 1, which is not possible, given the definition of E. This may be due to the fact that the definition of the surface that the beads can cover assumes that this surface is plane while this surface is actually curved. Another cause may be the fact that the surface fraction has been mesured for the opaque beads only.

VI.4 How the wrap affects the evaporation

The main feature of a Leidenfrost drop may be the fact that this drop evaporates. Hence, an obvious question that one can ask about our drops covered with particles is : does they evaporate in the same way than drops of pure liquid ? To answer the question, the easiest way is to measure the evolution of geometrical parameters such as the volume or the radius (seen from above) with time. Here, we chose to focus on the volume of the drop.

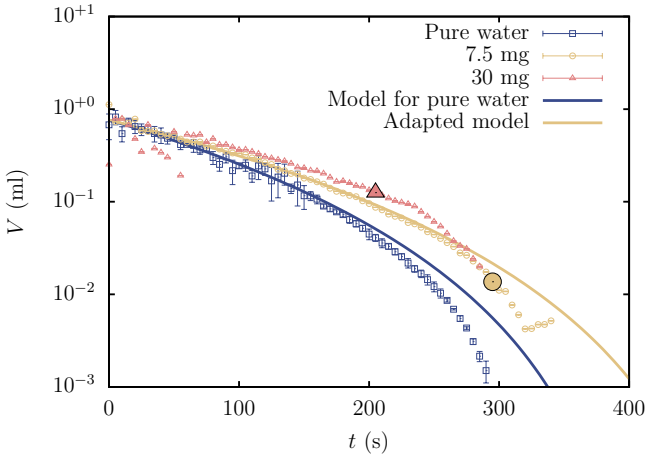

Figure VI.6: Volume of three different Leidenfrost drops made of water on an aluminium substrate at $300°C$ *as a function of time. The first drop contains no bead (blue squares); the second drop contains* 7.5 *mg of beads (yellow circles); the third drop contains* 30 *mg of beads (red triangles). The type of beads used here is the type II. The blue line is fit of the data for the pure water drop using Eq. (I.7). The yellow line is a fit of the data for the drop with* 7.5 *mg of beads using the same equation.*

In Fig. VI.6, we plot the evolution with time of the volume of three different drops. All of them are made of water. The first one contains no bead (blue squares), the second one contains 7.5 mg of beads (yellow circles), and the third one contains 30 mg of beads (red triangles). The type of bead used is the type II. The larger points indicate the time when the drop becomes fully covered by the monolayer of beads. We see that the drop without beads evaporates faster than the two others, that evaporates approximately at the same rate. Thus, the quantity of beads seems to have a negligible impact on the reduction of the evaporation above a threshold value that is below 7.5 mg for these beads. Several things can lead to a modification of the evaporation when some beads are added to the drops.

The first one comes from the fact that the beads are more dense than the water. Thus, as the drop evaporates, the density of the drop increases. In that case, using Biance's model (see Sec. I.2.1), we can modify Eq. (I.6), and, distinguishing the volume of the drop V_d and the volume of the beads V_b, we have

$$\dot{V}_d = -\left(\frac{\pi\rho_v g\ell_c^2}{6\eta_v}\right)^{1/4}\left(\frac{\kappa\Delta T}{\rho_l\mathcal{L}}\right)^{3/4} V_d^{3/4}\left(1+\frac{V_b}{V_d}\frac{\rho_b-\rho_l}{\rho_l}\right)^{1/4}. \qquad \text{(VI.6)}$$

In this equation, when the volume of the beads tends to the volume of the drop, *i.e.* when the drop is completely evaporated, the last factor tends to $(1+1.5)^{1/4} = 1.26$. Thus, the evaporation rate is only slightly increased at the end of the evaporation. Given that we assume that the volume of the drop is much larger than the volume of the beads, the increase is negligible.

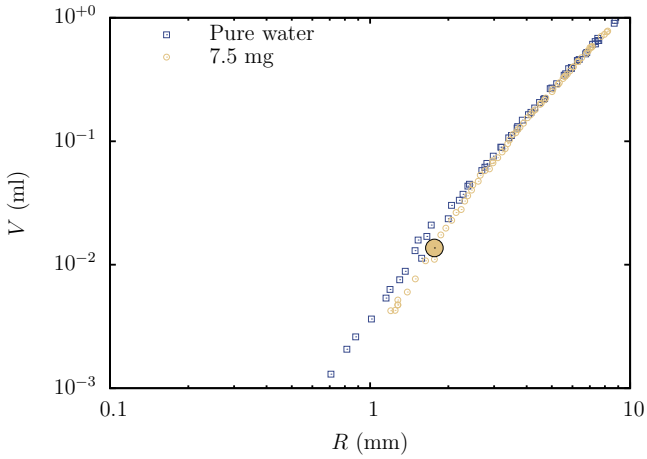

Figure VI.7: The volume of two drops is plotted as a function of their radius. The first one is a drop of water (blue squares), and the second one is a drop of water with 7.5 mg of beads (type II – yellow circles). The moment when the latter becomes fully covered is indicated by a large filled circle.

The second source for the modification of the evaporation comes from the fact that the beads can deform the drop. Indeed, grains are well known for their ability to form arches that redirects constraints towards edges. This effect is called the Janssen effect [17]. To see if this effect has an influence on the shape of our drops, we can plot the radius of the drops as a function

of their volume for a drop with beads and without beads. This is shown in Fig. VI.7. We see that there is no modification of the shape of the drop before the drop with beads becomes fully covered. Thus, the only arch that induces constraints on the edges of the drop is the global arch made by the whole layer of beads. Indeed, at that moment, an observation of the drop shows that the surface becomes less shiny, indicating a larger roughness induced by an increase of the dewetting of the beads.

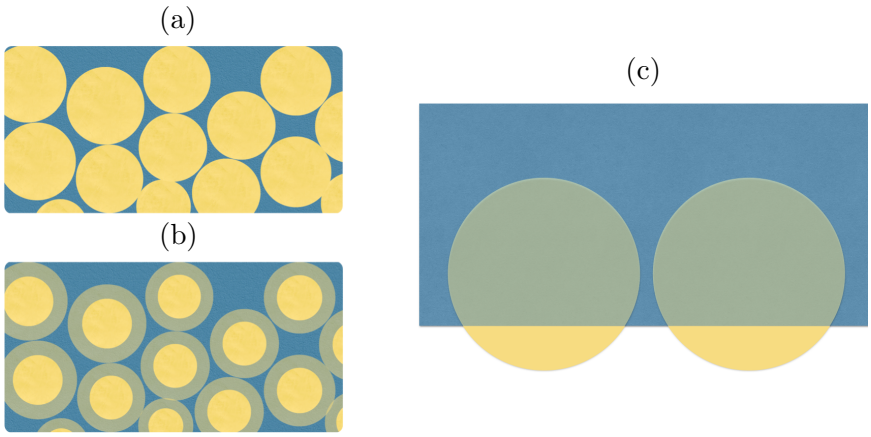

Figure VI.8: (a) Schematic view of the surface of a Leidenfrost drop covered with grains with $\Theta = 90°$*, and (b)* $\Theta < 90°$*. (c) Side view of the situation depicted in (b).*

The third source that can induce a change in the evaporation is linked to the dewetting of the beads. As emphasized by Eq. (I.3), the evaporation rate of the drop depends on the surface of fluid that is evaporating. This means that a fraction of the surface covered by a bead does not allow evaporation. This is illustrated in Fig. VI.8. As measured in Sec. VI.3, the beads occupy a fraction of the surface $\phi_b = 0.8$. However, not the whole projected area of the beads occupy a fraction of the surface. The effective surface of evaporation S_e can be expressed as

$$S_e \;=\; \pi R^2 \;(1-\phi_b) \;+\; \pi R^2 \;\phi_b \;\left(1-\cos^2\theta\right) \;. \tag{VI.7}$$

where θ is the angle between the plane of the contact line of the liquid on the bead and the diameter of the bead going through the contact line. The blue term is the term corresponding to the surface in blue in Fig. VI.8(b), and the term in greenish-grey is the term corresponding to the surface in the same color in Fig. VI.8(b). Θ is the complementary angle of θ, and is the contact angle of the liquid on the bead (see Fig. VI.2). We can thus rewrite Eq. (VI.7)

in terms of the contact angle Θ.

$$S_e \;=\; \pi R^2 \;\left(1 - \sin^2\Theta\;\phi_b\right) \tag{VI.8}$$

Taking back the theory of Biance *et al.* and replacing S_c by S_e in Eq. (I.3), we find the thickness of the vapor film

$$h = \left(\frac{3\kappa\Delta T\eta_v}{4\mathcal{L}\rho_v\rho_l g\ell_c}\right)^{1/4} \; R^{1/2} \;\left(1 - \sin^2\Theta\;\phi_b\right)^{1/4} \;. \tag{VI.9}$$

Following the same reasoning as in Biance's model, we finally find

$$\dot{V} = -A_{\text{beads}}\; V^{3/4} = -A_{\text{pure}}\; V^{3/4}\left(1 - \sin^2\Theta\;\phi_b\right)^{3/4} \;. \tag{VI.10}$$

In the end, we can simply express the reduction of the evaporation rate by the presence of the beads with the equation

$$\frac{A_{\text{beads}}}{A_{\text{pure}}} \;=\; \left(1 - \sin^2\Theta\;\phi_b\right)^{3/4} \;. \tag{VI.11}$$

Thus, knowing ϕ_b, we can extract the contact angle Θ from the fits of the curves of $V(t)$ with beads and without beads. This has been done for the type of beads I – IV and the results are shown in the table VI.2 along with the direct measurements of the contact angles previously reported in Sec. VI.2. The contact angle measured directly is noted Θ_d and the contact angle calculated from the reduction of the evaporation rate is noted Θ_i. The results are shown for two different temperatures of the substrate and the fraction of the surface of evaporation that is free for evaporation is also given.

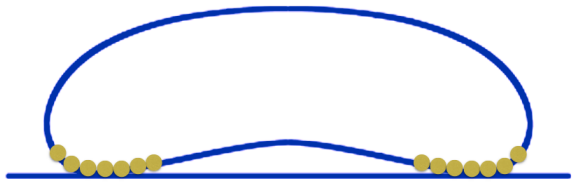

Figure VI.9: Schematic view of a large Leidenfrost drop with beads in it. The beads quickly occupy the neck region where the drop evaporates the most.

Note that these measurements have been done with different quantity of beads, from one type to another. However, in all cases, the beads initially cover only a portion of the surface that is close to the neck. This fraction

Type	T °C	ϕ_{free}	Θ_d	Θ_i
I	300	0.572	–	47°
I	350	0.612	–	44°
II	300	0.640	26°	42°
II	350	0.618	26°	44°
III	300	0.624	31°	43°
III	350	0.603	31°	45°
IV	300	0.527	30°	50°
IV	350	0.554	30°	48°

Table VI.2: For two different temperatures, we give the contact angles measured directly Θ_d and calculated from the reduction of the evaporation rates Θ_i. The fraction of the contact surface of the drop that is free of beads ϕ_{free} is also given.

of the surface is much lower than πR^2. However, we know that some of the assumptions behind the model from Biance *et al.* are too strong. Notably, the contact surface is not flat and Leidenfrost drops does not evaporate equally from the whole contact surface, but evaporate mostly on the neck, where the beads are present immediately after being poured (see Fig. VI.9). This is consistent with the fact that adding more beads to the drops does not change more the evaporation rate : a small quantity of beads cover the neck of the drop, and adding more beads just cover the parts of the contact surface that does not contribute highly to the evaporation of the drop.

VI.4.1 The case of highly wetting liquids

Up to now, we only investigate the case of drops made of water. Water, however, has some unusual features. Especially, its high surface tension makes water less wetting than other common liquids. Contact angles of liquids on a glass slide are respectively 6.5° for ethanol, 5.3° for acetone, and 49° for water. One can expect the same behavior than observed with water when beads are poured in Leidenfrost drops made of ethanol or acetone, with the only difference lying in a lower decrease of the evaporation rate because of a lower contact angle.

Nonetheless, this is not what is observed. Indeed, the trapping of the beads by the surface of the drop relies highly on the surface tension and on the contact angle. In the case of ethanol, the trapping is negligible and flows inside the drop carry most of the beads everywhere in the bulk of the drop. Only a small part accumulate at the bottom of the drops due to sedimentation.

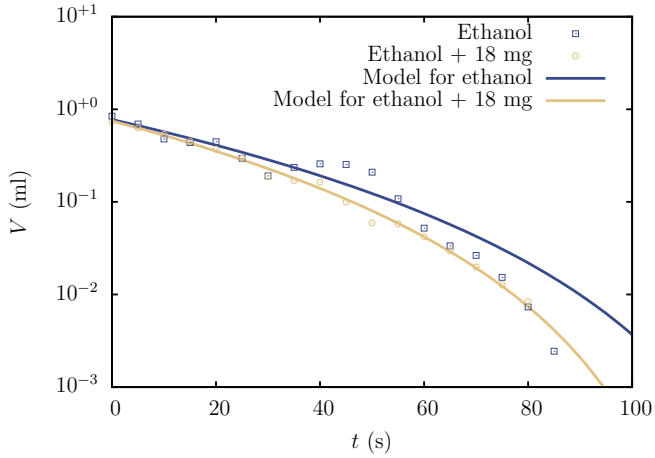

Figure VI.10: Volume of three different Leidenfrost drops made of water on an aluminium substrate at $300°C$ *as a function of time. The first drop contains no bead (blue squares); the second drop contains* 7.5 *mg of beads (yellow circles); the third drop contains* 30 *mg of beads (red triangles). The type of beads used here is the type II. The blue line is fit of the data for the pure water drop using Eq. (I.7). The yellow line is a fit of the data for the drop with* 7.5 *mg of beads using the same equation.*

In Fig. VI.10, we show the time evolution of the volume of drops of ethanol without beads (blue squares) and with 18 mg of beads (type II – yellow circles). We see that there is a negligible effect of the presence of the beads on the evaporation of an ethanol drops. The difference between the fits comes from an artifact of the measurements for the pure ethanol drop between $t = 35$ s and $t = 55$ s.

VI.5 How the drop ends its life

When the drop is fully covered, frustration between grains is happening in the monolayer. The surface of the drop reduces while the surface of the monolayer is constrained by contacts between the beads. Some beads begin to go from the surface to the bulk of the drop, and the layer of beads begins to buckle. At a point, the drop becomes closer to a wetted granular material and the evaporation at the bottom of the drop becomes unsufficient to maintain the levitation. The drop then contacts the substrate and evaporates quickly. At the end of this process, only the microbeads remain. The grains show an unexplained cohesion and form objects that are sometimes close to spheres that we called "basalt blackberries". An exemple is shown in Fig. VI.11. A few questions

can be asked about these objects. In what conditions these objects get closer to a sphere ? What makes the cohesion ? How the beads are organized inside ?

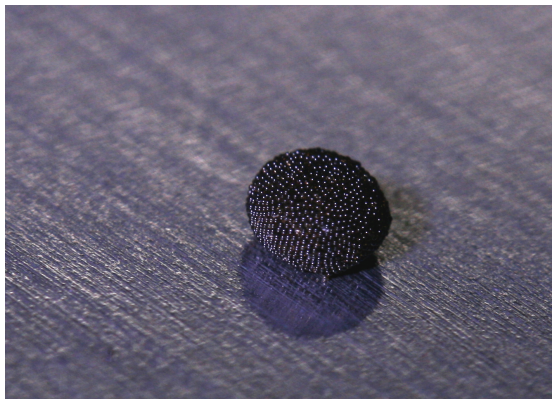

Figure VI.11: Residue of the evaporation of a Leidenfrost drop made of water with basalt beads in it: a so-called "basalt blackberry" The final object is cohesive and pretty much spherical. The size of the residue is approximately 2 *mm.*

On one hand, without any surprise, when there are too much beads, the drop is still flattened by gravity at the end of its evaporation, when the monolayer nuckles and grains begin to sink, and the final residue keeps a trace of this flattening. On the other hand, when there are very few beads, the discrete aspect of the beads appear. Moreover, the final shape can also be modified by violent events due to the rapid evaporation happening when the drop touches the substrate at the end of its life. In between these two extremes, residues like the one shown in Fig. VI.11 can be observed. In most cases, however, shapes can be sometimes very surprising as shown in Fig. VI.12, which shows residues composed of 17, 71, 205, and 563 beads. Figure VI.12(b) is particularly non-spherical and asymetric. This kind of shapes can be observed when nucleate boiling occurs when the drop touches the substrate.

In large residues, above 100 beads, we can wonder how the beads are organized in the residues. A first answer comes in the analysis of the packing fraction of these objects. Measuring the total volume of the residue from a side view and knowing the mass of beads in it, we calculate this packing fraction. In some cases, we observe packing fraction down to 0.4. Such a packing fraction is very low. Random Loose Packing of spheres usually goes down to 0.56 and even the thinnest regular packing (cubic lattice) has only a packing fraction of $\pi/6 \simeq 0.52$. The slight polydispersity of our beads should even increase the packing fraction of the residues compared to the case of monodis-

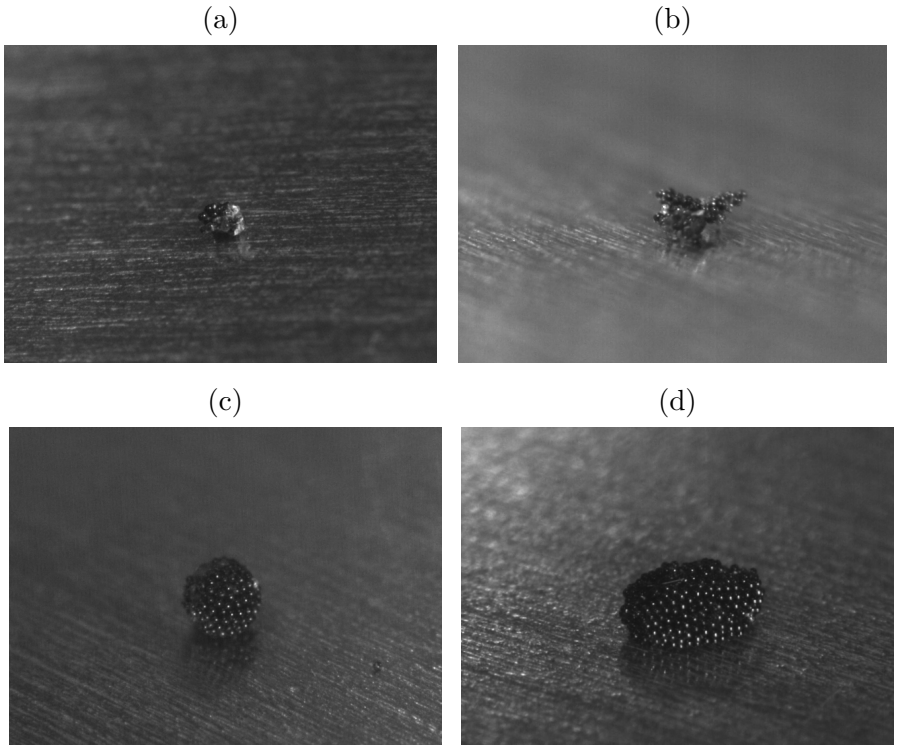

Figure VI.12: Images of the residues of the evaporation of Leidenfrost drops on a substrate at $300°C$*. The number of microbeads (type IV) in each of these residues is respectively 17, 71, 205, and 563 beads.*

perse spheres. The cohesion may stabilize some internal structures that would normally be unstable, like arches which may induce the presence of holes.

To observe the organization of the beads and see the presence of holes in the structure, a useful tool is the microtomography. The spatial resolution of this 3D imaging technique is of the order of 1 micron. The disadvantage of the technique is that the acquisition of a single 3D picture takes around 15 min. Thus, it is impossible to use this technique while the drop is still evaporating. In Fig. VI.13, we present the images of two horizontal slices of a single residue. The two slices are taken at the bottom (a) and at the middle (b) of the residue. We observe in Fig. VI.13(a) that the base of the drop keeps a trace of the shape of the bottom of the drop. The whole residue stands on a few beads that are part of an annular neck. This implies that there is a pocket with no beads under the residue. Thus, with a simple visualization from the side, we overestimate the volume of the object. Furthermore, in Fig. VI.13(b),

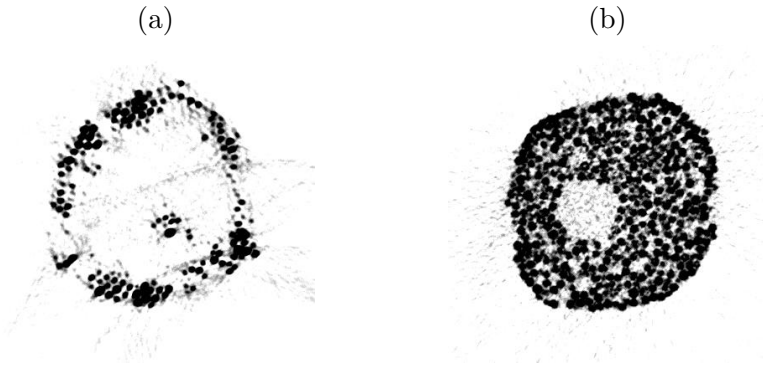

Figure VI.13: Images acquired by microtomography representing horizontal slices of the bottom (a) and of the middle (b) of a single residue.

we see that there is also a hole in the center of the drop. This may be a trace of the layered structure of the beads inside the drop during its evaporation, or a trace of a nucleate boiling event in the last moments of the life of the drop.

VI.6 Conclusion

We focused on an applied thematic related to Leidenfrost drops, *i.e.* the manipulation of particles by drops. Yet, we saw that one cannot focus on these applied thematics without taking care of the fundamental thematics. And more important, one *should* not !

We showed that microparticles from $\sim 10\,\mu m$ to $\sim 100\,\mu m$ are able to organize themselves in monolayers around Leidenfrost drops. This behavior can only happen when they are initially able to cover a small part of the surface of the drops, and overall, the wetting of the beads by the liquid has to be low. A highly wetting liquid does not lead to a surface organization, but only to a bulk organization.

The monolayers observed are highly stable and are able to cover the whole drop, notably because of the high surface fraction of their packing close to ~ 0.8. However, when the whole surface is covered, they begin to buckle as the drop keeps on evaporating.

Up to this complete cover, the drops with particles in them evaporate slower than drops made of pure water. We showed that the decrease of this evaporation rate is linked to the dewetting of the beads which reduces the

apparent surface of evaporation. This reduction of the surface evaporation depends on the contact angle between the water and the particle. Thus, a comparison between the evaporation of drops with and without particles allows to measure this contact angle.

Finally, we showed that the evaporation of these drops ends by leaving cohesives objects made of the particles. While this cohesion is still a mystery, the so-called "basalt blackberries" showed surprisingly low packing fraction, down to ~ 0.4. We showed that these low packing fractions are due to large holes in the structures made by the beads.

References

[1] F. Weyer, M. Ben Said, J. Hotzer, M. Berghoff, L. Dreesen, B. Nestler, and N. Vandewalle. *Compound droplets on fibers.* Langmuir, 31:7799–7805, 2015.

[2] R. M. Bain, C. J. Pulliam, F. Thery, and R. G. Cooks. *Accelerated Chemical Reactions and Organic Synthesis in Leidenfrost Droplets.* Angew. Chem. Int. Ed., 55:10478–10482, 2016.

[3] R. D. Deegan, O. Bakajin, T. F. Dupont, G. Huber, S. R. Nagel, and T. A. Witten. *Capillary flow as the cause of ring stains from dried liquid drops.* Nature, 389:827–829, 1997.

[4] H. Hu and R. G. Larson. *Marangoni effect reverses coffee-ring depositions.* J. Phys. Chem. B, 110:7090–7094, 2006.

[5] P. J. Yunker, T. Still, M. A. Lohr, and A. G. Yodh. *Suppression of the coffee-ring effect by shape-dependent capillary interactions.* Nature, 476:308–311, 2011.

[6] B.-J. de Gans, P. C. Duineveld, and U. S. Schubert. *Inkjet printing of polymers: state of the art and future developments.* Advanced materials, 16:203–213, 2004.

[7] N. Tsapis, E. R. Dufresne, S. S. Sinha, C. S. Riera, J. W. Hutchinson, L. Mahadevan, and D. A. Weitz. *Onset of buckling in drying droplets of colloidal suspensions.* Phys. Rev. Lett., 94:018302, 2005.

[8] M. Elbahri, D. Paretkar, K. Hirmas, S. Jebril, and R. Adelung. *Anti-lotus effect for nanostructuring at the Leidenfrost temperature.* Adv. Mater., 19:1262, 2007.

[9] R. Abdelaziz, D. Disci-Zayed, M. K. Hedayati, J.-H. Pöhls, A. U. Zillohu, B. Erkartal, V. S. K. Chakravadhanula, V. Duppel, L. Kienle, and M. Elbahri. *Green chemistry and nanofabrication in a levitated Leidenfrost drop.* Nat. Commun., 4, 2013.

[10] L. Maquet, P. Colinet, and S. Dorbolo. *Organization of microbeads in Leidenfrost drops.* Soft Matter, 10:4061–4066, 2014.

[11] P. S. Raux, H. Cockenpot, M. Ramaioli, D. Quéré, and C. Clanet. *Wicking in a Powder.* Langmuir, 29:3636–3644, 2013.

[12] D. Vella and L. Mahadevan. *The cheerios effect.* Am. J. Phys., 73(9):817–825, 2005.

[13] A.-L. Biance, C. Clanet, and D. Quéré. *Leidenfrost drops.* Phys. Fluids, 15:1632–1637, June 2003.

[14] P. Brunet and J. H. Snoeijer. *Star-drops formed by periodic excitation and on an air cushion ? A short review.* Eur. Phys. J. Special Topics, 192:207–226, 2011.

[15] J. G. Berryman. *Random close packing of hard spheres and disks.* Phys. Rev. A, 27:1053–1061, February 1983.

[16] D. Bideau and J. P. Troadec. *Compacity and mean coordination number of dense packings of hard discs.* J. Phys. C, 17:L731, 1984.

[17] H. A. Janssen. *Versuche über getreidedruck in silozellen.* Zeitschr. d. Vereines deutscher Ingenieure, 39:1045–1049, 1895.

VII

Overall Conclusion and Perspectives

This thesis is an experimental study of the Leidenfrost effect and of its limits. We especially focused on diverse situations that gave us the opportunity to increase the understanding of the apparition of the effect. Additionally, we took this opportunity to improve the way we see the evaporation of these drops and their usefulnes in different aspects.

In Chapter II, we examined one of the most conceptually simple situation involving the Leidenfrost effect : drops evaporating on a hot metallic substrate with a gravity larger than the earth gravity. Even though the concept was simple, the way to achieve it was not. The use of the Large Diameter Centrifuge at ESTEC center allowed us to reach $20g$. In doing so, we showed that the hypergravity is an interesting way in Leidenfrost experiments to get rid of the capillary regime. We also confirmed that the so-called chimneys that can be observed in large drops are due to a Rayleigh-Taylor-like instability implying a distance between chimneys that scales as the capillary length. However, the main goal of the experiment was different. We showed that the Leidenfrost Point increases slightly but clearly with the gravity. This led us to notice the importance of taking the precise shape of the vapor film to understand better the Leidenfrost Point.

In Chapter III, the experiment was still focused on the improvment of the knowledge of the Leidenfrost Point. Based on the fact that the roughness of solid substrates tends to disrupt the vapor film, we used one of the smoothest

substrate possible, an oil pool. We showed that the leviation of drops above this substrate is possible for superheats as low as 1°C for ethanol drops. We studied the shape of the drop and of the pool and built a model that reproduce well these shapes. The capillary length does not appear as a critical length for the shape of the drop as it is the case on solid substrates. As a consequence, there is only one regime of evaporation, and we showed that the decrease of the radius with time is linear in all cases. However, the rate of decrease saturates highly for low superheats, which is not explained by our model. This is due to the fact that the evaporation is not driven by the heat transfer in the vapor film anymore. We also showed that the presence of a Leidenfrost drop on a liquid pool has an effect on the oil in the pool. We observed and described buoyancy-driven convection cells under ethanol drops, and viscous entrainment-driven convection cells under drops made of HFE–7100.

Perspectives The drastic reduction of the Leidenfrost Point that we observed is very promising for enhancing the Leidenfrost effect. In this thesis, we always worked with deep pools. However, another interesting geometry is the impregnated substrate. Indeed, a very thin layer of oil should be able to damp any roughness of a substrate without a tiny amount of liquid. However, pre-manipulations showed that the reduction may not be as drastic as it is on a pool. The flows induced by the viscous entrainment, as well as the pressure imposed by the drop on the liquid layer may be in cause. Still, regarding the potential interest of a reduced Leidenfrost Point with a very simple setup, this system should be studied.

In Chapter IV, we introduced the various phenomenons happening in the impacts of Leidenfrost drops by revisiting the problem of the bouncing ball. We dropped drops over vertically oscillated hot substrates. The point was not to look at the suppression of the Leidenfrost effect, but instead to look at the motion of these drops when sumitted to particular forcings. Leidenfrost drops were observed to bounce with a contact time that was independent on the parameters of the forcing (frequency and maximum acceleration of the substrate), and that is simply equal to the capillary time up to a numerical factor. This leads to a prediction that large drops are not able to bounce if their contact time is too large compared to the period of an oscillation. We also observed that the drop can bounce in several modes, depending on the acceleration of the substrate and on the frequency of the oscillation. We then observe bifurcations from a robust mode $(1, 1)$ to modes $(2, 1)$ and $(2, 2)$ that are mixed for high reduced accelerations.

In Chapter V, we explored another phenomenon including impacts where the Leidenfrost drops are pushed to their limits. We showed that impacting drops on heated liquid pools made of silicone oil can lead to four very different regimes of impacts, depending on the impact velocity. The first one, at low impact velocities, is the bouncing of the drop on its vapor layer. In the second one, at larger velocities, the drop penetrates deep enough in the pool so that the liquid of the pool pinches-off above the drop, forming an antibubble stabilized by the evaporation of the drop. In those two first regimes, the Leidenfrost effect is maintained. In the third one, the same pinch-off occurs, but destabilize the vapor layer and suppress the Leidenfrost effect. In the last regime, the vapor layer is so much squeezed while the drop impacts that it breaks before any pinch-off, leading to hemispherical cavities.

Finally, in Chapter VI, we saw that Leidenfrost drops are highly resistant to dust contamination. Instead of problems to maintain the Leidenfrost effect, we observed that these drops have the surprising ability to organize microparticles at their surface. This organization takes the form of a monolayer constituted by a almost all microparticles present in the drop. This monolayer has observed to wrap completely the drops and to decrease the evaporation of the drops. This is due to the dewetting of the particles lying at the surface of the drop, reducing the surface of evaporation. We also observed that the complete evaporation of the drops was leading to compact and cohesive assemblies of microparticles with a surprisingly low packing fraction resulting from holes in the global structure.

Perspectives These results show once more how promising is the manipulation of microparticles by Leidenfrost drops. The possibility of a complete processing of such particles by drops is not so far from being realised. A deposition by complete evaporation, the transport via structured substrates are already quite well understood. Preliminary experiments have shown that the capture of particles is also possible. In Fig. VII.1, we show the capture rate of beads $R_b = 58$ μm by a water drop ($R = 3$ mm - represented by the blue zone). We see that all the beads are removed from the stripe on a large part of the drop (positive values of the capture rate) and only a small part is pushed toward the edges of the trajectory of the drop (negative values of the capture rate).

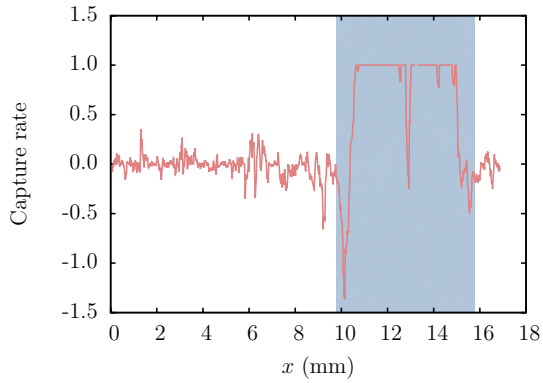

Figure VII.1: Capture rate of a drop of $R = 3$ mm passing on a stripe of beads ($R_b = 58$ μm).